Springer ThesesRecognizing Outstanding Ph.D. Research

Stathis Antoniou

Mathematical Modeling Through Topological Surgery and Applications



Springer Theses

Recognizing Outstanding Ph.D. Research

Aims and Scope

The series "Springer Theses" brings together a selection of the very best Ph.D. theses from around the world and across the physical sciences. Nominated and endorsed by two recognized specialists, each published volume has been selected for its scientific excellence and the high impact of its contents for the pertinent field of research. For greater accessibility to non-specialists, the published versions include an extended introduction, as well as a foreword by the student's supervisor explaining the special relevance of the work for the field. As a whole, the series will provide a valuable resource both for newcomers to the research fields described, and for other scientists seeking detailed background information on special questions. Finally, it provides an accredited documentation of the valuable contributions made by today's younger generation of scientists.

Theses are accepted into the series by invited nomination only and must fulfill all of the following criteria

- They must be written in good English.
- The topic should fall within the confines of Chemistry, Physics, Earth Sciences, Engineering and related interdisciplinary fields such as Materials, Nanoscience, Chemical Engineering, Complex Systems and Biophysics.
- The work reported in the thesis must represent a significant scientific advance.
- If the thesis includes previously published material, permission to reproduce this must be gained from the respective copyright holder.
- They must have been examined and passed during the 12 months prior to nomination.
- Each thesis should include a foreword by the supervisor outlining the significance of its content.
- The theses should have a clearly defined structure including an introduction accessible to scientists not expert in that particular field.

More information about this series at http://www.springer.com/series/8790

Stathis Antoniou

Mathematical Modeling Through Topological Surgery and Applications

Doctoral Thesis accepted by the National Technical University of Athens, Athens, Greece



Author
Dr. Stathis Antoniou
School of Applied Mathematical and
Physical Sciences, Department of
Mathematics
National Technical University of Athens
Athens, Greece

Supervisor
Prof. Sofia Lambropoulou
School of Applied Mathematical and
Physical Sciences, Department of
Mathematics
National Technical University of Athens
Athens, Greece

ISSN 2190-5053 ISSN 2190-5061 (electronic) Springer Theses ISBN 978-3-319-97066-0 ISBN 978-3-319-97067-7 (eBook) https://doi.org/10.1007/978-3-319-97067-7

Library of Congress Control Number: 2018949348

© Springer Nature Switzerland AG 2018

This work is subject to copyright. All rights are reserved by the Publisher, whether the whole or part of the material is concerned, specifically the rights of translation, reprinting, reuse of illustrations, recitation, broadcasting, reproduction on microfilms or in any other physical way, and transmission or information storage and retrieval, electronic adaptation, computer software, or by similar or dissimilar methodology now known or hereafter developed.

The use of general descriptive names, registered names, trademarks, service marks, etc. in this publication does not imply, even in the absence of a specific statement, that such names are exempt from the relevant protective laws and regulations and therefore free for general use.

The publisher, the authors and the editors are safe to assume that the advice and information in this book are believed to be true and accurate at the date of publication. Neither the publisher nor the authors or the editors give a warranty, express or implied, with respect to the material contained herein or for any errors or omissions that may have been made. The publisher remains neutral with regard to jurisdictional claims in published maps and institutional affiliations.

This Springer imprint is published by the registered company Springer Nature Switzerland AG The registered company address is: Gewerbestrasse 11, 6330 Cham, Switzerland

We are a way for the cosmos to know itself.

Carl Sagan

La réponse est l'homme, quelle que soit la question.

Louis Aragon

There is a theory which states that if ever anyone discovers exactly what the Universe is for and why it is here, it will instantly disappear and be replaced by something even more bizarre and inexplicable. There is another theory which states that this has already happened.

Douglas Adams

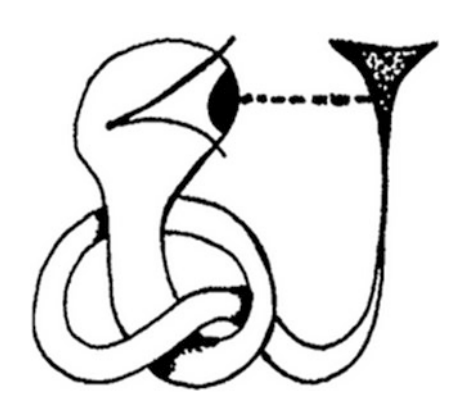


Illustration by L. H. Kauffman, see [Kauffman, L.H.: Knot Logic. In: Kauffman, L. (ed), Knots and Applications. World Scientific Pub. pp. $1-110\ (1994)$]

Supervisor's Foreword

Topology is the area of Mathematics that deals with the study of properties of topological spaces and subsets of theirs, meant as point sets, which remain invariant under transformations called homeomorphisms. A homeomorphism is a continuous bijective mapping with continuous inverse. So, the objects in Topology can be considered as elastically deformable, stretchable, squeezable, bendable, and twistable. For example, a circle is homeomorphic to a triangle, while an open interval or a circle with a point removed is homeomorphic to a line. The surface of a sphere is homeomorphic to the surface of a cube but not to the surface of a torus. Further, the surface of a sphere with a point removed is homeomorphic to a plane. An annulus is homeomorphic to the surface of a cylinder but not to the Möbius band. The annulus is also homeomorphic to a circular band which has undergone a full twist and has been reglued, since a cut followed by a point-by-point regluing is not visible by the homeomorphism. In this spirit, a circle is homeomorphic to any knot. One of the aims of Topology is to classify up to homeomorphism classes of point sets with respect to some given properties. The most typical example is the classification of compact, connected, orientable surfaces with no boundary, which comprises: the 2-sphere, the torus, the torus with two holes, the torus with three holes, etc.

If, however, a point set is embedded in a larger topological space and one requires a homeomorphism on it to extend to a homeomorphism of the whole surrounding space, then this may not be always possible. Such a "nice" homeomorphism is called *isotopy*. Hence, an isotopy can be perceived as a continuous elastic deformation of the ambient space, during which no cutting and regluing may take place. As an example, a circle embedded in our 3-space is not isotopic to any given knot. Hence, the question of classifying all knots up to isotopy now makes sense and this is one of the classical still unsolved problems of Mathematics. The classification of knots is a special case of the general placement problem: to understand the embeddings of a point set in some given topological space. In this work, topological spaces are restricted to *manifolds*. These are "nice" topological spaces, each point of which has a topological neighborhood of fixed dimension, the dimension of the manifold, and points have a separation property.

A basic aspect of Low-dimensional Topology is the use of cobordisms of 1-, 2-, and 3-manifolds to understand topological and geometric structure. Such cobordisms can be factored into elementary cobordisms called surgeries, which are elementary steps of topology change. Surgery on a manifold M is roughly the procedure of removing from the interior of M a manifold, which has boundary of one dimension lower than that of M, and gluing back another manifold with the same boundary. The "glue" is a homeomorphism along the common boundary. The new manifold will very likely be non-homeomorphic to the starting one. Hence, surgery is a topological technique that can be employed for changing the homeomorphism or the isotopy types of manifolds. Topological surgery was introduced independently by A. H. Wallace (1960) and J. W. Milnor (1961). It has been used in the study and classification of manifolds of dimension greater than three while also being an important topological tool in lower dimensions. For instance, by surgery on a knot one can switch a crossing and, very likely, produce a different knot. Surgery on a sphere can produce a torus and, successively, any other oriented surface. Further, surgery on the 3-sphere along any framed knot or link will produce a 3-manifold, in most cases non-homeomorphic to the 3-sphere and all closed, connected, orientable 3-manifolds arise in this way. Furthermore, R. Kirby (1978) described an equivalence relation on the set of all framed knots and links, such that two framed links are equivalent if and only if they give rise, after surgery, to homeomorphic 3-manifolds. It is also worth adding that in the proof of the Poincaré Conjecture, G. Y. Perelman used a modification of the standard Ricci flow called "Ricci flow with surgery", which involves excising singular regions.

In recent years, topology has been making its way from abstract mathematics to natural sciences. Its numerous applications range from Physics and Biology to Chemistry and Material Science. This work makes a very important contribution in this direction and opens new ways of using the general language of topology in natural sciences. More precisely, it initiates the exploration of the direct connection of topological surgery with various natural processes, which are—not surprisingly—abundantly present in both micro- and macroscales. We can see it, for example, during DNA recombination, the biological process where DNA strands are exchanged to produce new nucleotide sequence arrangements, but also during magnetic reconnection, the physical process in which the magnetic topology is rearranged and magnetic energy is converted to kinetic energy, thermal energy, and particle acceleration. One dimension up, topological surgery can be observed in bubble splitting and cell division, in the formation of tornados and hurricanes, as well as in the formation of the connected vortices in a pool of water (Falaco solitons), while it can be sought in many other processes of change and evolution of shapes in natural forms.

In order to pin down the connections between the abovementioned phenomena with topological surgery, the formal definition of surgery is enhanced by introducing "forces", by extending continuously the process to the interior of the original manifold (formulation of the continuity model) and by considering surgery on embedded manifolds. In this way, the enhanced models of the various types of surgery parallel the underlying mechanisms of these dynamical phenomena in nature. Further, the new notions introduced in the definition of surgery allow for viewing its mechanism across dimensions. Finally, in a rather unexpected direction,

the last part of the thesis presents a conjectured application of 3-dimensional surgery to black hole formation, a problem on which we currently work with Louis H. Kauffman and which we believe will be of considerable interest to cosmologists.

The seed of this work dates back several years ago, I believe 1990, when I heard a talk by Nikola Samardzija presenting their newly discovered, with Larry Greller, 3-dimensional generalization of the classical Lotka–Volterra one predator/one prey dynamical system. Their system of two predators/one prey demonstrates how, upon change of parameters, nested spherical solutions change topology to a toroidal nesting inside a fractal bead via a "hole-drilling" behavior along the slow manifold. This intriguing discovery, which clearly exhibits topological surgery as I immediately observed, reached out to The New York Times (1990). The connection of this dynamical system with topological surgery was pinned down already in the Diploma dissertation of Stathis in 2006. This means that phenomena exhibiting this type of surgery can be potentially modeled by the Samardzija—Greller dynamical system. Stathis was the student who inspired me to discuss this idea with him and I was right. Later on, he took the subject for his Ph.D. study and with his dedicated and inspired work as well as his interdisciplinary mind he raised it to a new mathematical direction. To quote one of the reviewers of our PLOS ONE paper: "...This paper is a ground-breaking review of instances of topological surgery in natural scientific situations. The examples given are convincing and of much significance both for mathematics and for natural science," while a reviewer of our Springer PROMS THALES paper wrote: "This is an intriguing paper that investigates how extensions of the traditional notion of topological surgery can be used to model naturally occurring phenomena. It would be wonderful to see scientists adopting this point of view, as it provides a formal manner for describing a wide range of phenomena." Our topological model indicates where to look for the forces causing surgery and what deformations should be observed in the local submanifolds involved. These predictions are significant for the study of such phenomena exhibiting surgery.

Stathis defended his Ph.D. thesis at the National Technical University of Athens (NTUA), in December 2017 receiving a unanimous "excellent". Apart from myself, the 3-member Advisory Committee included Louis H. Kauffman of the University of Illinois at Chicago and Antonios Charalambopoulos of the NTUA, while the 7-member Examining Committee was complemented with Cameron McA. Gordon of the University of Texas at Austin, Colin Adams of the Williams College, Theocharis Apostolatos, physicist at the National and Kapodistrian University of Athens, and Dimitrios Kodokostas of the NTUA.

In conclusion, this thesis is of much significance for both mathematics and natural sciences as it provides the formal language of topological surgery for describing and studying a wide range of phenomena. I believe this work is important not only because it provides a new bridge between topology and natural sciences, but also because its ideas open a plethora of new research directions which I expect to flourish in years to come.

Athens, Greece June 2018

Abstract

Topological surgery is a mathematical technique used for creating new manifolds out of known ones. We observe that it occurs in natural phenomena, where forces are applied and the manifold in which they occur changes type. For example, 1-dimensional surgery happens during chromosomal crossover, DNA recombination, and when cosmic magnetic lines reconnect, while 2-dimensional surgery happens in the formation of Falaco solitons, in drop coalescence, and in the cell mitosis. Inspired by such phenomena, we enhance topological surgery with the observed forces and dynamics. We then generalize these low-dimensional cases to a model, which extends the formal definition to a continuous process caused by local forces for an arbitrary dimension m. Next, for modeling phenomena which do not happen on arcs (respectively surfaces) but are 2-dimensional (respectively 3-dimensional), we fill in the interior space by defining the notion of solid topological surgery. We further present a dynamical system as a model for both natural phenomena exhibiting a "hole drilling" behavior and our enhanced notion of solid 2-dimensional 0-surgery. Moreover, we analyze the ambient space S^3 in order to introduce the notion of *embedded topological* surgery in S^3 . This notion is then used for modeling phenomena which involve more intrinsically the ambient space, such as the appearance of knotting in DNA and phenomena where the causes and effects of the process lie beyond the initial manifold, such as the formation of tornadoes. Moreover, we present a visualization of the 4-dimensional process of 3-dimensional surgery by using the new notion of decompactified 2-dimensional surgery and rotations. Finally, we propose a model for a phenomenon exhibiting 3-dimensional surgery: the formation of black holes from cosmic strings. We hope that through this study, the topology and dynamics of many natural phenomena, as well as topological surgery itself, will be better understood.¹

¹2010 Mathematics Subject Classification: 34D45, 34F10, 37B99, 37C70, 37G10, 37Mxx, 37Nxx, 57M25, 57M40, 57M99, 57N12, 57N13, 57R65, 58Z05, 65Pxx, 92B99.

Acknowledgements

I am grateful to my advisor Sofia Lambropoulou, who inspired me to change my career to science. She has supported me throughout the whole duration of my thesis in many ways. Her guidance and enthusiasm pushed me toward higher goals, taught me how to properly write in a scientific way and opened up new research directions.

I wish to express my gratitude to Louis H. Kauffman for his commitment to our meetings (real and virtual), which taught me how to tackle difficult problems and gave me the opportunity to expand not only my mathematical knowledge but also the way I am thinking. I would also like to thank Colin Adams, Cameron McA. Gordon, and Antonios Charalambopoulos for many insightful discussions and their support during my thesis.

I am grateful to my parents Ioannis and Aggeliki and my aunt Lena, who supported me in deciding to change my career to science; this decision which was undoubtedly the right one. Further, I would like to thank Danai, Orfeas, Rea, and all my family and friends. All of them supported me, directly or indirectly.

Finally, I am grateful for having the privilege of doing a funded Ph.D. during these unstable economic times for Greece. More precisely, I would like to thank the European Union (European Social Fund—ESF) and the Greek national funds for their funding through the Operational Program "Education and Lifelong Learning" and my teacher Sofia Lambropoulou who coordinated the Research Funding Program THALES. I would also like to thank the Papakyriakopoulos Foundation and the Department of Mathematics for the Papakyriakopoulos scholarship.

Contents

1	Intro	oduction	1				
	Refe	rences	3				
2	Useful Mathematical Notions						
	2.1						
	2.2	Non-technical Definition of a Manifold					
	2.3	Properties of Manifolds	6				
	2.4	Examples of Manifolds	6				
		2.4.1 1-Manifolds	6				
		2.4.2 2-Manifolds	7				
		2.4.3 3-Manifolds	7				
		2.4.4 <i>n</i> -Balls and <i>n</i> -Spheres	8				
		2.4.5 The Compactification of \mathbb{R}^n	8				
		2.4.6 Product Spaces	9				
	2.5		0				
		2.5.1 Hausdorff Space	lO				
			1				
			1				
	2.6 Homeomorphisms						
	2.7						
	2.8						
	Refe		3				
3	The	Formal Definition of Surgery	15				
	3.1		6				
	3.2	2-Dimensional 0-Surgery					
	3.3	2-Dimensional 1-Surgery					
	3.4	3-Dimensional 0- and 1-Surgery					
	Refe		9				
4	Cont	tinuity	21				

xvi Contents

	4.1 4.2	The Continuous Definition of Surgery	21 22					
5	5.1 5.2 5.3 5.4 5.5	Amics Dynamic 1-Dimensional Topological Surgery Modeling Phenomena Exhibiting 1-Dimensional Surgery Dynamic 2-Dimensional Topological Surgery Modeling Phenomena Exhibiting 2-Dimensional Surgery A Model for Dynamic m-Dimensional n-Surgery erences						
6	Solid	l Surgery	33					
	6.1	Solid 1-Dimensional Topological Surgery	34					
	6.2	Solid 2-Dimensional Topological Surgery	35					
	6.3	Modeling Phenomena Exhibiting Solid 2-Dimensional						
		0-Surgery	38					
	6.4							
	Dafa	1-Surgery	39					
		References						
7	-	Oynamical System Modeling Solid 2-Dimensional 0-Surgery 41						
	7.1	The Dynamical System and Its Steady State Points						
	7.2	Local Behavior and Numerical Simulations						
	7.3	Connecting the Dynamical System with Solid 2-Dimensional 0-Surgery						
	Refe	rences	48					
8	The	Ambient Space S ³	49					
_	8.1	Descriptions of S^3	49					
		8.1.1 Via \mathbb{R}^3	49					
		8.1.2 Via Two 3-Balls.	50					
		8.1.3 Via Two Solid Tori	51					
	8.2	Connecting the Descriptions of S^3	51					
		8.2.1 Via Corking	51					
		8.2.2 Via Surgery	52					
	8.3	Dynamical Systems Exhibiting the Topology of S^3	53					
		8.3.1 The 3-Dimensional Lotka–Volterra System	53					
		8.3.2 The Pair of Linear Harmonic Oscillators	53					
	Refe	rences	55					
9	Emb	edded Surgery	57					
	9.1	Embedded 1-Dimensional Surgery	57					
	9.2	Embedded 2-Dimensional Surgery						
	9.3	Modeling Phenomena Exhibiting Embedded Solid						
		2-Dimensional Surgery	59					

Contents xviii

		9.3.1	A Topological Model for the Density Distribution					
			in Black Hole Formation	59				
		9.3.2	A Topological Model for the Formation					
			of Tornadoes	62				
		9.3.3	Embedded Solid 2-Dimensional 1-Surgery					
			on $M = D^3$	64				
	Refer	ences		65				
10	3-Din	nensiona	d Surgery	67				
	10.1		pactified 2-Dimensional Surgery	67				
	10.2	Visuali	zing 3-Dimensional Surgery in \mathbb{R}^3	69				
		10.2.1	Initial and Final Steps	70				
		10.2.2	Intermediate Steps	71				
	10.3	The Co	ontinuity of 3-Dimensional Surgery	72				
	10.4	Modeli	ng Black Hole Formation from Cosmic Strings	74				
		10.4.1	Terminology	74				
		10.4.2	Black Holes from Cosmic Strings	75				
		10.4.3	Black Holes from 3-Dimensional 1-Surgery	76				
	References							
11	Conclusions							
Cui	riculu	m Vitae		81				
Ind	Index							

Chapter 1 Introduction



1

Topological surgery is a mathematical technique used for changing the homeomorphism type, or simply the shape, of a manifold. For example, all orientable surfaces may arise from the 2-dimensional sphere using surgery. The mathematical notions needed for understanding the definition of surgery can be found in Chap. 2. The examples of 1, 2- and 3-dimensional surgery are analyzed in Sects. 3.1, 3.2, 3.3 and 3.4.

Topological surgery is exhibited in nature in numerous, diverse processes of various scales. Surgery in nature is usually performed on basic manifolds with or without boundary, that undergo merging and recoupling. For example, in dimension 1 topological surgery can be seen in DNA recombination and during the reconnection of cosmic magnetic lines, while in dimension 2 it happens when genes are transferred in bacteria and during the formation of black holes. Such processes are initiated by attracting forces acting on a sphere of dimension 0 (that is, two points) or 1 (that is, a circle).

A large part of this work is dedicated to defining new theoretical concepts which are better adapted to the phenomena, to modeling such phenomena in dimensions 1, 2 and 3 and to presenting a generalized topological model for m-dimensional n-surgery which captures the observed dynamics. With our enhanced definitions and our model of topological surgery in hand, we match surgery patterns with natural phenomena and we study the physical implications of our modeling. Furthermore, we present a dynamical system that performs a specific type of surgery and we pin down its relation with topological surgery. Finally, we propose a new type of surgery, the decompactified 2-dimensional surgery, which allows the visualization of 3-dimensional surgery in \mathbb{R}^3 . More precisely, the new concepts are:

• Continuity and dynamics: In Chap. 4, we start by enhancing the formal definition of surgery with continuity, whereby an m-dimensional surgery is considered as the continuous local process of passing from an appropriate boundary component of an m+1-dimensional handle to its complement boundary component. We further notice that surgery in nature is caused by forces. For example, in dimension 1, during

2 1 Introduction

meiosis the pairing is caused by mutual attraction of the parts of the chromosomes that are similar or homologous, as detailed and illustrated in Sect. 5.1. In dimension 2, the creation of tornadoes is caused by attracting forces between the cloud and the earth (as detailed and illustrated in Sect. 9.3.2), while soap bubble splitting is caused by the surface tension of each bubble which acts as an attracting force (this is discussed in Sect. 5.4). In Sect. 5.5 we incorporate these dynamics to our continuous definition and present a model for m-dimensional n-surgery. These dynamics explain the intermediate steps of the formal definition of surgery and extend it to a continuous process caused by local forces. Note that these intermediate steps can also be explained by Morse theory but this approach does not involve the forces.

- Solid surgery: The interior of the initial manifold is now filled in. We observe that phenomena like tension on soap films or the merging of oil slicks are undergoing 1-dimensional surgery but they happen on surfaces instead of 1-manifolds. For example, an oil slick is seen as a disc, which is a continuum of concentric circles together with the center. Similarly, moving up one dimension, during the biological process of mitosis and during tornado formation, 2-dimensional surgery is taking place on 3-dimensional manifolds instead of surfaces. For example, during the process of mitosis, the cell is seen as a 3-ball, that is, a continuum of concentric spheres together with the central point (this is discussed in Sect. 6.4). Thus, in order to fit natural phenomena where the interior of the initial manifold is filled in, in Chap. 6, we extend the formal definition by introducing the notion of *solid topological surgery* in both dimensions 1 and 2.
- Connection with a dynamical system: We establish a connection between these new notions applied on 2-dimensional topological surgery and the dynamical system presented in [1]. In Chap. 7 we analyze how, with a slight perturbation of parameters, trajectories pass from spherical to toroidal shape through a 'hole drilling' process. We show that our new topological notions are verified by both the local behavior of the steady state points of the system and the numerical simulations of its trajectories. This result gives us on the one hand a mathematical model for 2-dimensional surgery and on the other hand a dynamical system that can model natural phenomena exhibiting this type of surgery.
- Embedded surgery: We notice that in some phenomena exhibiting topological surgery, the ambient space is also involved. For example in dimension 1, during DNA recombination the initial DNA molecule which is recombined can also be knotted. In other words, the initial 1-manifold can be a knot (an embedding of the circle) instead of an abstract circle (see description and illustration in Sect. 9.1). Similarly in dimension 2, the processes of tornado and black hole formation are not confined to the initial manifold and topological surgery is causing (or is caused by) a change in the whole space (see Sect. 9.3 and illustrations therein). We therefore define the notion of *embedded topological surgery* in Chap. 9 which allows us to model these kind of phenomena but also to view all natural phenomena exhibiting topological surgery as happening in 3-space instead of abstractly. We consider our ambient 3-space to be S^3 and an extensive analysis of its descriptions together with the presentation of dynamical systems exhibiting its topology is done in Chap. 8.

1 Introduction 3

• The visualization of 3-dimensional surgery: Finally, in Chap. 10, we present a way to visualize the 4-dimensional process of 3-dimensional surgery. In order to do so, we introduce the notion of decompactified 2-dimensional surgery which allows us to visualize the process of 2-dimensional surgery in \mathbb{R}^2 instead of \mathbb{R}^3 . Using this new notion and rotation, we present a way to visualize 3-dimensional surgery in \mathbb{R}^3 . This is done in Sect. 10.2. Further, in Sect. 10.4, we propose a model for a phenomenon exhibiting 3-dimensional surgery: the formation of black holes from cosmic strings.

This thesis gathers, links and completes the results presented in [2–5] while extending them one dimension higher. The material is organized as follows: In Chap. 2 we recall the topological notions that will be used and provide specific examples that will be of great help to readers that are not familiar with the topic. In Chap, 3, we present the formal definition of topological surgery for an arbitrary dimension m. In Chap. 4, we enhance the formal definition of surgery with continuity. In Chap. 5, we introduce dynamics to 1 and 2-dimensional surgery and we discuss natural processes exhibiting these types of surgeries. In Sect. 5.5, we present a generalized model for m-dimensional n-surgery. In Chap. 6 we define solid 1 and 2-dimensional surgery and discuss related natural processes. We then present the dynamical system connected to these new notions in Chap. 7. As all natural phenomena exhibiting surgery (1 or 2-dimensional, solid or usual) take place in the ambient 3-space, in Chap. 8 we present the 3-sphere S^3 and the duality of its descriptions. This allows us to define in Chap. 9 the notion of embedded surgery. Finally, in Chap. 10, we use lower dimensional surgeries to visualize 3-dimensional surgery and propose a topological model for black hole formation from cosmic strings.

References

- Samardzija N., Greller L.: Explosive route to chaos through a fractal torus in a generalized Lotka-Volterra model. Bull. Math. Biol. 50(5) 465–491 (1988). https://doi.org/10.1007/BF02458847
- Lambropoulou, S., Samardzija, N., Diamantis, I., Antoniou, S.: Topological surgery and dynamics. In: Mathematisches Forschungsinstitut Oberwolfach Report No. 26/2014, Workshop: Algebraic Structures in Low-Dimensional Topology (2014). https://doi.org/10.4171/OWR/2014/26
- Lambropoulou, S., Antoniou, S.: Topological surgery, dynamics and applications to natural processes. J. Knot Theor Ramif. 26(9) (2016). https://doi.org/10.1142/S0218216517430027
- Antoniou S., Lambropoulou S.: Extending topological surgery to natural processes and dynamical systems. PLOS ONE 12(9) (2017). https://doi.org/10.1371/journal.pone.0183993
- Antoniou S., Lambropoulou S.: Topological surgery in nature. Algebraic modeling of topological and computational structures and applications. In: Proceedings in Mathematics and Statistics, vol. 219. Springer (2017). https://doi.org/10.1007/978-3-319-68103-0_15

Chapter 2 Useful Mathematical Notions



In this chapter we introduce the basic notions related to topological surgery. Readers that are familiar with the formalism of the topic can directly move to the formal definition in Chap. 3.

In Sect. 2.1 we define the notion of topological space which allows us to give a non-technical definition of a manifold in Sect. 2.2. After discussing some properties of manifolds in Sect. 2.3, a plethora of examples, which are to be used in this work, are presented in Sect. 2.4. The rigorous definition of a manifold is then given in Sect. 2.5. In Sects. 2.6 and 2.7, we further present the notions of homeomorphisms and embeddings of manifolds. Finally, the idea of topological surgery which makes use of these notions is introduced in Sect. 2.8.

2.1 Topological Spaces

A topological space is a set X with a distinguished family τ of subsets possessing the following properties:

- the empty set and the whole set X belong to τ
- the intersection of a finite number of elements of τ belongs to τ
- the union of any subfamily of elements of τ belongs to τ

The family τ is said to be the *topology* on X. Any set belonging to τ is called *open*. A *neighborhood* of a point $x \in X$ is any open set containing x. Any set whose complement is open is called *closed*. The minimal closed set (with respect to inclusion) containing a given set $A \subset X$ is called the *closure* of A and is denoted by \overline{A} . The maximal open set contained in a given set $A \subset X$ is called the *interior* of A and is denoted by Int(A).

2.2 Non-technical Definition of a Manifold

- An *n-manifold without boundary* is a 'nice' topological space with the property that each point in it has a neighborhood that locally resembles the usual *n*-dimensional Euclidean space \mathbb{R}^n .
- Similarly, an *n-manifold with boundary* is a 'nice' topological space with the property that each point in it has a neighborhood that locally resembles either \mathbb{R}^n (if the point lies in the interior) or \mathbb{R}^n_+ (if the point lies on the boundary).

2.3 Properties of Manifolds

An n-manifold, M, is said to be:

- connected if it consists of only one piece,
- simply connected if a loop at any point can be continuously shrunk to a point
- *compact* if it can be enclosed in some *k*-dimensional ball,
- *orientable* if any oriented frame that moves along any closed path in *M* returns to a position that can be transformed to the initial one by a rotation.

2.4 Examples of Manifolds

In this section we start by giving examples of manifolds of dimensions 1, 2 and 3 in Sects. 2.4.1, 2.4.2 and 2.4.3 respectively. We then present some basic examples of manifolds in any dimension n. Namely, the n-balls, \mathbb{R}^n and its compactification the n-sphere are discussed in Sects. 2.4.4 and 2.4.5. Finally, the product space of two manifolds is discussed in Sect. 2.4.6.

2.4.1 1-Manifolds

Typical examples of 1-manifolds without boundary are lines while closed intervals are typical examples of 1-manifolds with boundary. It is easy to see that any open neighborhood of a point in a line or in the interior of a closed interval is topologically equivalent to \mathbb{R} while any open neighborhood of a boundary point of a closed interval is topologically equivalent to \mathbb{R}_+ . Other examples of 1-manifolds are circles and open intervals (without boundary) as well as half-lines and half-closed intervals (with boundary). In fact, any connected 1-manifold is homeomorphic to one of the following four manifolds: the real line \mathbb{R} , the half-line \mathbb{R}_+ , the closed interval I = [0, 1] or the circle $S^1 = \{(x, y) \in \mathbb{R}^2 | x^2 + y^2 = 1\}$. The proof of this theorem can be found in [1, 2].

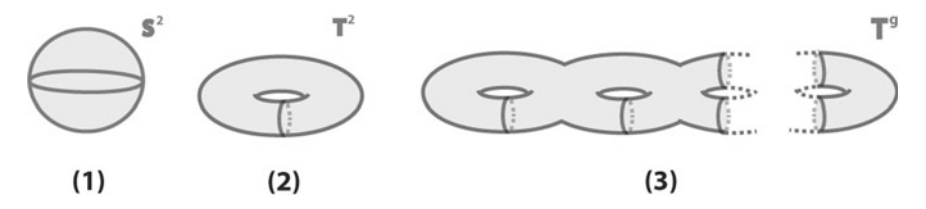


Fig. 2.1 (1) A sphere S^2 has genus 0 (2) A torus T^2 has genus 1 (3) The connected sum of g tori has genus g

2.4.2 2-Manifolds

Moving up one dimension, the plane \mathbb{R}^2 , the sphere $S^2=\{(x,y,z)\in\mathbb{R}^3|x^2+y^2+z^2=1\}$ and the torus $T^2=\{(x,y,z)\in\mathbb{R}^3|\left(b-\sqrt{x^2+y^2}\right)^2+z^2=a^2\}$ (where the inner and outer radii are b-a and b+a), which can be perceived as the boundary of a doughnut, are 2-manifolds without boundary, while a disc $D^2=\{(x,y)\in\mathbb{R}^2|x^2+y^2\leq 1\}$ or a cylinder $C=\{(x,y,z)\in\mathbb{R}^3|x^2+y^2=1,z\in[-1,1]\}$, which is homeomorphic to an annulus, are examples of 2-manifolds with boundary.

It is also worth mentioning that for every connected, orientable, compact 2-manifolds M without boundary, there is a $g \in \mathbb{N}$ such that M is homeomorphic to a surface of genus g. The proof of this classic theorem can be found, for example, in [3] or in [4]. The *genus* g represents the number of holes of the surface. For instance the sphere S^2 is a surface of genus g=0, see Fig. 2.1(1). Next, the torus T^2 is a surface of genus g=1, see Fig. 2.1(2). Note that the torus can also be obtained by gluing the two pairs of opposite sides of a square. Moreover, a surface of genus g can be obtained by joining together g copies of the torus, see Fig. 2.1(3). The joining process for every pair of tori can be seen as cutting a small circle out of each tori and gluing them together along their common boundary.

2.4.3 3-Manifolds

In dimension 3, the 3-dimensional space \mathbb{R}^3 , the 3-sphere $S^3 = \{(x, y, z, w) \in \mathbb{R}^4 | x^2 + y^2 + z^2 + w^2 = 1\}$ (which, as we explain in Sect. 2.4.5, is the compactification of \mathbb{R}^3) and the 3-torus T^3 (which can be obtained by gluing the three pairs of opposite faces of a cube) are classical examples 3-manifolds without boundary. The 3-ball $D^3 = \{(x, y, z) \in \mathbb{R}^3 | x^2 + y^2 + z^2 \le 1\}$ or the solid torus, which can be perceived as a whole doughnut, and which, for $b \ge a$, is the set $V = \{(x, y, z) \in \mathbb{R}^3 | (b - \sqrt{x^2 + y^2})^2 + z^2 \le a^2\}$, are examples of 3-manifolds with boundary.

A very important theorem which was proven in [5–7] is the Poincaré conjecture which states that every simply connected, compact 3-manifold without boundary is homeomorphic to the 3-sphere. This theorem remained an open problem for nearly a century.

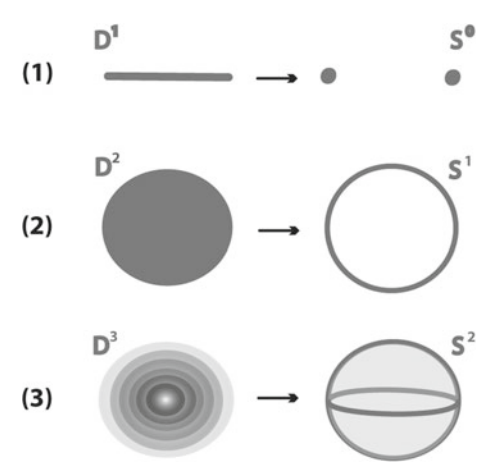


Fig. 2.2 (1) A segment D^1 is bounded by two points S^0 (2) A disc D^2 is bounded by a circle S^1 (3) A 3-ball D^3 is bounded by a sphere S^2

2.4.4 n-Balls and n-Spheres

Some manifolds can be generalized in every dimension n. For instance, the basic connected, oriented, compact n-manifold without boundary is the n-sphere, S^n , while the basic connected, oriented n-manifold with boundary is the n-ball, D^n . For n=1, D^1 is the closed unit interval, while S^1 is the circle. For n=2, we have the 2-disc D^2 and the 2-sphere S^2 and, for n=3, we have the 3-ball D^3 and the 3-sphere S^3 . Finally, for n=0, we have the 0-manifold D^0 which is a point and the space S^0 which is the disjoint union of two points. As seen in Fig. 2.2(1), by convention, we consider these two one-point spaces to be $\{+1\}$ and $\{-1\}$: $S^0=\{+1\}$ \coprod $\{-1\}$. More generally, we will follow this convention by considering that n-spheres and n-balls are centered at the origin of our coordinate system.

The above basic manifolds are related as follows: the n-sphere S^n is made by gluing two n-discs D^n along their boundaries. Indeed, the circle can be seen as the result of gluing two bended intervals, see Fig. 2.5(1), the 2-sphere can be seen as the result of gluing two bended 2-discs, see Fig. 2.5(2), the 3-sphere can be seen as the result of gluing two 3-balls, etc. Even for n = 0, S^0 is made of two points D^0 . The rigorous definition of 'gluing' can be found in Sect. 2.7.

Furthermore, another basic relation between the *n*-ball and the *n*-sphere is that the boundary of a *n*-dimensional ball is a (n-1)-dimensional sphere, $\partial D^n = S^{n-1}$. In Fig. 2.2, this relation is shown for n=1,2 and 3.

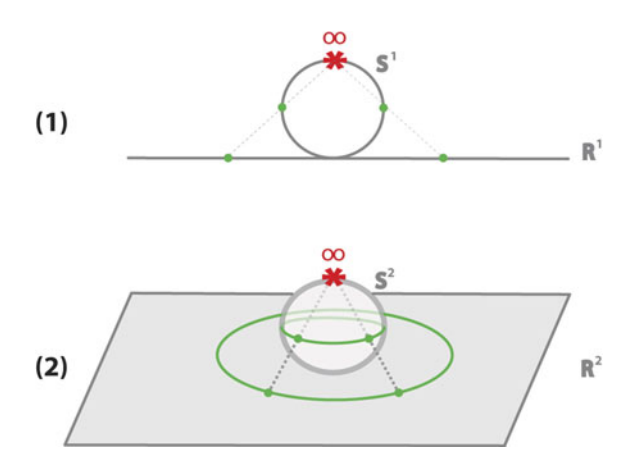


Fig. 2.3 (1) S^1 onto \mathbb{R}^1 (2) S^2 onto \mathbb{R}^2

2.4.5 The Compactification of \mathbb{R}^n

Besides creating the n-sphere S^n by gluing two n-discs, another way of creating the n-sphere is by compactifying the Euclidian space \mathbb{R}^n . *Compactification* is the process of making a topological space into a compact space. For each dimension n, the space \mathbb{R}^n with all points at infinity compactified to one single point is homeomorphic to S^n . So, S^n is also called the one-point compactification of \mathbb{R}^n . Conversely, the sphere S^n can be decompactified to the space \mathbb{R}^n by the so-called *stereographic projection*. For example, for n=1 we have that the circle S^1 is the one-point compactification of the real line \mathbb{R}^1 , see Fig. 2.3(1), while for n=2 the sphere S^2 is the one-point compactification of the plane \mathbb{R}^2 , see Fig. 2.3(2). The compactification of \mathbb{R}^3 is discussed and illustrated in Sect. 8.1.1.

It is worth pointing out that the two descriptions of S^n are very much related. Indeed, a closed neighborhood of the point at infinity in the compactification method is just one n-disc D^n while the remaining space is the second disc D^n .

2.4.6 Product Spaces

- If $X \times Y$ is the Cartesian product of the topological spaces X and Y (regarded as sets), then $X \times Y$ becomes a topological space (called the *product* of the spaces X and Y) if we declare open all the products of open sets in X and in Y and all possible unions of these products.
- The *product space* of two manifolds *X* and *Y* is the manifold made from their Cartesian product *X* × *Y*. This product space creates a new manifold *X* × *Y* out of known manifolds *X* and *Y*, whose dimension is the sum of the dimensions of *X* and *Y*.

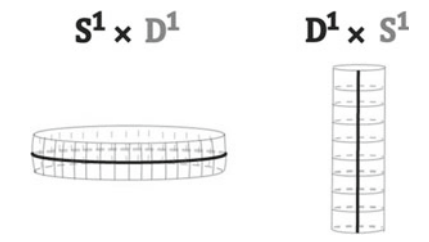


Fig. 2.4 Two ways of viewing a cylinder

• If X, Y are manifolds with boundary, the product space $X \times Y$ is a manifold with boundary:

$$\partial(X\times Y)=(\partial X\times Y)\cup(X\times\partial Y)(\star)$$

For example the next common connected, oriented, compact 2-manifold without boundary after S^2 is the torus, which can be seen as the product space $S^1 \times S^1$. Analogously, the solid torus is the product space $S^1 \times D^2$ and its boundary is a torus: $\partial(S^1 \times D^2) = S^1 \times \partial D^2 = S^1 \times S^1$.

Other product spaces that we will be using here are: the cylinder $S^1 \times D^1$ or $D^1 \times S^1$ (see Fig. 2.4), the solid cylinder $D^2 \times D^1$, which is homeomorphic to the 3-ball, and the spaces of the type $S^0 \times D^n$, which are the disjoint unions of two n-balls $D^n \coprod D^n$.

All the above examples are product spaces of the form $S^p \times D^q$ and can be viewed as q-thickenings of the p-sphere. For example, the 1-thickening of S^0 comprises two segments, the 2-thickening of S^0 comprises two discs, while the 3-thickening of S^0 comprises two 3-balls. Also, a solid torus is a 2-thickening of S^1 . It is also worth stressing that the product spaces $S^p \times D^q$ and $D^{p+1} \times S^{q-1}$ have the same boundary:

$$\partial(S^p \times D^q) = \partial(D^{p+1} \times S^{q-1}) = S^p \times S^{q-1}(\star\star).$$

2.5 Defining Manifolds

In order to give the rigorous definition of a manifold, we first need to define the notions of Hausdorff space and countable base.

2.5.1 Hausdorff Space

A topological space is said to be a *Hausdorff space* if any two distinct points of the space have nonintersecting neighborhoods.

2.5.2 Bases of Topological Spaces

- If (X, τ) is a topological space, a *base* of the space X is a subfamily $\tau' \subset \tau$ such that any element of τ can be represented as the union of elements of τ' . In other words, τ' is a family of open sets such that any open set of X can be represented as the union of sets from this family. To define the topology τ , it suffices to indicate a base for τ . In the case when at least one base of X is countable, we say that X is a space with *countable base*.
- For example, in the space $\mathbb{R}^n = \{(x_1, \dots, x_n) \mid x_i \in \mathbb{R}\}$, the standard topology is given by the base $U_{a,\epsilon} = \{x \in \mathbb{R}^n \mid |x a| < \epsilon\}$, where $a \in \mathbb{R}^n$ and $\epsilon > 0$. We can additionally require that all the coordinates of the point a, as well as the number ϵ , be rational; in this case we obtain a countable base.
- Another example is the topology of the *n*-dimensional sphere $S^n = \{x \in \mathbb{R}^{n+1} \mid |x|=1\}$. As stated in Sect. 2.4.5, this space is homeomorphic to the compactification of \mathbb{R}^n . To the set \mathbb{R}^n , we add the element ∞ and introduce in $\mathbb{R}^n \cup \{\infty\}$ the topology whose base is the base of \mathbb{R}^n to which we have added the family of sets $U_{\infty,R} = \{x \in \mathbb{R}^n \mid |x| > R\} \cup \{\infty\}$.

2.5.3 The Rigorous Definition of a Manifold

- A Hausdorff space M^n with countable base is said to be an *n*-dimensional topological manifold if any point $x \in M^n$ has a neighborhood homeomorphic to \mathbb{R}^n or to \mathbb{R}^n_+ , where $\mathbb{R}^n_+ = \{(x_1, \dots, x_n) \mid x_i \in \mathbb{R}, x_1 \geq 0\}$.
- The set of all points $x \in M^n$ that have no neigbourhoods homeomorphic to \mathbb{R}^n is called the *boundary* of the manifold M^n and is denoted by ∂M^n . When $\partial M^n = \emptyset$, we say that M^n is a *manifold without boundary*. If the boundary of a manifold M^n is nonempty, then it is an (n-1)-dimensional manifold.

2.6 Homeomorphisms

In Sect. 2.4 by 'topologically equivalent' we mean the following: two *n*-manifolds X and Y are *homeomorphic* or *topologically equivalent* if there exists a homeomorphism between them, namely a map $f: X \to Y$ with the properties that:

- f is continuous (i.e. the preimage of any open set is open)
- There exists the inverse function $f^{-1}: Y \to X$ (equivalently f is 1–1 and onto)
- f^{-1} is also continuous

For example, an elastic deformation of the space X to the space Y is a homeomorphism but a circle and a knotted circle are also homeomorphic.

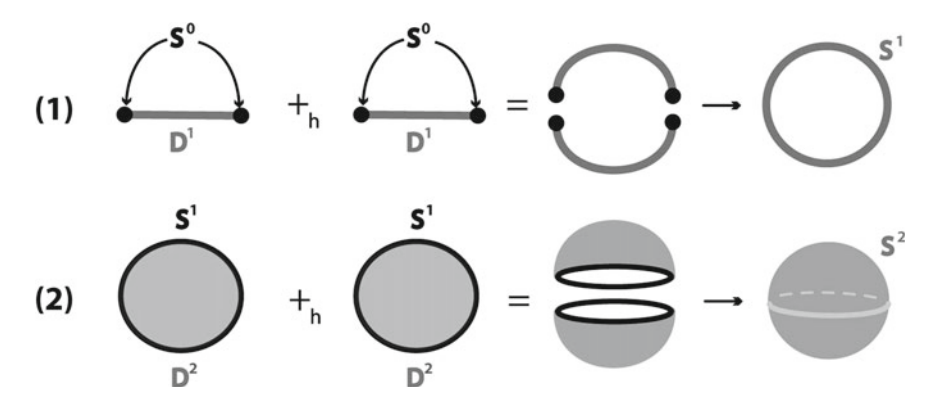


Fig. 2.5 (1) $D^1 \cup_h D^1 = S^1$ (2) $D^2 \cup_h D^2 = S^2$

2.7 Embeddings

- An *embedding* of an *n*-manifold N^n in an *m*-manifold M^m is a 1–1, continuous map $f: N \hookrightarrow M$ such that its restriction on the image f(N) is a homeomorphism between N and f(N). The notion of embedding allows to view spaces inside specific manifolds instead of abstractly. Embeddings even of simple manifolds can be very complex. For example, the embeddings of the circle S^1 in the 3-space \mathbb{R}^3 are the well-known knots whose topological classification is still an open problem of low-dimensional topology.
- An embedding of a submanifold $N^n \hookrightarrow M^m$ is *framed* if it extends to an embedding $N^n \times D^{m-n} \hookrightarrow M$.
- A *framed n-embedding in M* is an embedding of the (m-n)-thickening of the n-sphere, $h: S^n \times D^{m-n} \hookrightarrow M$, with core n-embedding $e = h_{|}: S^n = S^n \times \{0\} \hookrightarrow M$. For example, the framed 1-embeddings in \mathbb{R}^3 comprise embedded solid tori in the 3-space with core 1-embeddings being knots.
- Let X, Y be two n-manifolds with homeomorphic boundaries ∂X and ∂Y (which are (n-1)-manifolds). Let also h denote a homeomorphism $h: \partial X \to \partial Y$. Then, from $X \cup Y$ one can create a new n-manifold without boundary by 'gluing' X and Y along their boundaries. The gluing is realized by identifying each point $x \in \partial X$ to the point $h(x) \in \partial Y$. The map h is called *gluing homeomorphsim*. One important example is the gluing of two n-discs along their common boundary which gives rise to the n-sphere, see Fig. 2.5 for n = 1, 2. For n = 3, the gluing of two 3-balls yielding the 3-sphere S^3 is illustrated and discussed in Sect. 8.1.2. Another interesting example is the gluing of solid tori which also yield the 3-sphere. This is illustrated and discussed in Sect. 8.1.3.

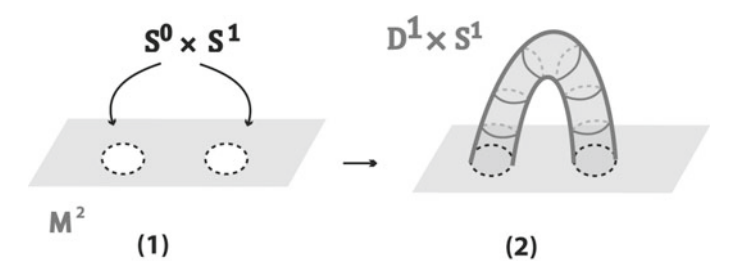


Fig. 2.6 (1) Remove $S^0 \times D^2$ (2) Glue $D^1 \times S^1$ along common boundary $S^0 \times S^1$

2.8 The Idea of Topological Surgery

As we will see in the next chapter, the notions of embedding and gluing homeomorphism together with property $(\star\star)$ described in Sect. 2.4.6 are the key ingredients needed to define topological surgery. In this section we present its key idea together with a simple example.

Topological surgery is a mathematical technique which creates new manifolds out of known ones. Given a manifold M, topological surgery describes a process which removes an embedding of $S^p \times D^q$ (a q-thickening of S^p) and glues back $D^{p+1} \times S^{q-1}$ (a (p+1)-thickening of S^{q-1}) along the common boundary $S^{p-1} \times S^{q-1}$. For instance, one type of 2-dimensional surgery opens two holes and adds a connecting tube between them. More precisely, the process starts by removing, from a 2-manifold M^2 , two discs $S^0 \times D^2$ which leave two holes bounded by two circles $S^0 \times S^1$, see Fig. 2.6(1). Then, it glues back a cylinder $D^1 \times S^1$ along the common boundary $S^0 \times S^1$, see Fig. 2.6(2). The effect of surgery has changed the initial manifold M^2 by first removing two unconnected discs $S^0 \times D^2$ and then connecting their boundaries via a tube $D^1 \times S^1$.

As we will see in Chaps. 5 and 10, the formal definition of topological surgery presented in next chapter provides a powerful mathematical tool for describing natural process exhibiting surgery.

For further reading on the above notions, introductory references include [1–4] while more technical references include [8–11].

References

- 1. Fuks, D.B., Rokhlin, V.A.: Beginner's course in topology. Geometric chapters. Translated from the Russian by A. Iacob. Series in Soviet Mathematics. Springer, Heidelberg (1984)
- 2. Gale, D.: The teaching of mathematics: the classification of 1-manifolds: a take-home exam. Amer. Math. Monthly **94**(2), 170–175 (1987)
- Kosniowski, C.: A First Course in Algebraic Topology. Cambridge University Press, Cambridge (1980). https://doi.org/10.1017/CBO9780511569296

- 4. Adams, C.: The knot book: an elementary introduction to the mathematical theory of knots. Am. Math, Soc (2004)
- 5. Perelman, G.: Finite extinction time for the solutions to the Ricci flow on certain three-manifolds (2002). https://arxiv.org/abs/math/0307245
- Perelman, G.: Ricci flow with surgery on three-manifolds (2003). https://arxiv.org/abs/math/ 0303109
- 7. Perelman, G.: The entropy formula for the Ricci flow and its geometric applications (2003). https://arxiv.org/abs/math/0211159
- 8. Ranicki, A.: Algebraic and Geometric Surgery. Clarendon Press, Oxford Mathematical Monographs (2002)
- Prasolov, V.V., Sossinsky, A.B.: Knots, Links, Braids and 3-Manifolds. AMS Translations of Mathematical Monographs, vol. 154 (1997)
- 10. Rolfsen, D.: Knots and Links. Publish or Perish Inc., AMS Chelsea Publishing (2003)
- 11. Saveliev N.: Lectures on the Topology of 3-Manifolds, 2nd edn. Walter de Gruyter (2012)

Chapter 3 The Formal Definition of Surgery



We recall the following well-known definition of surgery:

Definition 1 An *m-dimensional n-surgery* is the topological procedure of creating a new *m*-manifold M' out of a given *m*-manifold M by removing a framed *n*-embedding $h: S^n \times D^{m-n} \hookrightarrow M$, and replacing it with $D^{n+1} \times S^{m-n-1}$, using the 'gluing' homeomorphism h along the common boundary $S^n \times S^{m-n-1}$. Namely, and denoting surgery by χ :

$$M' = \chi(M) = \overline{M \setminus h(S^n \times D^{m-n})} \cup_{h|_{S^n \times S^{m-n-1}}} (D^{n+1} \times S^{m-n-1}).$$

The symbol ' χ ' of surgery comes from the Greek word ' $\chi \epsilon \iota \rho o \upsilon \rho \gamma \iota \kappa \dot{\eta}$ ' (cheirourgiki) whose term 'cheir' means hand. Note that from the definition, we must have $n+1 \leq m$. Also, the horizontal bar in the above formula indicates the topological closure of the set underneath.

Further, the *dual m-dimensional* (m-n-1)-surgery on M' removes a dual framed (m-n-1)-embedding $g: D^{n+1} \times S^{m-n-1} \hookrightarrow M'$ such that $g|_{S^n \times S^{m-n-1}} = h^{-1}|_{S^n \times S^{m-n-1}}$, and replaces it with $S^n \times D^{m-n}$, using the 'gluing' homeomorphism g (or h^{-1}) along the common boundary $S^n \times S^{m-n-1}$. That is:

$$M = \chi^{-1}(M') = \overline{M' \setminus g(D^{n+1} \times S^{m-n-1})} \cup_{h^{-1}|_{S^n \times S^{m-n-1}}} (S^n \times D^{m-n}).$$

The resulting manifold $\chi(M)$ may or may not be homeomorphic to M. From the above definition, it follows that $M = \chi^{-1}(\chi(M))$. Preliminary definitions behind the definition of surgery such as topological spaces, homeomorphisms, embeddings and other related notions are provided in Chap. 2. For further reading, excellent references on the subject are [1–4]. We shall now apply the above definition to dimensions 1 and 2.

3.1 1-Dimensional 0-Surgery

We only have one kind of surgery on a 1-manifold M, the 1-dimensional 0-surgery where m = 1 and n = 0:

$$M' = \chi(M) = \overline{M \setminus h(S^0 \times D^1)} \cup_{h|_{S^0 \times S^0}} (D^1 \times S^0).$$

The above definition means that two segments $S^0 \times D^1$ are removed from M and they are replaced by two different segments $D^1 \times S^0$ by reconnecting the four boundary points $S^0 \times S^0$ in a different way. In Figs. 3.1(a) and 3.2(a), $S^0 \times S^0 = \{1, 2, 3, 4\}$. As one possibility, if we start with $M = S^1$ and use as h the standard (identity) embedding denoted with h_s , we obtain two circles $S^1 \times S^0$. Namely, denoting by 1 the identity homeomorphism, we have $h_s : S^0 \times D^1 = D^1 \coprod D^1 \xrightarrow{1 \coprod 1} S^0 \times D^1 \hookrightarrow M$, see Fig. 3.1(a). However, we can also obtain one circle S^1 if h is an embedding h_t that reverses the orientation of one of the two arcs of $S^0 \times D^1$. Then in the substitution, joining endpoints 1–3 and 2–4, the two new arcs undergo a half-twist, see Fig. 3.2(a). More specifically, if we take $D^1 = [-1, +1]$ and define the homeomorphism $\omega : D^1 \to D^1$; $t \to -t$, the embedding used in Fig. 3.2(a) is $h_t : S^0 \times D^1 = D^1 \coprod D^1 \xrightarrow{1 \coprod 1} S^0 \times D^1 \hookrightarrow M$ which rotates one D^1 by 180°. The difference between the embeddings h_s and h_t of $S^0 \times D^1$ can be clearly seen by comparing the four boundary points 1, 2, 3 and 4 in Figs. 3.1(a) and 3.2(a).

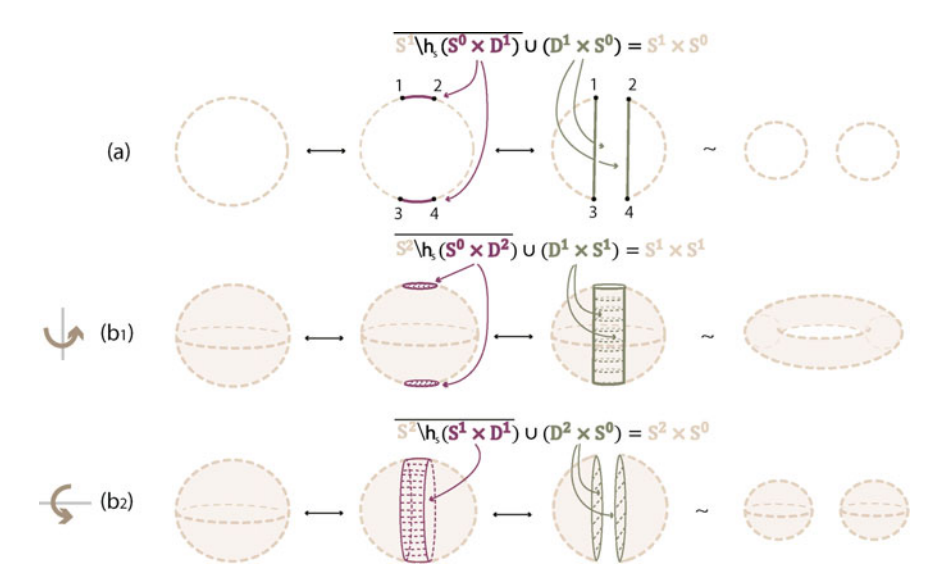


Fig. 3.1 Formal (a) 1-dimensional 0-surgery (b₁) 2-dimensional 0-surgery and (b₂) 2-dimensional 1-surgery using the standard embedding h_s

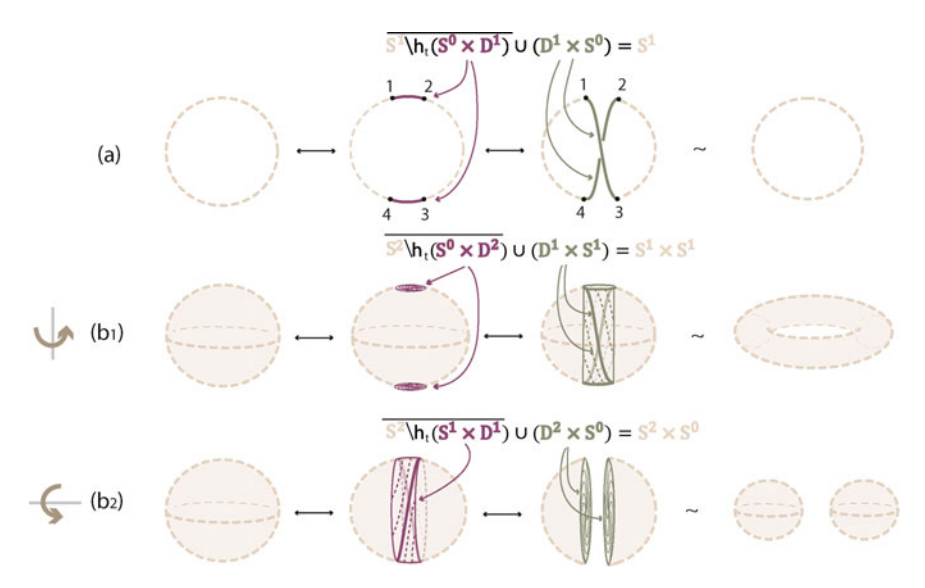


Fig. 3.2 Formal (a) 1-dimensional 0-surgery (b₁) 2-dimensional 0-surgery and (b₂) 2-dimensional 1-surgery using a twisting embedding h_t

Note that in dimension one, the dual case is also an 1-dimensional 0-surgery. For example, looking at the reverse process of Fig. 3.1(a), we start with two circles $M' = S^1 \coprod S^1$ and, if each segment of $D^1 \times S^0$ is embedded in a different circle, the result of the (dual) 1-dimensional 0-surgery is one circle: $\chi^{-1}(M') = M = S^1$.

3.2 2-Dimensional 0-Surgery

Starting with a 2-manifold M, there are two types of surgery. One type is the 2-dimensional 0-surgery, whereby two discs $S^0 \times D^2$ are removed from M and are replaced in the closure of the remaining manifold by a cylinder $D^1 \times S^1$, which gets attached via a homeomorphism along the common boundary $S^0 \times S^1$ comprising two copies of S^1 . The gluing homeomorphism of the common boundary may twist one or both copies of S^1 . For $M = S^2$ the above operation changes its homeomorphism type from the 2-sphere to that of the torus. View Fig. 3.1(b₁) for the standard embedding h_s and Fig. 3.2(b₁) for a twisting embedding h_t . For example, the homeomorphism $\mu: D^2 \to D^2$; $(t_1, t_2) \to (-t_1, -t_2)$ induces the 2-dimensional analogue h_t of the embedding defined in the previous example, namely: $h_t: S^0 \times D^2 = D^2 \coprod D^2 \xrightarrow{\coprod D^2} S^0 \times D^2 \hookrightarrow M$ which rotates one D^2 by 180°. When, now, the cylinder $D^1 \times S^1$ is glued along the common boundary $S^0 \times S^1$, the twisting of this boundary induces the twisting of the cylinder, see Fig. 3.2(b₁).

3.3 2-Dimensional 1-Surgery

The other possibility of 2-dimensional surgery on M is the 2-dimensional 1-surgery: here a cylinder (or annulus) $S^1 \times D^1$ is removed from M and is replaced in the closure of the remaining manifold by two discs $D^2 \times S^0$ attached along the common boundary $S^1 \times S^0$. For $M = S^2$ the result is two copies of S^2 , see Fig. 3.1(b₂) for the standard embedding h_s . Unlike Fig. 3.1(b₁) where the cylinder is illustrated vertically, in Fig. 3.1(b₂), the cylinder is illustrated horizontally. This choice was made so that the instances of 1-dimensional surgery can be obtained by crossections of the instances of both types of 2-dimensional surgeries, see further Remark 1. Figure 3.2(b₂) illustrates a twisting embedding h_t , where a twisted cylinder is being removed. In that case, taking $D^1 = \{h : h \in [-1, 1]\}$ and homeomorphism ζ :

$$\zeta: S^1 \times D^1 \to S^1 \times D^1;$$

$$\zeta: (t_1, t_2, h) \to (t_1 \cos \frac{(1-h)\pi}{2} - t_2 \sin \frac{(1-h)\pi}{2}, t_1 \sin \frac{(1-h)\pi}{2} + t_2 \cos \frac{(1-h)\pi}{2}, h)$$

the embedding h_t is defined as: $h_t: S^1 \times D^1 \xrightarrow{\zeta} S^1 \times D^1 \hookrightarrow M$. This operation corresponds to fixing the circle S^1 bounding the right side of the cylinder $S^1 \times D^1$, rotating the circle S^1 bounding the left side of the cylinder by 180° and letting the rotation propagate from left to right. This twisting of the cylinder can be seen by comparing the second instance of Fig. 3.1(b₂) with the second instance of Fig. 3.2(b₂), but also by comparing the third instance of Fig. 3.1(b₁) with the third instance of Fig. 3.2(b₁).

It follows from Definition 1 that a dual 2-dimensional 0-surgery is a 2-dimensional 1-surgery and vice versa. Hence, Fig. $3.1(b_1)$ shows that a 2-dimensional 0-surgery on a sphere is the reverse process of a 2-dimensional 1-surgery on a torus. Similarly, as illustrated in Fig. $3.1(b_2)$, a 2-dimensional 1-surgery on a sphere is the reverse process of a 2-dimensional 0-surgery on two spheres. In the figure the symbol \longleftrightarrow depicts surgeries from left to right and their corresponding dual surgeries from right to left.

Remark 1 The stages of the process of 2-dimensional 0-surgery on S^2 can be obtained by rotating the stages of 1-dimensional 0-surgeries on S^1 by 180° around a vertical axis, see Fig. 3.1(b₁). Similarly, the stages of 2-dimensional 1-surgery on S^2 can be obtained by rotating the stages of 1-dimensional 0-surgeries on S^1 by 180° around a horizontal axis, see Fig. 3.1(b₂). It follows from the above that 1-dimensional 0-surgery can be obtained as a cross-section of either type of 2-dimensional surgery.

3.4 3-Dimensional 0- and 1-Surgery

Starting with a 3-manifold M, there are three types of 3-dimensional surgeries. For m=3 and n=0, we have the 3-dimensional 0-surgery whereby two 3-balls $S^0 \times D^3$ are removed from M and are replaced in the closure of the remaining manifold by $D^1 \times S^2$:

$$\chi(M) = \overline{M \setminus h(S^0 \times D^3)} \cup_h (D^1 \times S^2)$$

Next, for m=3 and n=2, we have the 3-dimensional 2-surgery but we will not analyze this type of surgery as it is the reverse process of 3-dimensional 0-surgery. Finally, for m=3 and n=1, we have the 3-dimensional 1-surgery whereby a solid torus $S^1 \times D^2$ is removed from M and is replaced by another solid torus $D^2 \times S^1$:

$$\chi(M) = \overline{M \setminus h(S^1 \times D^2)} \cup_h (D^2 \times S^1)$$

Both processes will be analyzed and visualized in Chap. 10.

References

- Ranicki, A.: Algebraic and Geometric Surgery. Oxford Mathematical Monographs. Clarendon Press, Oxford (2002)
- Prasolov, V.V., Sossinsky, A.B.: Knots, links, braids and 3-manifolds. AMS Transl. Math. Monogr. 154 (1997)
- 3. Rolfsen, D.: Knots and Links. Publish or Perish Inc., AMS Chelsea Publishing (2003)
- 4. Saveliev, N.: Lectures on the Topology of 3-Manifolds, 2nd edn. Walter de Gruyter (2012)

Chapter 4 Continuity



As we will see in the following chapter, topological surgery happens in nature as a continuous process caused by local forces. However, the formal definition of surgery presented in Definition 1 gives only a static description of the initial and the final stage. In this section we define the continuous process of m-dimensional n-surgery as an extension of Definition 1. This new definition, enhanced with the observed dynamics, will become a topological model for natural phenomena exhibiting 1- and 2-dimensional surgery in Chap. 5 and for 3-dimensional surgery in Chap. 10.

4.1 The Continuous Definition of Surgery

Let us first notice that if we glue together the two m-manifolds involved in the process of m-dimensional n-surgery along their common boundary we obtain the m-sphere. Namely, from Definition 1 and using property (\star) discussed in Sect. 2.4.6, we can see that $(S^n \times D^{m-n}) \cup_h (D^{n+1} \times S^{m-n-1}) = (\partial D^{n+1} \times D^{m-n}) \cup_h (D^{n+1} \times \partial D^{m-n}) = \partial (D^{n+1} \times D^{m-n}) \cong \partial (D^{m+1}) = S^m$. This means that an m-dimensional n-surgery on an m-manifold M can be viewed as the process of cutting out a boundary component of $D^{n+1} \times D^{m-n}$ from M and gluing back the complement boundary component of $D^{n+1} \times D^{m-n}$ to the resulting manifold. Hence, a continuous analogue of Definition 1 is the following:

Definition 2 Given an m-manifold M and an embedding $h: S^n \times D^{m-n} \hookrightarrow M$, we consider the handle $D^{n+1} \times D^{m-n}$ which is bounded by $\partial(D^{n+1} \times D^{m-n}) = (S^n \times D^{m-n}) \cup_h (D^{n+1} \times S^{m-n-1})$. An m-dimensional n-surgery on a m-manifold M is the local process of continuously passing, within $D^{n+1} \times D^{m-n}$, from boundary component $(S^n \times D^{m-n}) \subset \partial(D^{n+1} \times D^{m-n})$ to its complement $(D^{n+1} \times S^{m-n-1}) \subset \partial(D^{n+1} \times D^{m-n})$, by going through the unique intersection point $D^{n+1} \cap D^{m-n}$. We will refer to this point as the *singular point*. Note that each 'slice' of the process is an

22 4 Continuity

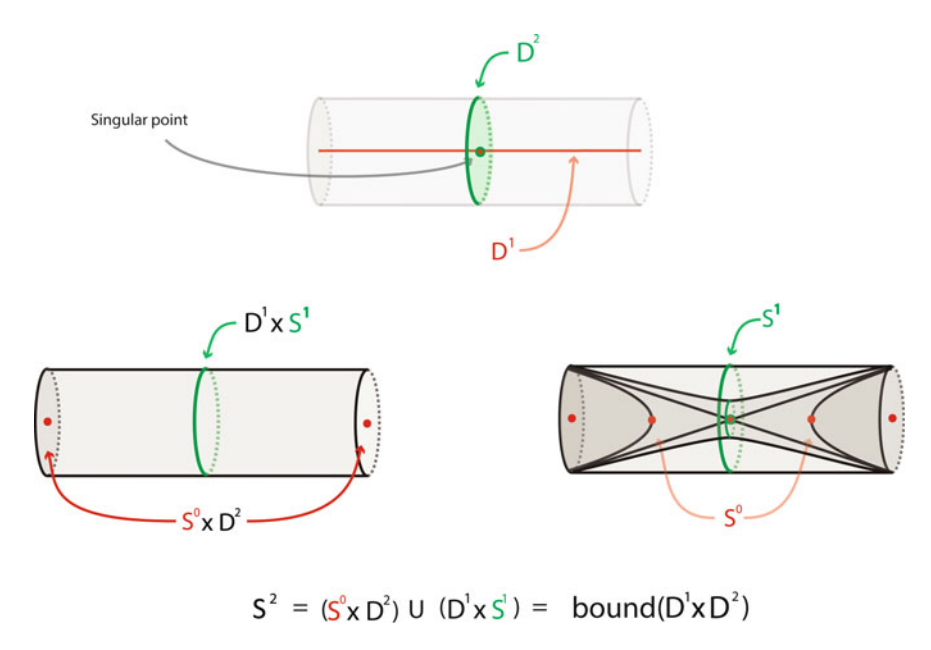


Fig. 4.1 Continuous 2-dimensional 0-surgery

m-dimensional manifold but the whole time evolution of the process requires m+1 dimensions in order to be visualized, as the whole process occurs inside the handle $D^{n+1} \times D^{m-n} \cong D^{m+1}$.

Given that the first boundary component $S^n \times D^{m-n}$ of $D^{n+1} \times D^{m-n}$ is a thickening of the core S^n and the second boundary component $D^{n+1} \times S^{m-n-1}$ is a thickening of the core S^{m-n-1} , both components can be seen as thickenings (or framings) of the cores (or spheres) to dimension m. Hence, the surgery process can be viewed locally as starting with the boundary $S^n = \partial D^{n+1}$ and considering it as the core of thickening $S^n \times D^{m-n}$. We then collapse the core S^n to the singular point from which the thickened S^{m-n-1} emerges, which is also the boundary $S^{m-n-1} = \partial D^{m-n}$. Note that these intermediate steps can also be explained through Morse theory. See Remark 2 for details.

4.2 Continuous 2-Dimensional 0-Surgery

For example, for m=2 and n=0 we have the case of 2-dimensional 0-surgery, where the boundary component $D^1 \times S^1$ is a cylinder with its two ends closed by the other boundary component $S^0 \times D^2$. The result is homeomorphic to the 2-sphere: $(S^0 \times D^2) \cup_h (D^1 \times S^1) = S^2$, see the left illustration of Fig. 4.1. The way of continuously passing from $(S^0 \times D^2)$ to $(D^1 \times S^1)$ is shown in the right illustration

of Fig. 4.1, where we see how the core S^0 of $S^0 \times D^2$ (in red) collapses to the unique intersection point (in red/green) from which the core S^1 of $D^1 \times S^1$ emerges (in green). The whole process happens inside the handle $D^1 \times D^2$, see also Fig. 4.1. This process together with continuous 1-dimensional surgery will be elaborated in much more details in the next chapter where dynamics are also introduced.

Chapter 5 **Dynamics**



In this chapter we present natural processes exhibiting topological surgery in dimensions 1 and 2 and we incorporate the observed dynamics to Definition 2, thus creating a model which extends surgery to a continuous process caused by local forces. Further, for each dimension, we go back to the phenomena and pin down the forces introduced by our models.

5.1 Dynamic 1-Dimensional Topological Surgery

We find that 1-dimensional 0-surgery is present in phenomena where 1-dimensional splicing and reconnection occurs. It can be seen for example during meiosis when new combinations of genes are produced, see Fig. 5.1(3), during magnetic reconnection, the phenomena whereby cosmic magnetic field lines from different magnetic domains are spliced to one another, changing their pattern of conductivity with respect to the sources, see Fig. 5.1(2) from [1] and in site-specific DNA recombination (see Fig. 9.1) whereby nature alters the genetic code of an organism, either by moving a block of DNA to another position on the molecule or by integrating a block of alien DNA into a host genome (see [2]). It is worth mentioning that 1-dimensional 0-surgery is also present during the reconnection of vortex tubes in a viscous fluid and quantized vortex tubes in superfluid helium. As mentioned in [3], these cases have some common qualitative features with the magnetic reconnection shown in Fig. 5.1(2).

Since all the above phenomena follow a dynamic process, in Fig. 5.1(1), we introduce dynamics to Definition 2 which shows how the intermediate steps of surgery are caused by local forces. The process starts with the two points (in red) specified on any 1-dimensional manifold, on which attracting forces are applied (in blue). We assume that these forces are caused by an attracting center (also in blue). Then, the two segments $S^0 \times D^1$, which are neighborhoods of the two points, get close

26 5 Dynamics

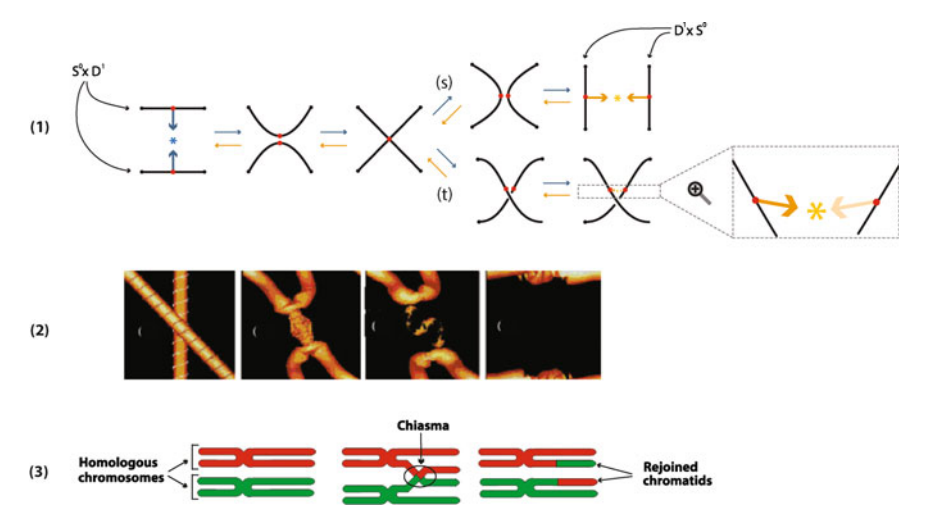


Fig. 5.1 (1) Dynamic 1-dimensional surgery locally (2) The reconnection of cosmic magnetic lines (3) Crossing over of chromosomes during meiosis

to one another. When the specified points (or centers) of the two segments reach the attracting center they touch and recoupling takes place, giving rise to the two final segments $D^1 \times S^0$, which split apart. In Fig. 5.1(1), case (s) corresponds to the identity embedding h_s described in Sect. 3.1, while (t) corresponds to the twisting embedding h_t described in Sect. 3.1.

As also mentioned in Sect. 3.1, the dual case is also a 1-dimensional 0-surgery, as it removes segments $D^1 \times S^0$ and replaces them by segments $S^0 \times D^1$. This is the reverse process which starts from the end and is illustrated in Fig. 5.1(1) as a result of the orange forces and attracting center which are applied on the 'complementary' points.

Note that these local dynamics produce different manifolds depending on where the initial neighborhoods are embedded. Taking the known case of the standard embedding h_s and $M = S^1$, we obtain $S^1 \times S^0$, see Fig. 5.2(a). Furthermore, as shown in Fig. 5.2(b), we also obtain $S^1 \times S^0$ even if the attracting center is outside S^1 . Note that these outcomes are not different than the ones shown in formal surgery (recall Fig. 3.1(a)) but we can now see the intermediate instances as a result of forces.

Remark 2 It is worth mentioning that the intermediate steps of surgery presented in Fig. 5.1(1) can also be viewed in the context of Morse theory [4]. By using the local form of a Morse function, we can visualize the process of surgery by varying parameter t of equation $x^2 - y^2 = t$. For t = -1 it is the hyperbola shown in the second stage of Fig. 5.1(1) where the two segments get close to one another. For t = 0 it is the two straight lines where the reconnection takes place as shown in the third stage of Fig. 5.1(1) while for t = 1 it represents the hyperbola of the two final segments shown in case (s) of the fourth stage of Fig. 5.1(1). This sequence can be generalized for higher dimensional surgeries as well. For example, for 2-dimensional

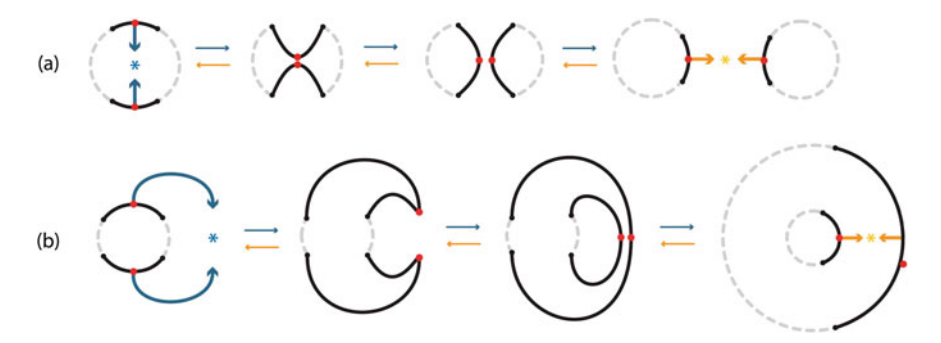


Fig. 5.2 1-dimensional surgery on one and two circles

surgery, we can visualize the process by varying parameter t of equation $x^2 + y^2 - z^2 = t$. We mention this approach because it gives us an algebraic formulation of surgery's time evolution. However, in this analysis we will not use it as we are focusing on the introduction of forces and the attracting center.

5.2 Modeling Phenomena Exhibiting 1-Dimensional Surgery

The aforementioned phenomena are all 1-dimensional in the sense that they involve happening 1-dimensional manifold. We will take a closer look at them and show that the described dynamics and attracting forces introduced by our model are present in all cases. Namely, **magnetic reconnection** (Fig. 5.1(2)) corresponds to a dual 1-dimensional 0-surgery (see case (t) of Fig. 5.1(1)) where $g: D^1 \times S^0 \hookrightarrow M'$ is a dual embedding of the twisting homeomorphism h_t defined in Sect. 3.1. The tubes are viewed as segments and correspond to an initial manifold $M = S^0 \times D^1$ (or $M = S^1$ if they are connected) on which the local dynamics act on two smaller segments $S^0 \times D^1$. Namely, the two magnetic flux tubes have a nonzero parallel net current through them, which leads to attraction of the tubes (cf. [5]). Between them, a localized diffusion region develops where magnetic field lines may decouple. Reconnection is accompanied with a sudden release of energy and the magnetic field lines break and rejoin in a lower energy state.

In the case of chromosomal crossover during **meiosis** (Fig. 5.1(3)), we have the same dual 1-dimensional 0-surgery as magnetic reconnection (see case (t) of Fig. 5.1(1)). During this process, the homologous (maternal and paternal) chromosomes come together and pair, or synapse, during prophase. The pairing is remarkably precise and is caused by mutual attraction of the parts of the chromosomes that are similar or homologous. Further, each paired chromosomes divide into two chromatids. The point where two homologous non-sister chromatids touch and exchange genetic material is called chiasma. At each chiasma, two of the chromatids have

28 5 Dynamics

become broken and then rejoined (cf. [6]). In this process, we consider the initial manifold to be one chromatid from each chromosome, hence the initial manifold is $M = S^0 \times D^1$ on which the local dynamics act on two smaller segments $S^0 \times D^1$.

For **site-specific DNA recombination** (see Fig. 9.1), we have a 1-dimensional 0-surgery (see case (t) of Fig. 5.1(1)). Here the initial manifold is a knot which is an embedding of $M = S^1$ in 3-space but this will be detailed in Sect. 9.1. As mentioned in [7], enzymes break and rejoin the DNA strands, hence in this case the seeming attraction of the two specified points is realized by the enzyme. Note that, while both are genetic recombinations, there is a difference between chromosomal crossover and site-specific DNA recombination. Namely, chromosomal crossover involves the homologous recombination between two similar or identical molecules of DNA and we view the process at the chromosome level regardless of the knotting of DNA molecules.

Finally, **vortices reconnect** following the steps of 1-dimensional 0-surgery with a standard embedding shown in (see case (s) of Fig. 5.1(1)). The initial manifold is again $M = S^0 \times D^1$. As mentioned in [8], the interaction of the anti-parallel vortices goes from attraction before reconnection, to repulsion after reconnection.

5.3 Dynamic 2-Dimensional Topological Surgery

Both types of 2-dimensional surgeries are present in nature, in various scales, in phenomena where 2-dimensional merging and recoupling occurs. For example, 2-dimensional 0-surgery can be seen during the formation of tornadoes, see Fig. 5.3(2) (this phenomenon will be detailed in Sect. 9.3.2). Further, it can be seen in the formation of Falaco solitons, see Fig. 5.3(3) (note that each Falaco soliton consists of a pair of locally unstable but globally stabilized contra-rotating identations in the water-air discontinuity surface of a swimming pool, see [9] for details). It can also be seen in gene transfer in bacteria where the donor cell produces a connecting tube called a 'pilus' which attaches to the recipient cell, see Fig. 5.3(4); in drop coalescence, the phenomenon where two dispersed drops merge into one, and in the formation of black holes (this phenomena will be discussed in Sect. 9.3.1), see Fig. 9.2(2) (Source: www.black-holes.org).

On the other hand, 2-dimensional 1-surgery can be seen during soap bubble splitting, where a soap bubble splits into two smaller bubbles, see Fig. 5.3(5) (Source: soapbubble.dk); when the tension applied on metal specimens by tensile forces results in the phenomena of necking and then fracture, see Fig. 5.3(6) and in the biological process of mitosis, where a cell splits into two new cells, see Fig. 5.3(7).

Phenomena exhibiting 2-dimensional 0-surgery are the results of *two colinear attracting forces which 'create' a cylinder*. These phenomena have similar dynamics and are characterized by their continuity and the attracting forces causing them. In order to model them topologically and understand 2-dimensional surgery through continuity and dynamics we introduce the model of Fig. 5.3(1) which shows the instances of dynamic 2-dimensional 0-surgery from left to right.

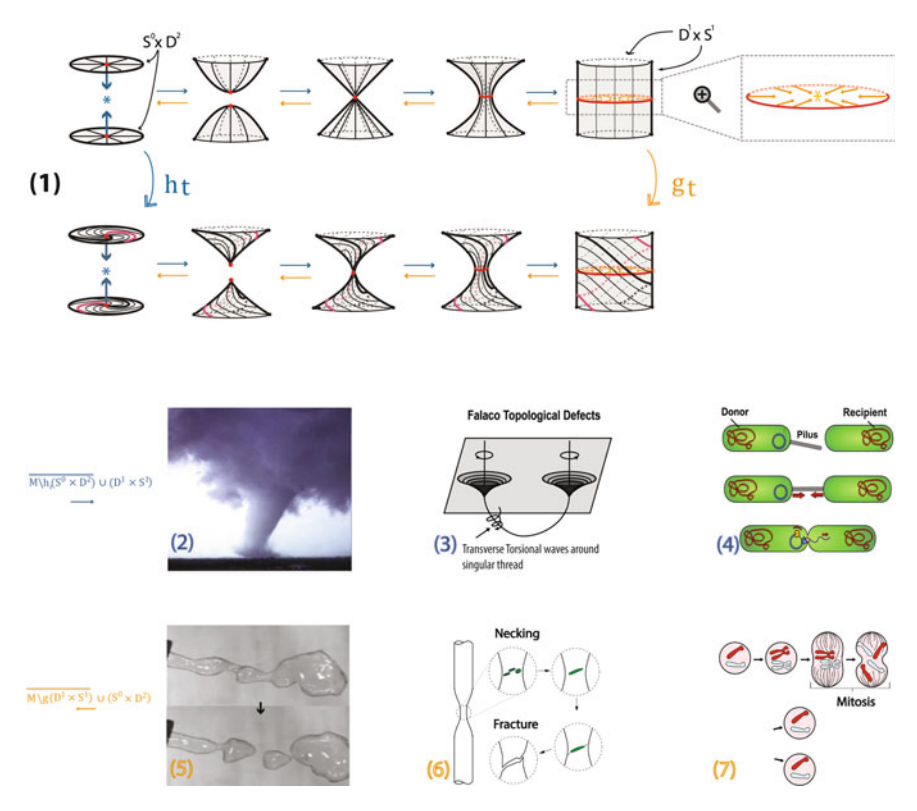


Fig. 5.3 (1) Dynamic 2-dimensional surgery locally (2) Tornadoes (3) Falaco solitons (4) Gene transfer in bacteria (5) Soap bubble splitting (6) Fracture (7) Mitosis

In Fig. 5.3(1), below the instances of the standard embedding, we also show the instances of these processes when a non-trivial embedding are used (recall Sect. 3.2). Note that these embeddings are more appropriate for natural processes involving twisting, such as tornadoes and Falaco solitons. In this example of *twisted 2-dimensional 0-surgery*, the two discs $S^0 \times D^2$ are embedded via a twisted homemorphism h_t while, in the dual case, the cylinder $D^1 \times S^1$ is embedded via a twisted homemorphism g_t . Here h_t rotates the two initial discs in opposite directions by an angle of $3\pi/4$ and we can see how this rotation induces the twisting of angle $3\pi/2$ of the final cylinder (which corresponds to homemorphism g_t rotating the top and bottom of the cylinder by $3\pi/4$ and $-3\pi/4$ respectively). More specifically, if we define the homeomorphism $\omega_1, \omega_2: D^2 \to D^2$ to be rotations by $3\pi/4$ and $-3\pi/4$ respectively, then h_t is defined as the composition $h_t: S^0 \times D^2 \xrightarrow{\omega_1 \coprod \omega_2} S^0 \times D^2 \xrightarrow{h} M$. The homeomorphism $g_t: D^1 \times S^1 \to M$ is defined analogously.

The process of *dynamic 2-dimensional 0-surgery* starts with two points, or poles, specified on the manifold (in red) on which attracting forces caused by an attracting center are applied (in blue). Then, the two discs $S^0 \times D^2$, neighbourhoods of the two

30 5 Dynamics

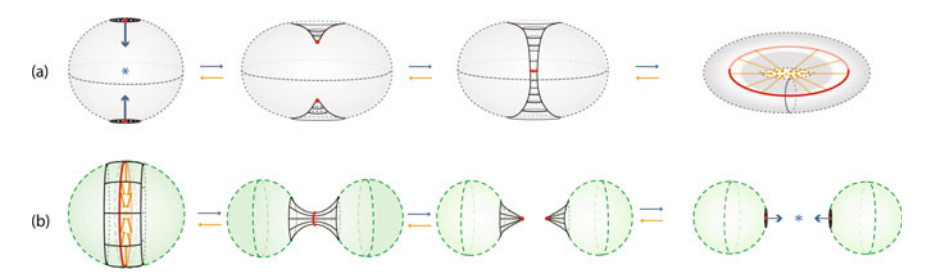


Fig. 5.4 (a) 2-dimensional 0-surgery on $M=S^2$ and 2-dimensional 1-surgery on $M'=S^0\times S^2$ (b) 2-dimensional 1-surgery on $M=S^2$ and 2-dimensional 0-surgery on $M'=S^0\times S^2$

poles, approach each other. When the centers of the two discs touch, recoupling takes place and the discs get transformed into the final cylinder $D^1 \times S^1$, see Fig. 5.3(1). The cylinder created during 2-dimensional 0-surgery can take various forms. For example, it is a tubular vortex of air in the case of tornadoes, a transverse torsional wave in the case of Falaco solitons and a pilus joining the genes in gene transfer in bacteria.

On the other hand, phenomena exhibiting 2-dimensional 1-surgery are the result of an infinitum of coplanar attracting forces which 'collapse' a cylinder, see Fig. 5.3(1) from the end. As mentioned in Sect. 3.3, the dual case of 2-dimensional 0-surgery is the 2-dimensional 1-surgery and vice versa. This is illustrated in Fig. 5.3(1) where the reverse process is the 2-dimensional 1-surgery which starts with the cylinder and a specified circular region (in red) on which attracting forces caused by an attracting center are applied (in orange). A 'necking' occurs in the middle which degenerates into a point and finally tears apart creating two discs $S^0 \times D^2$. This cylinder can be embedded, for example, in the region of the bubble's surface where splitting occurs, on the region of metal specimens where necking and fracture occurs or on the equator of the cell which is about to undergo a mitotic process.

In Fig. 5.4(a) and (b), we apply the local dynamics of Fig. 5.3(1) to the initial manifold $M = S^2$ and produce the same manifolds seen in formal 2-dimensional surgery (recall Fig. 3.1(b₁), (b₂) through a continuous process resulting of forces. Note that, as also seen in 1-dimensional surgery (Fig. 5.2(b)), if the blue attracting center in Fig. 5.4(a) was outside the sphere and the cylinder was attached on S^2 externally, the result would still be a torus.

Finally, it is worth pointing out that these local dynamics produce different manifolds depending on the initial manifold where they act. Taking examples from natural phenomena, 2-dimensional 0-surgery transforms an $M = S^0 \times S^2$ to an S^2 by adding a cylinder during gene transfer in bacteria (see Fig. 5.3(4)) but can also transform an $M = S^2$ to a torus by 'drilling out' a cylinder during the formation of Falaco solitons (see Fig. 5.3(3)) in which case S^2 is the pool of water and the cylinder is the boundary of the tubular neighborhood around the thread joining the two poles.

Remark 3 Note that Remark 1 is also true here. One can obtain Fig. 5.3(1) by rotating Fig. 5.1(1) and this extends also to the dynamics and forces. For instance, by rotating

the two points, or S^0 , on which the pair of forces of 1-dimensional 0-surgery acts (shown in red in the last instance of Fig. 5.1(1)) by 180° around a vertical axis we get the circle, or S^1 , on which the infinitum of coplanar attracting forces of 2-dimensional 1-surgery acts (shown in red in the last instance of Fig. 5.3(1)).

5.4 Modeling Phenomena Exhibiting 2-Dimensional Surgery

Looking back at the natural phenomema happening on surfaces, an example is **soap bubble splitting** during which a soap bubble splits into two smaller bubbles. This process is the 2-dimensional 1-surgery on $M = S^2$ shown in Fig. 5.4(b). The orange attracting force in this case is the surface tension of each bubble that pulls molecules into the tightest possible groupings.

If one looks closer at the other phenomena exhibiting 2-dimensional surgery shown in Fig. 5.3, one can see that these phenomena do not happen on surfaces but on 3-dimensional manifolds, therefore we can't model them as 2-dimensional surgeries. As we will see in Chap. 6, these processes are described by the notion of solid surgery. Therefore they will be analyzed after the introduction of this notion. For instance, gene transfer in bacteria, drop coalescence and the formation of Falaco solitons are discussed in Sect. 6.3 while mitosis and fracture will be discussed in Sect. 6.4.

Moreover, as we will see in Chap. 9, the ambient space is also involved in the process of tornado formation, see Fig. 5.3(2). Therefore it will analyzed in Sect. 9.3.2, after the introduction of the notion of embedded surgery.

5.5 A Model for Dynamic *m*-Dimensional *n*-Surgery

As mentioned in Sect. 4.1, surgery can be viewed as collapsing the thickened core S^n to a singular point and then uncollapsing the thickened core S^{m-n-1} . As seen in Fig. 5.3(1), in the case of 2-dimensional 0-surgery, forces (in blue) are applied to core S^0 , whose thickening comprises the two discs, while in the case of the 2-dimensional 1-surgery, forces (in orange) are applied on the core S^1 , whose thickening is the cylinder. In other words, the forces that model 2-dimensional n-surgery are always applied to the core n-embedding $e = h_1 : S^n = S^n \times \{0\} \hookrightarrow M$ of the framed n-embedding $h : S^n \times D^{2-n} \hookrightarrow M$.

This observation can be generalized as follows: The process followed by natural phenomena exhibiting topological surgery is modeled by Definition 2 enhanced with attracting forces acting on the cores S^n and S^{m-n-1} of embeddings $S^n \times D^{m-n}$ and $D^{n+1} \times S^{m-n-1}$. Moreover, we view this continuous passage as a result of forces towards the attracting center, which is identified with the singular point.

32 5 Dynamics

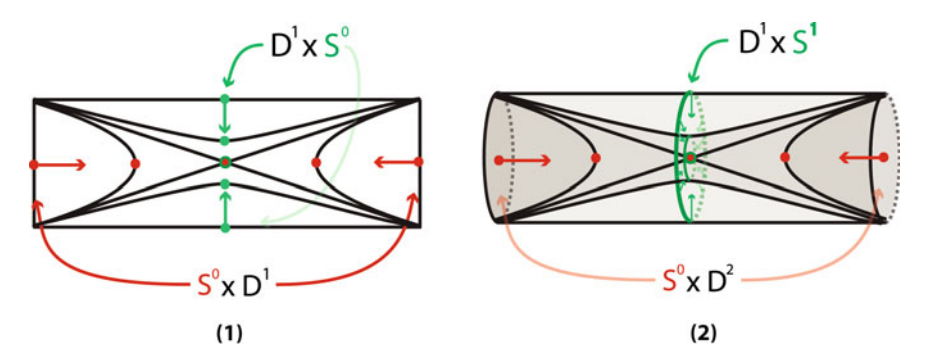


Fig. 5.5 (1) Model for dynamic 1-dimensional 0-surgery (2) Model for dynamic 2-dimensional 0-surgery

The above are shown in Fig. 5.5(1) and (2) for dimensions 1 and 2 respectively. This figure completes Fig. 4.1 with the observed dynamics.

References

- Dahlburg, R.B., Antiochos, S.K.: Reconnection of antiparallel magnetic flux tubes. J. Geophys. Res. 100(A9), 16991–16998 (1995). https://doi.org/10.1029/95JA01613
- Sumners, D.: Lifting the curtain: using topology to probe the hidden action of enzymes. Not Am. Math. Soc. 42(5):528–537 (1995). http://www.ams.org/notices/199505/sumners.pdf
- Laing, C.E., Ricca, R.L., Sumners, D.: Conservation of writhe helicity under anti-parallel reconnection. Sci. Rep. 5, 9224 (2014). https://doi.org/10.1038/srep09224
- 4. Milnor, J.: Morse Theory. Princeton University Press (1963)
- Kondrashov, D., Feynman, J., Liewer, P.C., Ruzmaikin, A.: Three-dimensional magnetohydrodynamic simulations of the interaction of magnetic flux tubes. Astrophys. J. 519, 884–898 (1999). https://doi.org/10.1086/307383
- Pujari, S.: Useful notes on the mechanism of crossing over. Your article library (2015). http://www.yourarticlelibrary.com/biology/useful-notes-on-the-mechanism-of-crossing-over-biology-810-words/6634/
- Johnson, A.B., Lewis, J., et al.: Molecular Biology of the Cell. Garland Science (2002). http://www.ncbi.nlm.nih.gov/books/NBK26845/
- Kerr, R.M.: Fully developed hydrodynamic turbulence from a chain reaction of reconnection events. Procedia IUTAM 9: 57–68 (2013). https://doi.org/10.1016/j.piutam.2013.09.006. http:// www.sciencedirect.com/science/article/pii/S2210983813001284
- Kiehn, R.M.: Non-equilibrium Systems and Irreversible Processes

 –Adventures in Applied Topology. Non-equilibrium thermodynamics, vol. 1, pp. 147

 –150. University of Houston Copyright CSDC Inc. (2013)

Chapter 6 Solid Surgery



Looking closer at the phenomena exhibiting 2-dimensional surgery shown in Fig. 5.3, one can see that, with the exception of soap bubble splitting that involves surfaces, all others involve 3-dimensional manifolds. For instance, what really happens during a mitotic process is that a solid cylindrical region located in the center of the cell collapses and a D^3 is transformed into an $S^0 \times D^3$. Similarly, during tornado formation, the created cylinder is not just a cylindrical surface $D^1 \times S^1$ but a solid cylinder $D^2 \times S^1$ containing many layers of air (this phenomena will be detailed in Sect. 9.3.2). Of course we can say that, for phenomena involving 3-dimensional manifolds, the outer layer of the initial manifold is undergoing 2-dimensional surgery. In this chapter we will define topologically what happens to the whole manifold.

The need of such a definition is also present in dimension 1 for modeling phenomena such as the merging of oil slicks and tension on membranes (or soap films). These phenomena undergo the process of 1-dimensional 0-surgery but happen on surfaces instead of 1-manifolds.

We will now introduce the notion of solid surgery (in both dimensions 1 and 2) where the interior of the initial manifold is filled in. There is one key difference compared to the dynamic surgeries discussed in the previous chapter. While the local dynamics described in Figs. 5.1 and 5.3 can be embedded in any manifold, here we also have to fix the initial manifold in order to define solid surgery. For example, as we will see next, we define separately the processes of solid 1-dimensional 0-surgery on D^2 and solid 1-dimensional 0-surgery on $D^2 \times S^0$. However, the underlying features are common in both.

34 6 Solid Surgery

6.1 Solid 1-Dimensional Topological Surgery

Solid 1-dimensional 0-surgery on the 2-disc D^2 is the topological procedure whereby a ribbon $D^1 \times D^1$ is being removed, such that the closure of the remaining manifold comprises two discs $D^2 \times S^0$. The reader is referred to Fig. 3.1(a) where the interior is now supposed to be filled in. This process is equivalent to performing 1-dimensional 0-surgeries on the whole continuum of concentric circles included in D^2 , see Fig. 6.1. More precisely, and introducing at the same time dynamics, we define:

Definition 3 Solid 1-dimensional 0-surgery on D^2 is the following process. We start with the 2-disc of radius 1 with polar layering:

$$D^2 = \bigcup_{0 < r < 1} S_r^1 \cup \{P\},\,$$

where r the radius of a circle and P the limit point of the circles, which is the center of the disc and also the circle of radius zero. We specify colinear pairs of antipodal points, all on the same diameter, with neighbourhoods of analogous lengths, on which the same colinear attracting forces act. See Fig. 6.1(1) where these forces and the attracting center are shown in blue. Then, in (2), the antipodal segments get closer to one another or, equivalently, closer to the attracting center. Note that here, the attracting center coincides with the limit point of all concentric circles, which is shown in green from instance (2) and on. Then, as shown from (3) to (9), we perform 1-dimensional 0-surgery on the whole continuum of concentric circles. The natural order of surgeries is as follows: first, the center of the segments that are closer to the center of attraction touch, see (4). After all other points have also reached the center, see (5), decoupling starts from the central or limit point. We define 1-dimensional 0-surgery on the limit point P to be the two limit points of the resulting surgeries. That is, the effect of solid 1-dimensional 0-surgery on a point is the creation of two new points, see (6). Next, the other segments reconnect, from the inner, see (7), to the outer ones, see (8), until we have two copies of D^2 , see (9) and (10). The proposed order of reconnection, from inner to outer, is the same as the one followed by skin healing, namely, the regeneration of the epidermis starts with the deepest part and then migrates upwards.

The above process is the same as first removing the center P from D^2 , doing the 1-dimensional 0-surgeries and then taking the closure of the resulting space. The resulting manifold is

$$\chi(D^2) := \bigcup_{0 < r \le 1} \chi(S_r^1) \cup \chi(P),$$

which comprises two copies of D^2 .

We also have the reverse process of the above, namely, solid 1-dimensional 0-surgery on two discs $D^2 \times S^0$ is the topological procedure whereby a ribbon $D^1 \times D^1$ joining the discs is added, such that the closure of the remaining manifold comprise one disc D^2 . This process is the result of the orange forces and attracting center which are applied on the 'complementary' points, see Fig. 6.1 in reverse order. This operation is equivalent to performing 1-dimensional 0-surgery on the whole

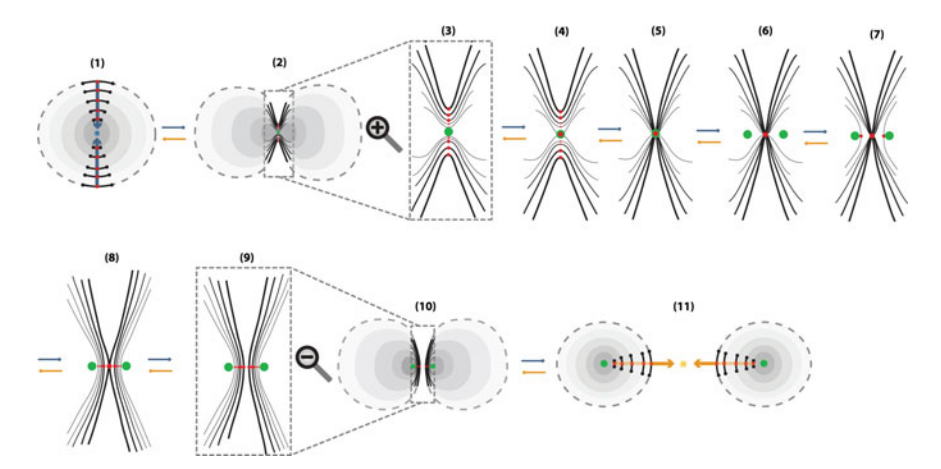


Fig. 6.1 Solid 1-dimensional surgery

continuum of pairs of concentric circles in D^2 \coprod D^2 . We only need to define solid 1-dimensional 0-surgery on two limit points to be the limit point P of the resulting surgeries. That is, the effect of *solid 1-dimensional 0-surgery on two points is their merging into one point*. The above process is the same as first removing the centers from the $D^2 \times S^0$, doing the 1-dimensional 0-surgeries and then taking the closure of the resulting space. The resulting manifold is

$$\chi^{-1}(D^2 \times S^0) := \bigcup_{0 < r < 1} \chi^{-1}(S_r^1 \times S^0) \cup \chi^{-1}(P \times S^0),$$

which comprises one copy of D^2 .

6.2 Solid 2-Dimensional Topological Surgery

Moving up one dimension, there are two types of solid 2-dimensional surgery on the 3-ball, D^3 , analogous to the two types of 2-dimensional surgery. Both are shown in Fig. 6.2(b₁) and (b₂) in relation with solid 1-dimensional surgery, see Fig. 6.2(a). The first one is the *solid 2-dimensional 0-surgery* which is the topological procedure of removing a solid cylinder homeomorphic to the product set $D^1 \times D^2$, $h(D^1 \times D^2)$ (such that the part $S^0 \times D^2$ of its boundary lies in the boundary of D^3) and taking the closure of the remaining manifold $D^3 \setminus h(D^1 \times D^2)$, which is a regular (or twisted) solid torus. See Fig. 3.1(b₁) where the interior is supposed to be filled in. The second type is the *solid 2-dimensional 1-surgery* which is the topological procedure of removing a solid cylinder homeomorphic to the product set $D^2 \times D^1$, $h(D^2 \times D^1)$, (such that the part $S^1 \times D^1$ of its boundary lies in the boundary of D^3) and taking the closure of the remaining manifold $D^3 \setminus h(D^2 \times D^1)$, which is two copies of

36 6 Solid Surgery

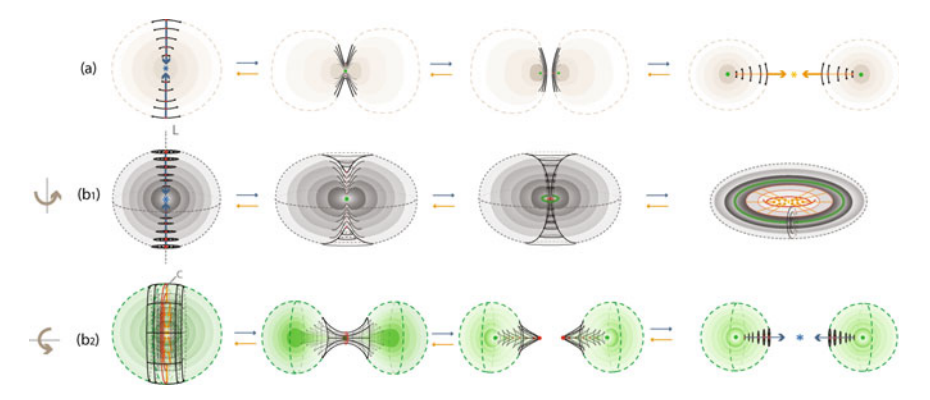


Fig. 6.2 (a) Solid 1-dimensional 0-surgery on D^2 (b₁) Solid 2-dimensional 0-surgery on D^3 (b₂) Solid 2-dimensional 1-surgery on D^3

 D^3 . See Fig 3.1(b₂) where the interior is supposed to be filled in. Those processes are equivalent to performing 2-dimensional surgeries on the whole continuum of concentric spheres included in D^3 . More precisely we have:

Definition 4 We start with the 3-ball of radius 1 with polar layering:

$$D^3 = \bigcup_{0 < r \le 1} S_r^2 \cup \{P\},\,$$

where r the radius of the 2-sphere S_r^2 and P the limit point of the spheres, that is, their common center and the center of the ball. *Solid 2-dimensional 0-surgery on D*³ is the topological procedure whereby 2-dimensional 0-surgery takes place on each spherical layer that D^3 is made of. More precisely, as illustrated in Fig. 6.2(b₁), on all spheres S_r^2 colinear pairs of antipodal points are specified, all on the same diameter, on which the same colinear attracting forces act. The poles have disc neighborhoods of analogous areas. Then, 2-dimensional 0-surgeries are performed on the whole continuum of the concentric spheres using the same embedding h (recall Sect. 3.2). Moreover, 2-dimensional 0-surgery on the limit point P is defined to be the limit circle of the nested tori resulting from the continuum of 2-dimensional 0-surgeries. That is, the effect of 2-dimensional 0-surgery on a point is defined to be the creation of a circle.

The process is characterized on one hand by the 1-dimensional core L of the solid cylinder which joins the two selected antipodal points of the outer shell and intersects each spherical layer at its two corresponding antipodal points, and on the other hand by the embedding h. The process results in a continuum of layered tori and can be viewed as drilling out a tunnel along L according to h. Note that in Fig. 6.2, the identity embedding has been used. However, a twisting embedding, which is the case shown in Fig. 5.3(1), agrees with our intuition that, for opening a hole, *drilling with twisting* seems to be the easiest way. Examples of these two embeddings can be found in Sect. 3.2.

Furthermore, solid 2-dimensional 1-surgery on D^3 is the topological procedure where on all spheres S_r^2 nested cylindrical peels of the solid cylinder of analogous areas are specified and the same coplanar attracting forces act on all spheres, see Fig. 6.2(b₂). Then, 2-dimensional 1-surgeries are performed on the whole continuum of the concentric spheres using the same embedding h. Moreover, 2-dimensional 1-surgery on the limit point P is defined to be the two limit points of the nested pairs of 2-spheres resulting from the continuum of 2-dimensional surgeries. That is, the effect of 2-dimensional 1-surgery on a point is the creation of two new points. The process is characterized by the 2-dimensional central disc of the solid cylinder and the embedding h, and it can be viewed as squeezing the central disc C or, equivalently, as pulling apart the left and right hemispheres with possible twists, if h is a twisting embedding. This agrees with our intuition that for cutting a solid object apart, pulling with twisting seems to be the easiest way. Examples of the identity and the twisting embedding can be found in Sect. 3.3.

For both types of solid 2-dimensional surgery, the above process is the same as: first removing the center P from D^3 , performing the 2-dimensional surgeries and then taking the closure of the resulting space. Namely we obtain:

$$\chi(D^3) := \cup_{0 < r \le 1} \chi(S_r^2) \cup \chi(P),$$

which is a solid torus in the case of solid 2-dimensional 0-surgery and two copies of D^3 in the case of solid 2-dimensional 1-surgery.

As seen in Fig. 6.2, we also have the two dual solid 2-dimensional surgeries, which represent the reverse processes. As already mentioned in Sect. 3.3, the dual case of 2-dimensional 0-surgery is the 2-dimensional 1-surgery and vice versa. More precisely:

Definition 5 The dual case of solid 2-dimensional 0-surgery on D^3 is the solid 2dimensional 1-surgery on a solid torus $D^2 \times S^1$ whereby a solid cylinder $D^1 \times D^2$ filling the hole is added, such that the closure of the resulting manifold comprises one 3-ball D^3 . This is the reverse process shown in Fig. 6.2(b₁) which results from the orange forces and attracting center. Given that the solid torus can be written as a union of nested tori together with the core circle: $D^2 \times S^1 = (\bigcup_{0 \le r \le 1} S^1_r \cup \{0\}) \times S^1$, solid 2-dimensional 1-surgeries are performed on each toroidal layer starting from specified annular peels of analogous sizes where the same coplanar forces act on the central rings of the annuli. These forces are caused by the same attracting center lying outside the torus. It only remain to define the solid 2-dimensional 1-surgery on the limit circle to be the limit point P of the resulting surgeries. That is, the effect of solid 2-dimensional 1-surgery on the core circle is that it collapses into one point, the attracting center. The above process is the same as first removing the core circle from $D^2 \times S^1$, doing the 2-dimensional 1-surgeries on the layered tori, with the same coplanar acting forces, and then taking the closure of the resulting space. Hence, the resulting manifold is

38 6 Solid Surgery

$$\chi^{-1}(D^2 \times S^1) := \cup_{0 < r \le 1} \chi^{-1}(S^1_r \times S^1) \cup \chi^{-1}(\{0\} \times S^1),$$

which comprises one copy of D^3 .

Further, the dual case of solid 2-dimensional 1-surgery on D^3 is the solid 2-dimensional 0-surgery on two 3-balls D^3 whereby a solid cylinder $D^2 \times D^1$ joining the balls is added, such that the closure of the resulting manifold comprise of one 3-ball D^3 . This is the reverse process shown in Fig. 6.2(b₂) which results from the blue forces and attracting center. We only need to define the solid 2-dimensional 0-surgery on two limit points to be the limit point P of the resulting surgeries. That is, as in solid 1-dimensional surgery (see Fig. 6.2(a)), the effect of solid 2-dimensional 0-surgery on two points is their merging into one point. The above process is the same as first removing the centers from the $D^3 \times S^0$, doing the 2-dimensional 0-surgeries on the nested spheres with the same colinear forces and then taking the closure of the resulting space. The resulting manifold is

$$\chi^{-1}(D^3 \times S^0) := \bigcup_{0 < r < 1} \chi^{-1}(S_r^2 \times S^0) \cup \chi^{-1}(P \times S^0),$$

which comprises one copy of D^3 .

Note that Remarks 1 and 3 are also true here. One can obtain the instances of solid 2-dimensional surgeries (Fig. $6.2(b_1)$ and (b_2)) by rotating the instances of solid 1-dimensional surgery (Fig. 6.2(a)) respectively by 180° around a vertical axis and by 180° around a horizontal axis.

Remark 4 The notions of 2-dimensional (resp. solid 2-dimensional) surgery, can be generalized from S^2 (resp. D^3) to a surface (resp. a handlebody) of genus g creating a surface (resp. a handlebody) of genus $g \pm 1$ or a disconnected surface (resp. handlebody).

6.3 Modeling Phenomena Exhibiting Solid 2-Dimensional 0-Surgery

We will now describe the phenomena mentioned in Sect. 5.4 which undergo the process of solid 2-dimensional 0-surgery.

For **gene transfer in bacteria**, see Fig. 5.3(4) (also, for description and instructive illustrations see [1]), the donor cell produces a connecting tube called a 'pilus' which attaches to the recipient cell, brings the two cells together and transfers the donor's DNA. This process is similar to the one shown earlier in Fig. 6.2(b₂) as two copies of D^3 merge into one, but here the attracting center is located on the recipient cell. This process is a solid 2-dimensional 0-surgery on two 3-balls $M = D^3 \times S^0$.

Similarly, the process of **drop coalescence** is also a solid 2-dimensional 0-surgery on two 3-balls $M = D^3 \times S^0$, see Fig. 6.2(b₂). The process of drop coalescence also exhibits the forces of our model. Namely, the surfaces of two drops must be in

contact for coalescence to occur. This surface contact is dependent on both the van der Waals attraction and the surface repulsion forces between two drops. When the van der Waals forces cause rupture of the film, the two surface films are able to fuse together, an event more likely to occur in areas where the surface film is weak. The liquid inside each drop is now in direct contact, and the two drops are able to merge into one.

Moreover, as already mentioned in Sect. 5.3, the formation of Falaco solitons is a natural phenomenon exhibiting solid 2-dimensional 0-surgery, see Fig. 5.3(3) (for photos of pairs of Falaco solitons in a swimming pool, see [2]). Note that the term 'Falaco Soliton' appears in 2001 in [3]. These pairs of singular surfaces (poles) are connected by means of a stabilizing thread. The two poles get connected and their rotation propagates below the water surface along the joining thread and the tubular neighborhood around it. This process is a solid 2-dimensional 0-surgery with a twisted homeomorphism (see Fig. 5.3(1)) where the initial manifold is the water contained in the volume of the pool where the process happens, which is homeomorphic to a 3-ball, that is $M = D^3$. It is also worth mentioning that the creation of Falaco solitons is immediate and does not allow us to see whether the transitions of solid 2-dimensional 0-surgery shown in Fig. 6.2(b₁) are followed or not. However, these dynamics are certainly visible during the annihilation of Falaco solitons. Namely, when the topological thread joining the poles is cut, the tube tears apart and slowly degenerates to the poles until they both stops spinning and vanish. Therefore, the continuity of our dynamic model is clearly present during the reverse process which corresponds to a solid 2-dimensional 1-surgery on a pair of Falaco solitons, that is, a solid torus $D^2 \times S^1$ degenerating into a still swimming pool D^3 , see the reverse process of Fig. $6.2(b_1)$.

Note that it is conjectured in [2] that the coherent topological features of the Falaco solitons and, by extension, the process of solid 2-dimensional 0-surgery appear in both macroscopic level (for example in the Wheeler's wormholes) and microscopic level (for example in the spin pairing mechanism in the microscopic Fermi surface). For more details see [2].

6.4 Modeling Phenomena Exhibiting Solid 2-Dimensional 1-Surgery

We will now describe the phenomena mentioned in Sect. 5.4 which undergo the process of solid 2-dimensional 1-surgery.

As already mentioned, the collapsing of the central disc of the sphere caused by the orange attracting forces in Fig. $6.2(b_2)$ can also be caused by pulling apart left and right hemispheres of the 3-ball D^3 , that is, the causal forces can also be repelling. For example, during the fracture of metal specimens under tensile forces, solid 2-dimensional 1-surgery is caused by forces that pull apart each end of the specimen.

40 6 Solid Surgery

On the other hand, in the biological process of mitosis, both attracting and repelling forces are present. We will now describe these two processes in details.

When the tension applied on metal specimens by tensile forces results in **necking** and then **fracture**, the process exhibits solid 2-dimensional 1-surgery. More precisely, in experiments in mechanics, tensile forces (or loading) are applied on a cylindrical specimen made of dactyle material (steel, aluminium, etc.). Up to some critical value of the force the deformation is homogeneous (the cross-sections have the same area). At the critical value the deformation is localized within a very small area where the cross-section is reduced drastically, while the sections of the remaining portions increase slightly. This is the 'necking phenomenon'. Shortly after, the specimen is fractured (view [4] for details). In Fig. 5.3(6) are the basic steps of the process: void formation, void coalescence (also known as crack formation), crack propagation, and failure or fracture. Here, the process is not as smooth as our theoretical model and the tensile forces applied on the specimen are equivalent to repelling forces. The specimen of Fig. 5.3(6) is homeomorphic to the sphere shown in Fig. 6.2(b₂) hence the initial manifold is $M = D^3$.

Solid 2-dimensional 1-surgery on $M=D^3$ also happens in the biological process of **mitosis**, where a cell splits into two new cells. See Fig. 5.3(7) (for description and instructive illustrations see for example [5]). We will see that both aforementioned forces are present here. During mitosis, the chromosomes, which have already duplicated, condense and attach to fibers that pull one copy of each chromosome to opposite sides of the cell (this pulling is equivalent to repelling forces). The cell pinches in the middle and then divides by cytokinesis. The structure that accomplishes cytokinesis is the contractile ring, a dynamic assembly of filaments and proteins which assembles just beneath the plasma membrane and contracts to constrict the cell into two (this contraction is equivalent to attracting forces). In the end, two genetically-identical daughter cells are produced.

References

- 1. Hartwell, L.H., Hood, L., Goldberg, M.L., Reynolds, A.E., Silver, L.M., Veres, R.C.: Genetics, from Genes to Genomes, p. 486. McGraw Hill (2000)
- Kiehn, R.M.: Non-equilibrium Systems and Irreversible Processes—Adventures in Applied Topology. Non-equilibrium Thermodynamics, vol. 1, pp. 147–150. University of Houston Copyright CSDC Inc. (2013)
- Kiehn, R.M.: Falaco Solitons, cosmic strings in a swimming pool. http://arXiv.org/pdf/gr-qc/ 0101098v1 (2001)
- Zhigilei, L.V.: Lecture Notes, Chapter 8: Failure. University of Virginia, Department of Materials Science. http://people.virginia.edu/~lz2n/mse209/Chapter8.pdf (2010)
- Keeton, W.T., McFadden, C.H.: Elements of Biological Science, p. 395. W.W. Norton & Company Inc. (1983)

Chapter 7



A Dynamical System Modeling Solid 2-Dimensional 0-Surgery

So far, inspired by natural processes undergoing surgery, we have extended the formal definition of topological surgery by introducing new notions such as continuity and solid surgery and presented a model showing where the observed forces act. However, in our model, time and dynamics were not introduced by differential equations. In this chapter we connect topological surgery, enhanced with these notions, with a dynamical system. We will see that, with a small change in parameters, the trajectories of its solutions are performing solid 2-dimensional 0-surgery. Therefore, this dynamical system constitutes a specific set of equations modeling natural phenomena undergoing solid 2-dimensional 0-surgery. More specifically, we will see that the change of parameters of the system affects the eigenvectors and induces a flow along a segment joining two steady state points. The induced flow represents the attracting forces shown in Fig. $6.2(b_1)$. Finally, we will see how our topological definition of solid 2-dimensional 0-surgery presented in Sect. 6.2 is verified by our numerical simulations and, in particular, that surgery on a steady point creates a limit cycle.

7.1 The Dynamical System and Its Steady State Points

In [1], N. Samardzija and L. Greller study the behavior of the following dynamical system (Σ) that generalizes the classical Lotka–Volterra problem [2, 3] into three dimensions:

$$\left\{ \begin{array}{l} \frac{dX}{dt} = X - XY + CX^2 - AZX^2 \\ \\ \frac{dY}{dt} = -Y + XY \\ \\ \frac{dZ}{dt} = -BZ + AZX^2 \end{array} \right\} A, B, C > 0$$
 (Σ)

In subsequent work [4], the authors present a slightly different model, provide additional numerical simulations and deepen the qualitative analysis done in [1]. Since both models coincide in the parametric region we are interested in, we will use the original model and notation and will briefly present some key features of the analyses done in [1, 4].

The system (Σ) is a two-predator and one-prey model, where the predators Y, Z do not interact directly with one another but compete for prey X. As X, Y, Z are populations, only the positive solutions are considered in this analysis. It is worth mentioning that, apart from a population model, (Σ) may also serve as a biological model and a chemical model, for more details see [1].

The parameters A, B, C are analyzed in order to determine the bifurcation properties of the system, that is, to study the changes in the qualitative or topological structure of the family of differential equations (Σ). As parameters A, B, C affect the dynamics of constituents X, Y, Z, the authors were able to determine conditions for which the ecosystem of the three species results in steady, periodic or chaotic behavior. More precisely, the authors derive five steady state solutions for the system but only the three positive ones are taken into consideration. These points are:

$$S_1 = \begin{pmatrix} 0 \\ 0 \\ 0 \end{pmatrix}, \quad S_2 = \begin{pmatrix} 1 \\ 1+C \\ 0 \end{pmatrix}, \quad S_3 = \begin{pmatrix} \sqrt{B/A} \\ 0 \\ \frac{1+C\sqrt{B/A}}{\sqrt{AB}} \end{pmatrix}$$

It is worth reminding here that a steady state (or singular) point of a dynamical system is a solution that does not change with time.

7.2 Local Behavior and Numerical Simulations

Let, now, $J(S_i)$ be the Jacobian of (Σ) evaluated at S_i for i=1,2,3 and let the sets $\Gamma\{J(S_i)\}$ and $W\{J(S_i)\}$ to be, respectively, the eigenvalues and the corresponding associated eigenvectors of $J(S_i)$. These are as follows:

$$\Gamma\{J(S_1)\} = \{1, -1, -B\}; \quad W\{J(S_1)\} = \left\{ \begin{bmatrix} 1\\0\\0 \end{bmatrix}, \begin{bmatrix} 0\\1\\0 \end{bmatrix}, \begin{bmatrix} 0\\0\\1 \end{bmatrix} \right\}$$

$$\Gamma\{J(S_2)\} = \left\{ A - B, (C + \sqrt{(C-2)^2 - 8})/2, (C - \sqrt{(C-2)^2 - 8})/2 \right\}$$

$$W\{J(S_2)\} = \left\{ \begin{bmatrix} 1\\(C+1)/(A-B)\\\frac{B+C-A+(C+1)/(B-A)}{2} \end{bmatrix}, \begin{bmatrix} \frac{1}{C-\sqrt{(C-2)^2 - 8}}\\\frac{2}{0} \end{bmatrix}, \begin{bmatrix} \frac{1}{C+\sqrt{(C-2)^2 - 8}}\\\frac{2}{0} \end{bmatrix} \right\}$$

$$\Gamma\{J(S_3)\} = \left\{ \sqrt{\frac{B}{A}} - 1, \frac{-1 + \sqrt{1 - 8B(1 + C\sqrt{B/A})}}{2}, \frac{-1 - \sqrt{1 - 8B(1 + C\sqrt{B/A})}}{2} \right\}$$

$$W\{J(S_3)\} = \left\{ \begin{bmatrix} 1 \\ -1 - \frac{2\sqrt{AB(1 + C\sqrt{B/A})}}{\sqrt{B/A - 1}} \\ \frac{2(1 + C\sqrt{B/A})}{\sqrt{B/A - 1}} \end{bmatrix}, \begin{bmatrix} 1 \\ 0 \\ \frac{-1 - \sqrt{1 - 8B(1 + C\sqrt{B/A})}}{2B} \end{bmatrix}, \begin{bmatrix} 1 \\ 0 \\ \frac{-1 + \sqrt{1 - 8B(1 + C\sqrt{B/A})}}{2B} \end{bmatrix} \right\}$$

Using the sets of eigenvalues and eigenvectors presented above, the authors characterize in [1, 4] the local behavior of the dynamical system around these three points using the Hartman-Grobman (or linearization) Theorem. Since 1 > 0 and -1, -B < 0, S_1 is a saddle point for all values of parameters A, B, C. However, the behavior around S_2 and S_3 changes as parameters A, B, C are varied. The authors show that the various stability conditions can be determined by only two parameters: C and B/A. It is also shown in [1] that stable solutions are generated left of and including the line B/A = 1 while chaotic/periodic regions appear on the right of the line B/A = 1. We are interested in the behavior of (Σ) as it passes from stable to chaotic/periodic regions. Therefore we will focus and analyze the local behavior around S_2 and S_3 and present numerical simulations for: stable region (a) where B/A = 1 and $(1/8B - 1)\sqrt{A/B} < C \le 2(1 + \sqrt{2})$ and chaotic/periodic region (b) where B/A > 1 and $(1/8B - 1)\sqrt{A/B} < C < 2(1 + \sqrt{2})$.

• Region (a)

Setting B/A = 1 and equating the right side of (Σ) to zero, one finds as solution the one-dimensional singular manifold:

$$L = \{(X, Y, Z); X = 1, Z = (1 + C - Y)/A\}$$

that passes through the points S_2 and S_3 . Since all points on L are steady state points, there is no motion along it. For $(1/8B-1)\sqrt{A/B} < C \le 2(1+\sqrt{2})$, S_2 is an unstable center while S₃ is a stable center (for a complete analysis of all parametric regions see [1]). This means that if λ_1 , λ_2 , λ_3 denote the eigenvalues of either S_2 or S_3 with $\lambda_1 \in \mathbb{R}$ and $\lambda_2, \lambda_3 \in \mathbb{C}$, then $\lambda_1 = 0$ and $Re(\lambda_2) = Re(\lambda_3) > 0$ for S_2 while $\lambda_1 = 0$ and $Re(\lambda_2) = Re(\lambda_3) < 0$ for S_3 . Moreover, the point (X, Y, Z) = (1, 1, C/A) is the center of L. The line segment X = 1, 0 < Y < 1 and (1 + C)/A < Z < C/Asupports attracting type singularities (and includes S_3) while the line segment defined by X = 1, 1 < Y < 1 + C and 0 < Z < C/A supports unstable singularities (and includes S_2), for details see [4]. More precisely, each attracting point corresponds to an antipodal repelling point, the only exception being the center of L which can be viewed as the spheroid of 0-diameter. The local behavior of (Σ) around S_2 and S_3 in this region together with line L are shown in Fig. 7.1(a). A trajectory (or solution) initiated near L in the repelling segment expands until it gets trapped by the attracting segment, forming the upper and lower hemisphere of a distinct sphere. Hence, a nest of spherical shells surrounding line L is formed, see Fig. 7.2(a). Moreover, the nest fills the entire positive space with stable solutions.

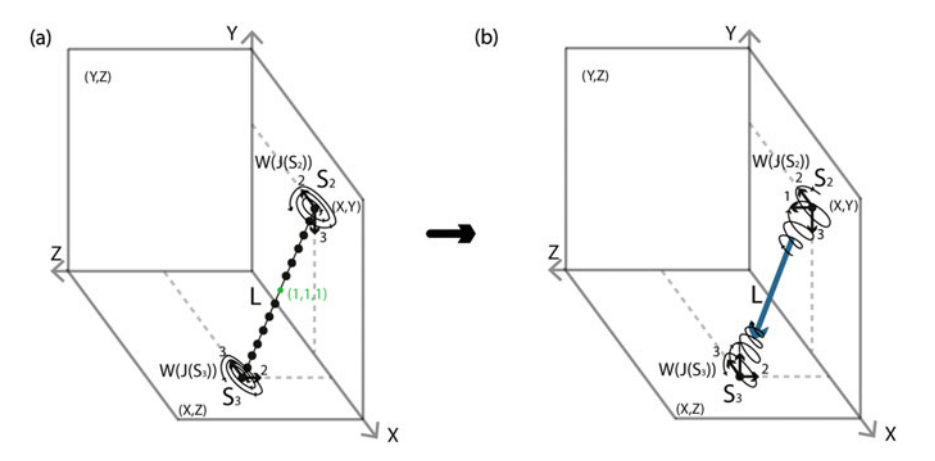


Fig. 7.1 Local behavior. Flow induced along L by changing parameter space from (a) B/A = 1 to (b) B/A > 1. Indices 1,2 and 3 indicate the first, second and third component in $W(J(S_2))$ and $W(J(S_3))$

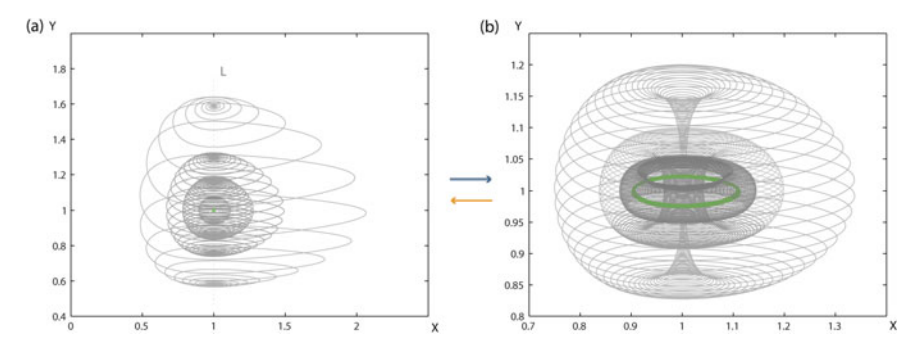


Fig. 7.2 Solid 2-dimensional 0-surgery by changing parameter space from (a) B/A=1 to (b) B/A>1

• Region (b)

For B/A > 1 and $(1/8B - 1)\sqrt{A/B} < C \le 2(1 + \sqrt{2})$, S_2 is an inward unstable vortex and S_3 is an outward stable vortex. This means that in both cases they must satisfy the conditions $\lambda_1 \in \mathbb{R}$ and $\lambda_2, \lambda_3 \in \mathbb{C}$ with $\lambda_3 = \lambda_2^*$, the conjugate of λ_2 . The eigenvalues of S_2 must further satisfy $\lambda_1 < 0$ and $Re(\lambda_2) = Re(\lambda_3) > 0$, while the eigenvalues of S_3 must further satisfy $\lambda_1 > 0$ and $Re(\lambda_2) = Re(\lambda_3) < 0$. The local behaviors around S_2 and S_3 for this parametric region are shown in Fig. 7.1(b). It is worth mentioning that Fig. 7.1(b) reproduces Fig. 1 of [1] with a change of the axes so that the local behaviors of S_2 and S_3 visually correspond to the local behaviors of the trajectories in Fig. 7.2(b) around the north and the south pole.

Note now that the point S_2 as well as the eigenvectors corresponding to its two complex eigenvalues, all lie in the xy-plane. On the other hand, the point S_3 and also

the eigenvectors corresponding to its two complex eigenvalues all lie in the xz-plane. The flow along line L produced by the actions of these eigenvectors forces trajectories initiated near S_2 to wrap around L and move toward S_3 in a motion reminiscent of hole drilling. The connecting manifold L is also called the 'slow manifold' in [1] due to the fact that trajectories move slower when passing near it. As trajectories reach S_3 , the eigenvector corresponding to the real eigenvalue of S_3 breaks out of the xz-plane and redirects the flow toward S_2 . As shown in Fig. 7.2(a) and (b), as B/A = 1 moves to B/A > 1, this process transforms each spherical shell to a toroidal shell. The solutions scroll down the toroidal surfaces until a limit cycle (shown in green in Fig. 7.2(b)) is reached. It is worth pointing out that this limit cycle is a torus of 0-diameter and corresponds to the sphere of 0-diameter, namely, the central steady point of L also shown in green in Fig. 7.2(a).

However, as the authors elaborate in [4], while for B/A=1 the entire positive space is filled with nested spheres, when B/A>1, only spheres up to a certain volume become tori. More specifically, quoting the authors: "to preserve uniqueness of solutions, the connections through the slow manifold L are made in a way that higher volume shells require slower, or higher resolution, trajectories within the bundle". As they further explain, to connect all shells through L, (Σ) would need to possess an infinite resolution. As this is never the case, the solutions evolving on shells of higher volume are 'choked' by the slow manifold. This generates solution indetermination, which forces higher volume shells to rapidly collapse or dissipate. The behavior stabilizes when trajectories enter the region where the choking becomes weak and weak chaos appears. As shown in both [1, 4], the outermost shell of the toroidal nesting is a fractal torus. Note that in Fig. 7.2(b) we do not show the fractal torus because we are interested in the interior of the fractal torus which supports a topology stratified with toroidal surfaces. Hence, all trajectories are deliberately initiated in its interior where no chaos is present.

It is worth pointing out that Fig. 7.2 reproduces the numerical simulations done in [4]. More precisely, Fig. 7.2(a) represents solutions of (Σ) for A=B=C=3 and trajectories initiated at points [1, 1.59, 0.81], [1, 1.3, 0.89], [1, 1.18; 0.95], [1, 1.08, 0.98] and [1, 1, 1]. Figure 7.2(b) represents solutions of (Σ) for A=2.9851.

B = C = 3 and trajectories initiated at points [1.1075, 1, 1], [1, 1, 0.95], [1, 1, 0.9] and [1, 1, 1].

In Fig. 7.3(a), we also present the outermost fractal torus as a trajectory initiated at point [1.45, 1, 1.45] for the same parameters used in Fig. 7.2, namely A = 2.9851 and B = C = 3. On the inside of the fractal torus, one can still see the periodic toroidal nesting. By zooming on the slow manifold of the outermost fractal torus shell, in Fig. 7.3(b) we can view the 'hole drilling' behavior of the trajectories.

As already mentioned, as B/A=1 changes to B/A>1, S_2 changes from an unstable center to an inward unstable vortex and S_3 changes from a stable center to an outward stable vortex. It is worth reminding that this change in local behavior is true not only for the specific parametrical region simulated in Figs. 7.2 and 7.3, but applies to all cases satisfying $(1/8B-1)\sqrt{A/B} < C \le 2(1+\sqrt{2})$. For details we refer the reader to Tables 2 and 3 in [1] that recapitulate the extensive diagrammatic analysis done therein.

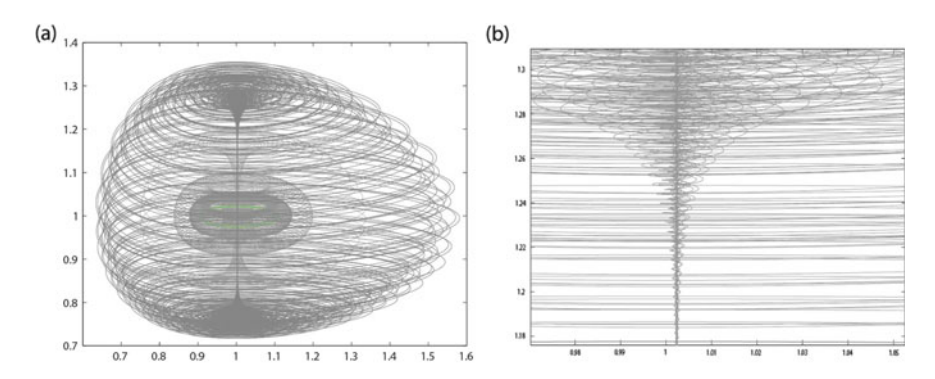


Fig. 7.3 (a) The fractal torus for B/A > 1 (b) Zooming on the slow manifold of the fractal torus

Finally, it is worth observing the changing of the local behavior around S_2 and S_3 in our numerical simulations. In Fig. 7.2(a), for B/A = 1 we have:

$$\Gamma\{J(S_2)\} = \{\mathbf{0.0000}, 1.500 - 1.3229i, 1.500 + 1.3229i\},\$$

$$\Gamma\{J(S_3)\} = \{\mathbf{0.0000}, -1.000 + 4.8780i, -1.000 - 4.878i\}$$

while in Fig. 7.2(b), for B/A > 1, both centers change to vortices (inward unstable and outward stable) through the birth of the first eigenvalue shown in bold (negative and positive respectively):

$$\Gamma\{J(S_2)\} = \{-0.0149, 1.500 - 1.3229i, 1.500 + 1.3229i\},\$$

$$\Gamma\{J(S_3)\} = \{0.0025, -1.000 + 4.8780i, -1.000 - 4.878i\}$$

Remark 5 The use of different numerical methods may affect the shape of the attractor. For example, as mentioned in [4], higher resolution produces a larger fractal torus and a finer connecting manifold. However, the 'hole drilling' process and the creation of a toroidal nesting is always a common feature.

7.3 Connecting the Dynamical System with Solid 2-Dimensional 0-Surgery

In this section, we will focus on the process of solid 2-dimensional 0-surgery on a 3-ball D^3 viewed as a continuum of concentric spheres together with their common center: $D^3 = \bigcup_{0 < r \le 1} S_r^2 \cup \{P\}$. Recall from Sect. 6.2 that the process is defined as the union of 2-dimensional 0-surgeries on the whole continuum of concentric spheres S_r^2 and on the limit point P. For each spherical layer, the process starts with attracting forces acting between $S^0 \times D^2$, i.e. two points, or poles, centers of two discs.

Having presented the dynamical system (Σ) in Sect. 7.1 and its local behavior in Sect. 7.2, its connection with solid 2-dimensional 0-surgery on a 3-ball is now straightforward. To be precise, surgery is performed on the manifold formed by the trajectories of (Σ) . Indeed, as seen in Fig. 7.2(a) and (b), with a slight perturbation of parameters, trajectories pass from spherical to toroidal shape through a 'hole drilling' process along a slow manifold L which pierces all concentric spheres. The spherical and toroidal nestings in Figs. $6.2(b_1)$ and 7.2 are analogous. The attracting forces acting between the two poles shown in blue in the first instance of Fig. $6.2(b_1)$ are realized by the flow along L (also shown in blue in Fig. 7.1(b)). When B/A > 1, the action of the eigenvectors is an attracting force between S_2 and S_3 acting along L, which drills each spherical shell and transforms it to a toroidal shell.

Furthermore, in order to introduce solid 2-dimensional 0-surgery on D^3 as a new topological notion, we had to define that 2-dimensional 0-surgery on a point is the creation of a circle. This new topological definition also has a meaning in the language of dynamical systems. Namely, the limit point P in the spherical nesting of trajectories shown in green in Fig. 7.2(a) is a steady state point and the core of the toroidal nesting of trajectories shown in green in Fig. 7.2(b) is a limit cycle. In other words, surgery on the limit point P creates the limit cycle. As mentioned in [4], this type of bifurcation is a 'Hopf bifurcation', so surgery on the trajectories can be also seen as a Hopf bifurcation.

Hence, instead of viewing surgery as an abstract topological process, we may now view it as a property of a dynamical system. Moreover, natural phenomena exhibiting 2-dimensional topological surgery through a 'hole-drilling' process, such as the creation of Falaco solitons, the formation of tornadoes, of whirls, of wormholes, etc., may be modeled mathematically by the dynamical system (Σ) . This system enhances the topological model presented in Fig. $6.2(b_1)$ with analytical formulation of the underlying dynamics. Indeed, if we link the three time-dependent quantities X, Y, Z to physical parameters of related phenomena undergoing 2-dimensional 0-surgery, system (Σ) can provide time forecasts for these phenomena.

Remark 6 In [5] R.M. Kiehn studies how the Navier-Stokes equations admit bifurcations to Falaco solitons. In other words, the author looks at another dynamical system modeling this natural phenomenon which, as mentioned in Sect. 5.3, exhibits solid 2-dimensional 0-surgery. To quote the author: "It is a system that is globally stabilized by the presence of the connecting 1-dimensional string" and "The result is extraordinary for it demonstrates a global stabilization is possible for a system with one contracting direction and two expanding directions coupled with rotation". It is also worth quoting Langford [6] which states that computer simulations indicate that "the trajectories can be confined internally to a sphere-like surface, and that Falaco Soliton minimal surfaces are visually formed at the North and South pole". One possible future research direction would be to investigate the similarities between this system and (Σ) in relation to surgery.

References

- Samardzija, N., Greller, L.: Explosive route to chaos through a fractal torus in a generalized Lotka-Volterra model. Bull. Math. Biol. 50(5): 465–491 (1988). https://doi.org/10.1007/BF02458847
- 2. Lotka, A.J.: Undamped oscillations derived from the law of mass action. J. Am. Chem. Soc. 42(8):1595–1599 (1920)
- 3. Volterra, V.: Leçons sur la Théorie Mathématique de la lutte pour la vie, Paris, Gauthier-Villars. Gabay, J. (1931, reissued 1990). https://doi.org/10.1090/S0002-9904-1936-06292-0
- Samardzija, N., Greller, L.: Nested tori in a 3-variable mass action model. Proc. R. Soc. Lond. A Math. Phys. Sci. 439(1907):637–647 (1992). https://doi.org/10.1098/rspa.1992.0173
- Kiehn R.M.: Non-equilibrium Systems and Irreversible Processes

 –Adventures in Applied Topology. Non-equilibrium Thermodynamics, vol. 1, pp. 147

 –150. University of Houston Copyright CSDC Inc. (2013)
- Langford, L.D.: A review of interactions of Hopf and steady-state bifurcations. In: Barrenblatt, G.I., Iooss, G., Joseph, D.D., Non-Linear Dynamics and Turbulence, Pitman, Boston, pp. 215– 237 (1983)

Chapter 8 The Ambient Space S³



All natural phenomena exhibiting surgery (1- or 2-dimensional, solid or usual) take place in the ambient 3-space. Moreover, as mentioned in Sect. 5.4, the ambient space can play an important role in the process of surgery. This will be detailed in next chapter where the notion of embedded surgery in 3-space is introduced. By 3-space we mean here the compactification of \mathbb{R}^3 which is the 3-sphere S^3 . This choice, as opposed to \mathbb{R}^3 , takes advantage of the duality of the descriptions of S^3 . In this section we present the three most common descriptions of S^3 (see Sect. 8.1) in which this duality is apparent and which will set the ground for defining the notion of embedded surgery in S^3 (see Chap. 9). Beyond that, in Sect. 8.2, we also demonstrate how these descriptions are interrelated. Finally, in Sect. 8.3, we pin down how the trajectories of the dynamical system (Σ) presented in Chap. 7 are related to the descriptions of S^3 and further introduce a Hamiltonian system exhibiting the topology of S^3 .

8.1 Descriptions of S^3

In dimension 3, the simplest closed, connected, orientable 3-manifolds are: the 3-sphere S^3 and the lens spaces L(p,q). In this analysis however, we will focus on S^3 . We start by recalling its three most common descriptions:

8.1.1 Via \mathbb{R}^3

 S^3 can be viewed as \mathbb{R}^3 with all points at infinity compactified to one single point: $S^3 = \mathbb{R}^3 \cup \{\infty\}$, see Fig. 8.1(a) and (a') where the point at infinity is symbolized with a red star. Given that \mathbb{R}^3 can be viewed as an unbounded continuum of nested 2-spheres centered at the origin together with the point at the origin, see Fig. 8.1(a'),

 S^3 minus the point at the origin and the point at infinity can be viewed as a continuous nesting of 2-spheres.

8.1.2 Via Two 3-Balls

 S^3 can be viewed as the union of two 3-balls: $S^3 = B^3 \cup D^3$, see Fig. 8.1(b). This second description of S^3 is clearly related to the first one, since a (closed) neighborhood of the point at infinity can stand for one of the two 3-balls. Note that, when removing the point at infinity, see the passage from Fig. 8.1(b) to 8.1(b'), we can see the concentric spheres of the 3-ball B^3 (in red) wrapping around the concentric spheres of the 3-ball D^3 . Note that, in both cases B^3 represents the hole space outside D^3 which means that the spherical nesting of B^3 in Fig. 8.1(b') extends to infinity, even though only a subset of B^3 is shown. This is another way of viewing \mathbb{R}^3 as the decompactification of S^3 . This picture is the analogue of the stereographic projection of S^2 on the plane \mathbb{R}^2 (recall Fig. 2.3), whereby the projections of the concentric circles of the south hemisphere together with the projections of the concentric circles of the north hemisphere form the well-known polar description of \mathbb{R}^2 with the unbounded continuum of concentric circles.

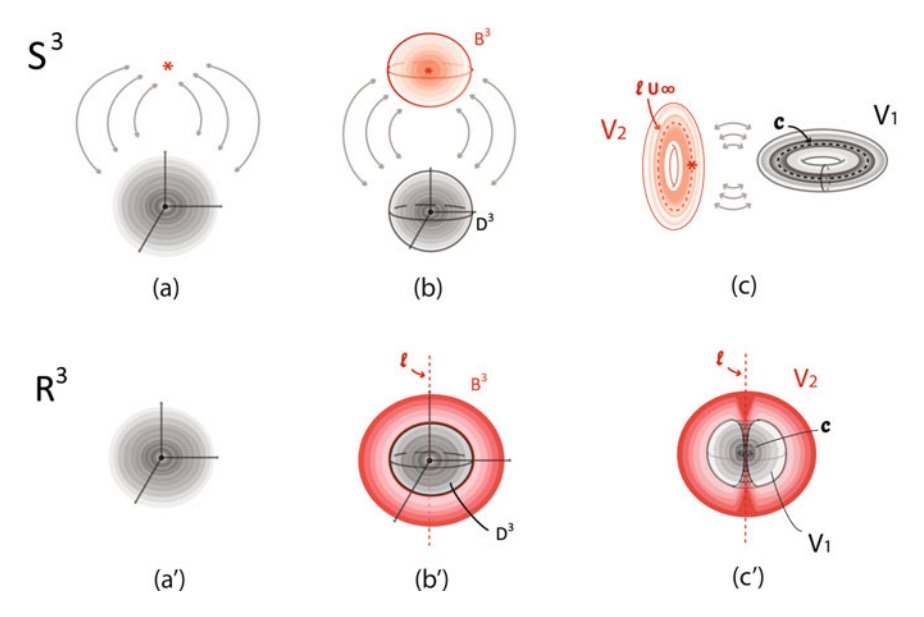


Fig. 8.1 (a) S^3 as the compactification of \mathbb{R}^3 (b) S^3 as the union of two 3-balls (c) S^3 as the union of two solid tori (a'), (b'), (c') corresponding decompacitified views in \mathbb{R}^3

8.1.3 Via Two Solid Tori

The third well-known representation of S^3 is as the union of two solid tori along their common boundary: $S^3 = V_1 \cup_{\vartheta} V_2$, via the torus homeomorphism ϑ along the common boundary, see Fig. 8.1(c). ϑ maps a meridian of V_2 to a longitude of V_1 which has linking number zero with the core curve c of V_1 . The illustration in Fig. 8.1(c) gives an idea of this splitting of S^3 . In the figure, the core curve c of V_1 is in dashed black. So, the complement of a solid torus V_1 in S^3 is another solid torus V_2 whose core curve l (shown in dashed red) may be assumed to pass by the point at infinity. Note that, S^3 minus the core curves c and c of c and c and c of c and c of

When removing the point at infinity in the representation of S^3 as a union of two solid tori, the core of the solid torus V_2 becomes an infinite line l and the nested tori of V_2 can now be seen wrapping around the nested tori of V_1 , see the passage from Fig. 8.1(c) to 8.1(c'). Therefore, \mathbb{R}^3 can be viewed as an unbounded continuum of nested tori, together with the core curve c of V_1 and the infinite line l. This line l joins pairs of antipodal points of all concentric spheres of the first description. Note that in the nested spheres description (Fig. 8.1(b')) the line l pierces all spheres while in the nested tori description the line l is the 'untouched' limit circle of all tori.

Remark 7 It is also worth mentioning that another way to visualize S^3 as two solid tori is the **Hopf fibration**, which is a map of S^3 into S^2 . The parallels of S^2 correspond to the nested tori of S^3 , the north pole of S^2 correspond to the core curve l of V_2 while the south pole of S^2 corresponds to the core curve c of c an insightful animation of the Hopf fibration can be found in [1].

8.2 Connecting the Descriptions of S^3

8.2.1 Via Corking

The connection between the first two descriptions of S^3 was already discussed in previous section. The third description is a bit harder to connect with the first two. We shall do this here. A way to see this connection is the following. Consider the description of S^3 as the union of two 3-balls, B^3 and D^3 (Fig. 8.1(b')). Combining with the third description of S^3 (Fig. 8.1(c')) we notice that both 3-balls are pierced by the core curve l of the solid torus V_2 . Therefore, D^3 can be viewed as the solid torus V_1 to which a solid cylinder $D^1 \times D^2$ is attached via the homeomorphism ϑ :

$$D^3 = V_1 \cup_{\vartheta} (D^1 \times D^2).$$

This solid cylinder is part of the solid torus V_2 , a 'cork' filling the hole of V_1 . Its core curve is an arc L, part of the core curve l of V_2 . View Fig. 8.2(a). The second

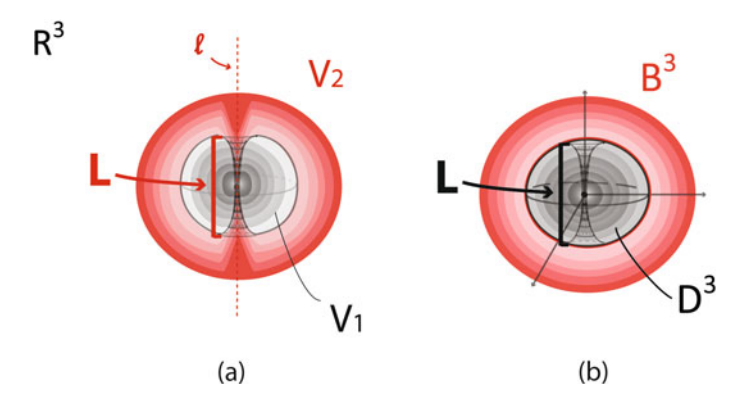


Fig. 8.2 Passing from (a) S^3 as two solid tori to (b) S^3 as two balls

ball B^3 (Fig. 8.2(b)) can be viewed as the remaining of V_2 after removing the 'cork' $D^1 \times D^2$:

$$B^3 = \overline{V_2 \setminus_{\vartheta} (D^1 \times D^2)}.$$

In other words the solid torus V_2 is cut into two solid cylinders, one comprising the 'cork' of V_1 and the other comprising the 3-ball B^3 .

Remark 8 If we remove a whole neighborhood B^3 of the point at infinity and focus on the remaining 3-ball D^3 , the line l of the previous picture is truncated to the arc L and the solid cylinder V_2 is truncated to the 'cork' of D^3 .

Remark 9 This arc L corresponds to the segment L joining the steady state points of the dynamical system of Chap. 7.

8.2.2 Via Surgery

We can also pass from the two-ball description to the two-tori description of S^3 via solid 2-dimensional 0-surgery (with the standard embedding homeomorphism) along the arc L of D^3 , see Figs. 9.2 and 9.3. As this process requires the notion of embedded surgery, it will be analyzed in Sect. 9.3.1. It is worth mentioning that this connection between the descriptions of S^3 and solid 2-dimensional 0-surgery is a dynamic way to visualize the connection established in Sect. 8.2.1.

8.3 Dynamical Systems Exhibiting the Topology of S^3

In this section, we go back to the 3-dimensional Lotka–Volterra system (Σ) and see how its trajectories relate to the descriptions of S^3 and further present a 4-dimensional Hamiltonian system exhibiting the topology of S^3 .

8.3.1 The 3-Dimensional Lotka-Volterra System

We will now pin down how the trajectories of (Σ) presented in Chap. 7 relate to the topology of S^3 . We start with the spherical nesting of Fig. 7.2(a) which can be viewed as the 3-ball D^3 shown in Fig. 8.1(b) and (b'). Surgery on its central point creates the limit cycle which is the core curve c of V_1 shown in Fig. 8.1(c) and (c'). If we extend the spherical shells of Fig. 7.2 to all of \mathbb{R}^3 and assume that the entire nest resolves to a toroidal nest, then the slow manifold L becomes the infinite line l. In the two-ball description of S^3 , l pierces all spheres, recall Fig. 8.1(b'), while in the two-tori description, it is the core curve of V_2 or the 'untouched' limit circle of all tori, recall Fig. 8.1(c) and (c').

8.3.2 The Pair of Linear Harmonic Oscillators

A toroidal nesting similar to the one exhibited in (Σ) and shown in Fig. 7.2 can be found in the trajectories of the Hamiltonian system of a pair of linear harmonic oscillators, see Fig. 8.3. Given that H is the sum of the energy functions of two harmonic oscillators with frequencies m and n and assuming that H is at least C^1 , m > 0 and n > 0, the time evolution of this system is given by the following system of four ODE of Hamilton:

$$\begin{cases} \dot{x}_i(s) = \frac{\partial H}{\partial y_i} \\ \dot{y}_i(s) = -\frac{\partial H}{\partial x_i} \end{cases} \text{ for } i = 1, 2$$
 (8.1)

$$H: \mathbb{R}^4 \to \mathbb{R}; H(x_1, x_2, y_1, y_2) = \frac{1}{2}m(x_1^2 + y_1^2) + \frac{1}{2}n(x_2^2 + y_2^2);$$
 (8.2)

As analyzed in [2], except from H, L is also a conserved quantity or first integral: $L(x_1, x_2, y_1, y_2) = \frac{1}{2}m(x_1^2 + y_1^2) - \frac{1}{2}n(x_2^2 + y_2^2)$.

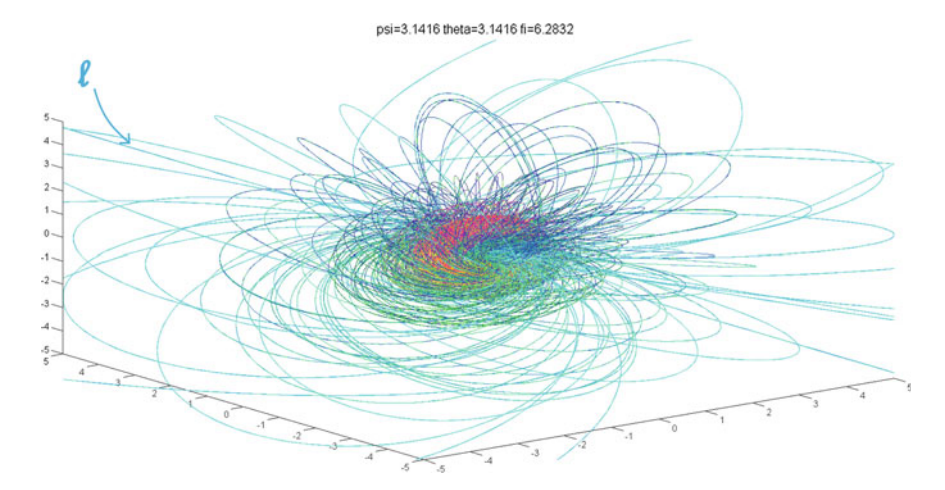


Fig. 8.3 The decompactified view of the orbits of a pair of linear harmonic oscillators

As the authors further elaborate: 'A constant energy surface $H^{-1}(h)$ of the harmonic oscillators is diffeomorphic to the three-sphere S^3 . Such a constant energy surface is the union of two critical circles $S_{h^+}^1 = \{(x_1, 0, y_1, 0) \in \mathbb{R}^4 \mid \frac{1}{2}m(x_1^2 + y_1^2) = h\}$, and $S_{h^-}^1 = \{(0, x_2, 0, y_2) \in \mathbb{R}^4 \mid \frac{1}{2}n(x_2^2 + y_2^2) = h\}$, and a one-parameter family of tori 'in between' parametrized by the values of the first integral L. This foliation of S^3 is indeed intricate; the two critical circles are linked, and concentric tori enveloping the critical circles fill the rest of S^3 '.

In Fig. 8.3, the orbits of the Hamiltonian system of a pair of linear harmonic oscillators with frequencies m=1 and n=1 were computed using matlab software. The system was solved for 1000 trajectories initiated on the unit 3-sphere S^3 . To make sure all of S^3 is covered, the hyperspherical coordinates (ψ, θ, ϕ) were used for $r=1, \psi, \theta \in [o, \pi]$ and $\phi \in [o, 2\pi]$: $(x_1, x_2, x_3, x_4) = (rcos(\psi), rsin(\psi)cos(\theta), rsin(\psi)sin(\theta)cos(\phi), rsin(\psi)sin(\theta)sin(\phi))$

These solutions were projected from S^3 to \mathbb{R}^3 using the stereographic projection which can be though of as removing the point at infinity and 'unwrapping' S^3 into \mathbb{R}^3 . More specifically, vectors $\mathbf{x} = (x_1, x_2, x_3, x_4) \in S^3$ were projected to vectors $\mathbf{u} = (u_1, u_2, u_3) = \frac{1}{1-x_4}(x_1, x_2, x_3) \in \mathbb{R}^3$, which corresponds to a projection from the pole (0, 0, 0, 1).

We will now identify the topology of S^3 in Fig. 8.3. The two critical circle $S_{h^+}^1$ and $S_{h^-}^1$ mentioned above are the core curve c of V_1 and the infinite line l respectively, see Fig. 8.1(c) and (c'). While l can be seen in both Figs. 8.1 and 8.3, the core curve c can only be seen if we visualize the trajectories of Fig. 8.3 step by step. Indeed, in Fig. 8.4(a) we see the core curve c which is quickly covered by the other trajectories. The first three toroidal layers are shown in Fig. 8.4(b), (c) and (d). Note that, comparing the trajectories of Fig. 8.4 with those of (Σ) shown in Fig. 7.2(b), a key difference is that here, as opposed to system (Σ) , the nesting of tori does extend to infinity.

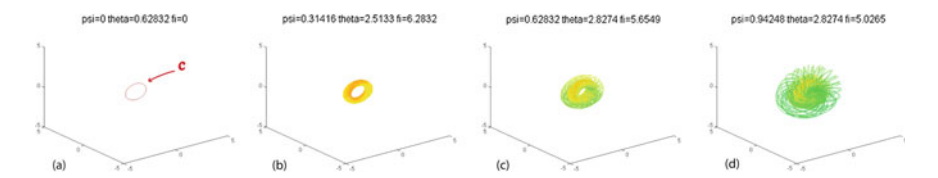


Fig. 8.4 Nesting of orbits of a pair of linear harmonic oscillators

To close the topological analogy, one can visualize $S^3 = V_1 \cup_{\vartheta} V_2$ by considering that V_1 is any finite number of toroidal nestings. For example V_1 could be any of the tori shown in Fig. 8.4(b), (c) or (d) while, in each of these case, V_2 is naturally defined as the complement space.

References

- 1. Johnson, N.: A visualization of the Hopf fibration. http://nilesjohnson.net/hopf.html
- Hale, J.K., Kocak, H.: Dynamic and Bifucation. Springer, New York (1996). Chapter 18:00 Dimension Four

Chapter 9 Embedded Surgery



In this chapter we will examine how the ambient space can be involved in the process of surgery and introduce the notion of embedded surgery in order to model such phenomena. As we will see, depending on the dimension of the manifold, the ambient space either leaves 'room' for the initial manifold to assume a more complicated configuration or it participates more actively in the process. Independently of dimensions, embedding surgery has the advantage that it allows us to view surgery as a process happening inside a space instead of abstractly. We define it as follows:

Definition 6 An embedded m-dimensional n-surgery is a m-dimensional n-surgery following the process described in Definition 2 where the initial manifold is an m-embedding $e: M \hookrightarrow S^d$, $d \ge m$ of some m-manifold M, and the result is also viewed as embedded in S^d . Namely:

$$M'=\chi(e(M))=\overline{e(M)\backslash h(S^n\times D^{m-n})}\cup_{h|_{S^n\times S^{m-n-1}}}D^{n+1}\times S^{m-n-1}\hookrightarrow S^d.$$

Since in this analysis we focus on phenomena exhibiting embedded 1- and 2-dimensional surgery in 3-space, from now on we fix d=3 and, for our purposes, we consider S^3 or \mathbb{R}^3 as our standard 3-space.

9.1 Embedded 1-Dimensional Surgery

In dimension 1, the notion of embedded surgery allows the topological modeling of phenomena with more complicated initial 1-manifolds. Let us demonstrate this with the example of site-specific **DNA recombination**. In this process, the initial manifold is a (circular or linear) DNA molecule. With the help of certain enzymes, site-specific recombination performs a 1-dimensional 0-surgery on the molecule, causing possible knotting or linking of the molecule.

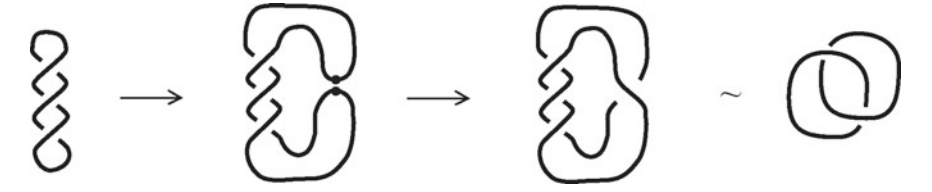


Fig. 9.1 DNA Recombination as an example of embedded 1-dimensional 0-surgery

58

The first electron microscope picture of knotted DNA was presented in [1]. In this experimental study, we see how genetically engineered circular DNA molecules can form DNA knots and links through the action of a certain recombination enzyme. A similar picture is presented in Fig. 9.1, where site-specific recombination of a DNA molecule produces the Hopf link. It is worth mentioning that there are infinitely many knot types and that 1-dimensional 0-surgery on a knot may change the knot type or even result in a two-component link (as shown in Fig. 9.1). Since a knot is by definition an embedding of $M = S^1$ in S^3 or \mathbb{R}^3 , in this case embedded 1-dimensional surgery is the so-called *knot surgery*. A good introductory book on knot theory is [2] among many others.

We can summarize the above by stating that for $M = S^1$, embedding in S^3 allows the initial manifold to become any type of knot. More generally, in dimension 1 the ambient space which is of codimension 2 gives enough 'room' for the initial 1-manifold to assume a more complicated homeomorphic configuration.

Remark 10 Of course we also have, in theory, the notion of embedded solid 1-dimensional 0-surgery whereby the initial manifold is an embedding of a disc in 3-space.

9.2 Embedded 2-Dimensional Surgery

Passing now to 2-dimensional surgeries, let us first note that an embedding of a sphere $M=S^2$ in S^3 presents no knotting because knotting requires embeddings of codimension 2. However, in this case the ambient space plays a different role. Namely, embedding 2-dimensional surgeries allows the complementary space of the initial manifold to participate actively in the process. Indeed, while some natural phenomena undergoing surgery can be viewed as 'local', in the sense that they can be considered independently from the surrounding space, some others are intrinsically related to the surrounding space. This relation can be both causal, in the sense that the ambient space is involved in the triggering of the forces causing surgery, and consequential, in the sense that the forces causing surgery can have an impact on the ambient space in which they take place.

As mentioned in the introduction of Chap.6, in most natural phenomena that exhibit 2-dimensional surgery, the initial manifold is a *solid* 3-dimensional object.

Hence, in the next sections, we describe natural phenomena undergoing solid 2-dimensional surgeries which exhibit the causal or consequential relation to the ambient space mentioned above and are therefore better described by considering them as embedded in S^3 or in \mathbb{R}^3 . In parallel, we describe how these processes are altering the whole space S^3 or \mathbb{R}^3 .

9.3 Modeling Phenomena Exhibiting Embedded Solid 2-Dimensional Surgery

In each of the following sections a natural phenomena undergoing embedding solid 2-dimensional surgery is analyzed. As we will see, the topological considerations of these processes also have physical implications.

9.3.1 A Topological Model for the Density Distribution in Black Hole Formation

Let us start by considering the density distribution in **black hole** formation. Most black holes are formed from the remnants of a large star that dies in a supernova explosion. Their gravitational field is so strong that not even light can escape. In the simulation of a black hole formation in [3], the density distribution at the core of a collapsing massive star is shown. Figure 9.2(2) shows three instants of this simulation, which indicate that matter performs solid 2-dimensional 0-surgery as it collapses into a black hole. In fact, matter collapses at the center of attraction of the initial manifold $M = D^3$ creating the singularity, that is, the center of the black hole (shown as a black dot in instance (c) of Fig. 9.2(2)), which is surrounded by the toroidal accretion disc (shown in white in instance (c) of Fig. 9.2(2)). Let us be reminded here that an accretion disc is a rotating disc of matter formed by accretion.

Note now that the strong gravitational forces have altered the space surrounding the initial star and that the singularity is created outside the final solid torus. This means that the process of surgery in this phenomenon has moreover altered matter outside the manifold in which it occurs. In other words, the effect of the forces causing surgery propagates to the complement space, thus causing a more global change in 3-space. This fact makes black hole formation a phenomenon that topologically undergoes embedded solid 2-dimensional 0-surgery.

In Fig. 9.2(1), we present a model of embedded solid 2-dimensional 0-surgery on $M = D^3$. From the descriptions of S^3 in Sect. 9.2, it becomes apparent that embedded solid 2-dimensional 0-surgery on one 3-ball describes the passage from the two-ball description to the two-solid tori description of S^3 . This can be seen in \mathbb{R}^3 in instances (a)–(c) of Fig. 9.2(1) but is more obvious by looking at instances (a)–(c) of Fig. 9.3 which show the corresponding view in S^3 .

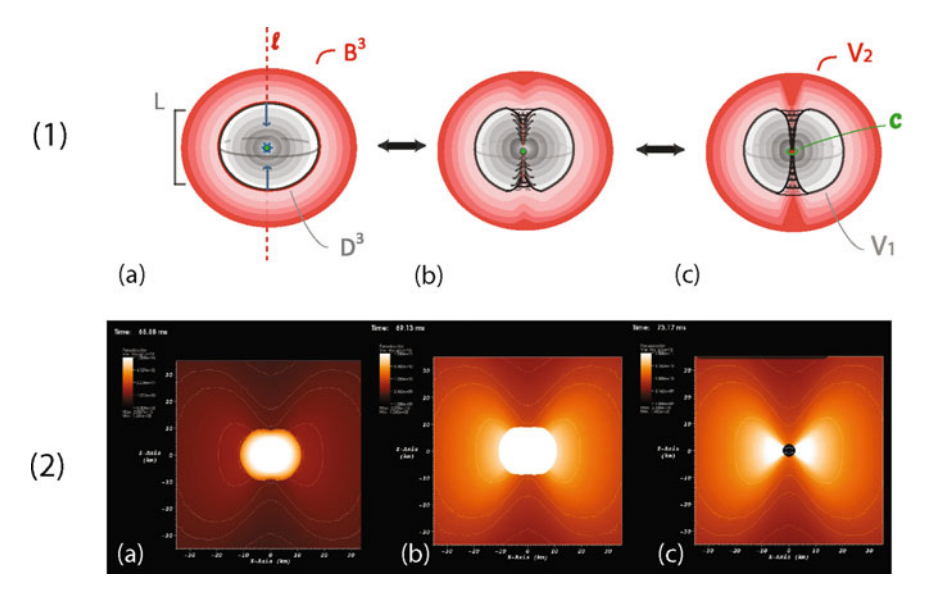


Fig. 9.2 (1) Embedded solid 2-dimensional 0-surgery on $M = D^3$ (in \mathbb{R}^3) (2) Black hole formation

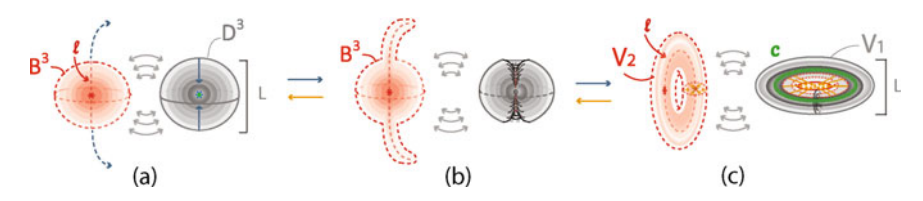


Fig. 9.3 Embedded solid 2-dimensional 0-surgery on $M = D^3$ (in S^3)

We will now detail the instances of the process of embedded solid 2-dimensional 0-surgery on $M=D^3$ by referring to both the view in S^3 and the corresponding decompacified view in \mathbb{R}^3 . Let $M=D^3$ be the solid ball having arc L as a diameter and the complement space be the other solid ball B^3 containing the point at infinity; see instances (a) of Fig. 9.3 and (a) of Fig. 9.2. Note that, in both cases B^3 represents the hole space outside D^3 which means that the spherical nesting of B^3 in instance Fig. 9.2(a) extends to infinity, even though only a subset of B^3 is shown. This joining arc L is seen as part of a simple closed curve l passing by the point at infinity. In instances (b) of Fig. 9.3 and (b) of Fig. 9.2, we see the 'drilling' along L as a result of the attracting forces. This is exactly the same process as in Fig. 6.2(b₁) if we restrict it to D^3 . But since we have embedded the process in S^3 or \mathbb{R}^3 , the complement space B^3 participates in the process and, in fact, it is also undergoing solid 2-dimensional 0-surgery. Indeed, the 'matter' that is being drilled out from the interior of D^3 can be viewed as 'matter' of the outer sphere B^3 invading D^3 . In instances (c) of Fig. 9.3 and (c) of Fig. 9.2, we can see that, as surgery transforms the solid ball D^3 into the

solid torus V_1 , B^3 is transformed into V_2 . That is, the nesting of concentric spheres of D^3 (respectively of B^3) is transformed into the nesting of concentric tori in the interior of V_1 (respectively of V_2). The point at the origin (in green), which is also the attracting center, turns into the core curve c of V_1 (in green) which, by Definition 4 is 2-dimensional 0-surgery on a point. As seen in instance (c) of Fig. 9.3 and (c) of Fig. 9.2(1), the result of surgery is the two solid tori V_1 and V_2 forming S^3 .

The described process can be viewed as a double surgery resulting from a single attracting center which is inside the first 3-ball D^3 and outside the second 3-ball B^3 . This attracting center is illustrated (in blue) in instance (a) of Fig. 9.2 but also in (a) of Fig. 9.3, where it is shown that the colinear attracting forces causing the double surgery can be viewed as acting on D^3 (the two blue arrows) and also as acting on the complement space B^3 (the two dotted blue arrows), since they are applied on the common boundary of the two 3-balls. Note that in both cases, the attracting center coincides with the limit point of the spherical layers that D^3 is made of, that is, their common center and the center of D^3 (shown in green in (a) of Fig. 9.2 and (a) of Fig. 9.3).

The reverse process of embedded solid 2-dimensional 0-surgery on D^3 is an embedded solid 2-dimensional 1-surgery on the solid torus V_2 , see instances of Fig. 9.3 in reverse order. This process is the embedded analog of the solid 2-dimensional 1-surgery on a solid torus $D^2 \times S^1$ defined in Definition 5 and shown in Fig. 6.2(b₁) in reverse order. Here too, the process can be viewed as a double surgery resulting from one attracting center which is outside the first solid torus V_1 and inside the second solid torus V_2 . This attracting center is illustrated (in orange) in instance (c) of Fig. 9.3 where it is shown that the coplanar forces causing surgery are applied on the common boundary of V_1 and V_2 and can be viewed as attracting forces along a longitude when acting on V_1 and as attracting forces along a meridian when acting on the complement space V_2 .

One can now directly appreciate the correspondence of the physical phenomena (instances (a), (b), (c) of Fig. 9.2(2)) with our model (instances (a), (b), (c) of Fig. 9.2(1)). Indeed, if one looks at the density distribution during the formation of a black hole and examines it as an isolated event in space, this process shows a decompactified view of the passage from a two 3-ball description of S^3 , that is, the core of the star and the surrounding space, to a two solid tori description, namely the toroidal accretion disc surrounding the black hole (shown in white in instance (c) of Fig. 9.2(2)) and the surrounding space.

Finally, it is worth pinning down the following spatial duality of embedded solid 2-dimensional 0-surgery for $M=D^3$: the attraction of two points lying on the boundary of segment L by the center of D^3 can be equivalently viewed in the complement space as the repulsion of these points by the center of B^3 (that is, the point at infinity) on the boundary of the segment l-L (or the segments, if viewed in \mathbb{R}^3). Hence, the aforementioned duality tells us that the attracting forces from the attracting center that are collapsing the core of the star can be equivalently viewed as repelling forces from the point at infinity lying in the surrounding space.

9.3.2 A Topological Model for the Formation of Tornadoes

Another example of global phenomenon is the formation of **tornadoes**, recall Fig. 5.3(2). As mentioned in Chap. 6 this phenomenon can be modelled by solid 2-dimensional 0-surgery. However, here, the initial manifold is different than D^3 . Indeed, if we consider a 3-ball around a point of the cloud and another 3-ball around a point on the ground, then the initial manifold is $M = D^3 \times S^0$ and the process followed is the one shown in Fig. 6.2(b₂) (from right to left). More precisely, if certain meteorological conditions are met, an attracting force between the cloud and the earth beneath is created. This force is shown in blue in see Fig. 9.4(1). Then, funnel-shaped clouds start descending toward the ground, see Fig. 9.4(2). Once they reach it, they become tornadoes, see Fig. 9.4(3). The only difference compared to our model is that here the attracting center is on the ground, see Fig. 9.4(1), and only one of the two 3-balls (the 3-ball of cloud) is deformed by the attraction. This lack of symmetry in the process can be obviously explained by the big difference in the density of the materials.

During this process, a solid cylinder $D^2 \times S^1$ containing many layers of air is created. Each layer of air revolves in a helicoidal motion which is modeled using a twisting embedding as shown in Fig. 5.3(1) (for an example of a twisting embedding, the reader is referred Sect. 3.2). Although all these layers undergo local dynamic 2-dimensional 0-surgeries which are triggered by local forces (shown in blue in Fig. 9.4(1)), these local forces are not enough to explain the dynamics of the phenomenon. Indeed, the process is triggered by the difference in the conditions of the lower and upper atmosphere which create an air cycle. This air cycle lies in the complement space of the initial manifold $M = D^3 \times S^0$ and of the solid cylinder $D^2 \times S^1$, but is also involved in the creation of the funnel-shaped clouds that will join the two initial 3-balls. Therefore in this phenomenon, surgery is the outcome of global changes and this fact makes tornado formation an example of embedded solid 2-dimensional 0-surgery on $M = D^3 \times S^0$.

It is worth mentioning that the complement space containing the aforementioned air cycle is also undergoing solid 2-dimensional 0-surgery. The process can be seen in \mathbb{R}^3 in instances (a)–(d) of Fig. 9.5 while the corresponding view in S^3 is shown in instances (a') to (d') of Fig. 9.5.



Fig. 9.4 (1) Attracting force between the cloud and the earth (2) Funnel-shaped clouds (3) Tornado

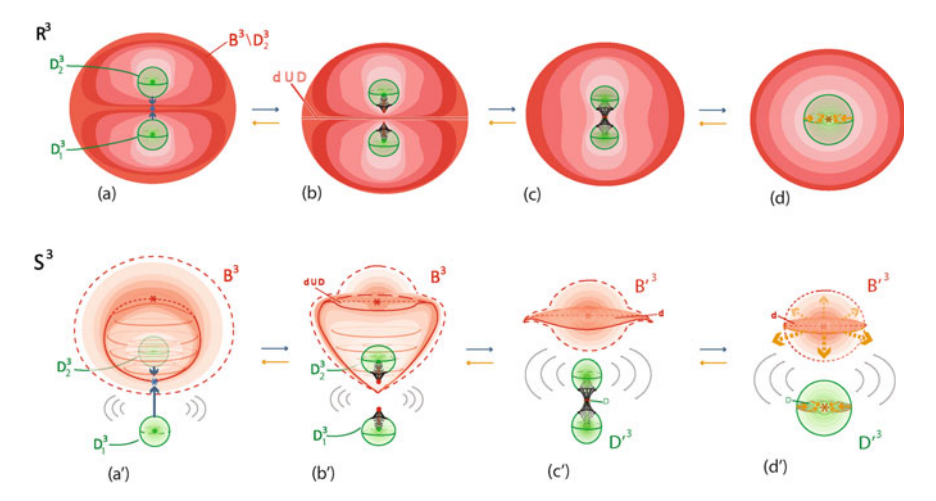


Fig. 9.5 Embedded solid 2-dimensional 0-surgery on $D_1^3 \coprod D_2^3$ (from left to right) and embedded solid 2-dimensional 1-surgery on $D^{\prime 3}$ (from right to left)

More precisely, let us name the two initial 3-balls D_1^3 and D_2^3 , hence $M=D^3\times S^0=D_1^3\coprod D_2^3$. Further, let B^3 be the complement of D_1^3 in S^3 . This setup is shown in (a') of Fig. 9.5 where S^3 is viewed as the union of the two 3-balls $D_1^3\cup B^3$, and here too, B^3 represents everything outside D_1^3 . The complement space of the initial manifold, $S^3\backslash M=B^3\setminus D_2^3$, is the 3-ball B^3 where D_2^3 has been removed from its interior and its boundary consists in two spheres $S^2\times S^0$, one bounding B^3 or, equivalently, D_1^3 (the outside sphere) and one bounding D_2^3 (the inside sphere). Next, D_1^3 and D_2^3 approach each other, see Fig. 9.5(b'). In (c') of Fig. 9.5, D_1^3 and D_2^3 merge and become the new 3-ball $D^{\prime 3}$, see Fig. 9.5(c') or Fig. 9.5(d') for a homeomorphic representation.

At the moment of merging, the spherical boundary of D_2^3 punctures the boundary of B^3 ; see the passage from (b') to (c') of Fig. 9.5. As a result, the complement space is transformed from $B^3 \setminus D_2^3$ to the new deformed 3-ball B'^3 , see Fig. 9.5(c') or Fig. 9.5(d') for a homeomorphic representation. Note that, although the complement space undergoes a type of surgery that is different from the ones defined in Chap. 6 and shown in Fig. 6.2, it can still be defined analogously. In short, we have a double solid 2-dimensional 0-surgery which turns $M = D_1^3 \coprod D_2^3$ into D'^3 and the complement space $S^3 \setminus (D_1^3 \coprod D_2^3)$ into B'^3 . This process is initiated by the attracting center shown (in blue) in Fig. 9.5(a'). The created colinear forces can be viewed as acting on $D_1^3 \coprod D_2^3$ or, equivalently, as acting on the complement space $S^3 \setminus (D_1^3 \coprod D_2^3)$ (see the two blue arrows for both cases).

Going back to the formation of tornadoes, the above process describes what happens to the complement space and provides a topological description of the behavior of the air cycle during the formation of tornadoes. The complement space $B^3 \setminus D_2^3$ in \mathbb{R}^3 is shown in red in Fig. 9.5(a) and its behavior during the process can be seen

in instances (b)–(d) of Fig. 9.5. Note that in Fig. 9.5(a), $B^3 \setminus D_2^3$ represents the hole space outside D_1^3 , which means that the red layers of Fig. 9.5(a) extend to infinity and only a subset is shown.

9.3.3 Embedded Solid 2-Dimensional 1-Surgery on $M = D^3$

We will now discuss the process of *embedded solid 2-dimensional 1-surgery* in S^3 . Taking $M = D^{3}$ as the initial manifold, embedded solid 2-dimensional 1-surgery is the reverse process of embedded solid 2-dimensional 0-surgery on $D^3 \times S^0$ and is illustrated in Fig. 9.5 from right to left. The process is initiated by the attracting center shown (in orange) in (d') of Fig. 9.5. The created coplanar attracting forces are applied on the circle which is the common boundary of the meridian of D^{3} and the meridian of $B^{\prime 3}$ and they can be viewed as acting on the meridional disc D of the 3-ball $D^{\prime 3}$ (see orange arrows) or, equivalently, in the complement space, on the meridional disc d of $B^{\prime 3}$ (see dotted orange arrows). As a result of these forces, in Fig. 9.5(c'), we see that while disc D of $D^{\prime 3}$ is getting squeezed, disc d of $B^{\prime 3}$ is enlarged. In Fig. 9.5(b'), the central disc d of $B^{\prime 3}$ engulfs disc D and becomes $d \cup D$, which is a separating plane in \mathbb{R}^3 , see Fig. 9.5(b). At this point the initial 3-ball $D^{\prime 3}$ is split in two new 3-balls D_1^3 and D_2^3 ; see Fig. 9.5(b') or Fig. 9.5(a') for a homeomorphic representation. The center point of $D^{\prime 3}$ (which coincides with the orange attracting center) evolves into the two centers of D_1^3 and D_2^3 (in green) which by Definition 4, is 2-dimensional 1-surgery on a point. This is exactly the same process as in Fig. 6.2(b₂) if we restrict it to $D^{\prime 3}$, but since we are in S^3 , the complement space $B^{\prime 3}$ is also undergoing, by symmetry, solid 2-dimensional 1-surgery.

All natural phenomena undergoing embedded solid 2-dimensional 1-surgery take place in the ambient 3-space. The converse, however, is not true. For example, the phenomena exhibiting 2-dimensional 1-surgery discussed in Sect. 5.3 are all embedded in 3-space, but they do not exhibit the intrinsic properties of embedded 2-dimensional surgery, since they do not demonstrate the causal or consequential effects discussed in Sect. 9.2 involving the ambient space. Yet one could, for example, imagine taking a solid material specimen, stress it until necking occurs and then immerse it in some liquid until its pressure causes fracture to the specimen. In this case the complement space is the liquid and it triggers the process of surgery. Therefore, this is an example of embedded solid 2-dimensional 1-surgery where surgery is the outcome of global changes.

Remark 11 Note that the spatial duality described in embedded solid 2-dimensional 0-surgery, in Sect. 9.3.2, is also present in embedded solid 2-dimensional 1-surgery. Namely, the attracting forces from the circular boundary of the central disc D to the center of $D^{\prime 3}$ shown in (d') of Fig. 9.5, can be equivalently viewed in the complement space as repelling forces from the center of $B^{\prime 3}$ (that is, the point at infinity) to the boundary of the central disc d, which coincides with the boundary of D.

Remark 12 One can sum up the processes described in this section as follows. The process of embedded solid 2-dimensional 0-surgery on D^3 consists in taking a solid cylinder such that the part $S^0 \times D^2$ of its boundary lies in the boundary of D^3 , removing it from D^3 and adding it to B^3 . Similarly, the reverse process of embedded solid 2-dimensional 1-surgery on V_2 consists of taking a solid cylinder such that the part $S^1 \times D^1$ of its boundary lies in the boundary of V_2 , removing it from V_2 and adding it to V_1 . Following the same pattern, embedded solid 2-dimensional 1surgery on $M = D^3$ consists of taking a solid cylinder in D^3 such that the part $S^1 \times D^1$ of its boundary lies in the boundary of $D^{\prime 3}$, removing it from $D^{\prime 3}$ and adding it to $B^{\prime 3}$. Similarly, the reverse process of embedded solid 2-dimensional 0-surgery on $S^3 \setminus (D_1^3 \coprod D_2^3)$ consists of taking a solid cylinder such that the two parts $S^0 \times D^2 = D_1^2 \coprod D_2^2$ of its boundary lie in the corresponding two parts of the boundary of $S^3 \setminus (D_1^3 \coprod D_2^3)$, removing it from $S^3 \setminus (D_1^3 \coprod D_2^3)$ and adding it to $D_1^3 \coprod D_2^3$. Note that, for clarity, in the above descriptions the attracting centers causing surgery are always inside the initial manifold. Of course a similar description starting with the complement space as an initial manifold and the attracting center outside of it would also have been correct.

References

- Wasserman, S.A., Dungan, J.M., Cozzarelli, N.R.: Discovery of a predicted DNA knot substantiates a model for site-specific recombination. Science 229, 171–174 (1985)
- 2. Adams, C.: The knot book: an elementary introduction to the mathematical theory of knots. American Mathematical Society (2004)
- 3. Ott, C.D., et al.: Dynamics and gravitational wave signature of collapsar formation. Phys. Rev. Lett. **106**, 161103 (2011). https://doi.org/10.1103/PhysRevLett.106.161103

Chapter 10 3-Dimensional Surgery



In this chapter we present a novel way of visualizing 3-dimensional surgery as well as a phenomenon exhibiting it. In Sect. 10.1, we introduce the notion of decompactified 2-dimensional surgery which allows us to visualize the process of 2-dimensional surgery in \mathbb{R}^2 instead of \mathbb{R}^3 . Using this new notion and rotation, in Sect. 10.2, we present a way to visualize the 4-dimensional process of 3-dimensional surgery in \mathbb{R}^3 . In Sect. 10.3, we analyze the concept of continuity introduced in Chap. 4 in the case of 3-dimensional surgery by looking at the local process inside the 4-dimensional handle. Finally, in Sect. 10.4, we model a phenomenon exhibiting 3-dimensional surgery: the formation of black holes from cosmic strings.

10.1 Decompactified 2-Dimensional Surgery

We present here the notion of *decompactified 2-dimensional surgery* which allows us to visualize 2-dimensional surgery in \mathbb{R}^2 instead of \mathbb{R}^3 .

Let us first recall from Chap. 4 that an m-dimensional n-surgery happens inside the handle $D^{n+1} \times D^{m-n}$. In Fig. 10.1, the cases of dimensions 1 and 2 are shown in the first two rows where m-dimensional n-surgeries are symbolized with [m-n]. For example, in 2-dimensional 0-surgery, see Fig. 10.1 [2–0], a homeomorphic representation of S^2 is formed by gluing the two discs $S^0 \times D^2$ to the cylinder $D^1 \times S^1$. The whole time evolution of 2-dimensional 0-surgery is a way of passing from $S^0 \times D^2$ to $D^1 \times S^1$ and the frames of this evolution are included in $D^1 \times D^2$.

Let us now point out that one can obtain all instances of 2-dimensional 0-surgery by rotating Fig. 10.1 [1–0] by 180° around a horizontal axis, see Fig. 10.1 [2–0]. Note that this observation is just the generalization of Remark 1, including now the intermediate instances of surgery. From this observation it follows that 1-dimensional 0-surgery is a crossection of 2-dimensional 0-surgery and that 2-dimensional 0-surgery can be obtained as a union of 1-dimensional 0-surgeries. While not shown

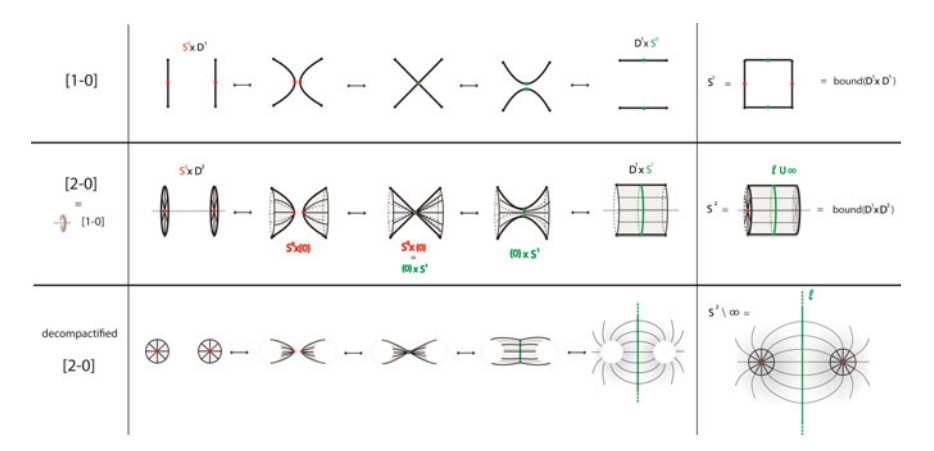


Fig. 10.1 From top to bottom row: 1-dimensional 0-surgery, 2-dimensional 0-surgery, decompactified 2-dimensional 0-surgery

here, it is also worth pointing out that, by symmetry, the instances of 2-dimensional 1-surgery can also be obtained by rotating the instances of 1-dimensional 0-surgery by 180° around a vertical axis, perpendicular to the one shown in Fig. 10.1 [2–0].

In analogy, for m=3, 3-dimensional surgery can be viewed as a way of passing from one boundary component of $D^{n+1}\times D^{3-n}\cong D^4$ to its complement, recall Chap. 4 for m=3. Hence, the initial and final instances of the process form $S^3=\partial D^4$, which is a 180° rotation of the S^2 that is made of the initial and final instances of 2-dimensional surgery. To grasp this last observation, recall that S^1 is obtained by a 180° rotation of S^0 and S^2 is obtained by a 180° rotation of S^1 . Moving up one dimension, since S^2 is embedded in \mathbb{R}^3 , the S^3 created by rotation requires a fourth dimension in order to be visualized.

In order to overcome this difficulty we project stereographically S^2 in \mathbb{R}^2 , as shown in Fig. 10.2. Note that the two great circles $l \cup \{\infty\}$ and $l' \cup \{\infty\}$ in S^2 are projected to the two perpendicular infinite lines l and l' in \mathbb{R}^2 . With the stereographic projection of S^2 at hand, it is now easy to see that S^3 is obtained as 180° rotation of S^2 . Indeed, rotating $\mathbb{R}^2 = S^2 \setminus \{\infty\}$ in Fig. 10.2 around axis l by 180° we obtain $\mathbb{R}^3 = S^3 \setminus \{\infty\}$. We can now introduce the notion of decompactified 2-dimensional 0-surgery which is depicted in Fig. 10.1 decompactified [2–0]:

Definition 7 The process of *decompactified 2-dimensional 0-surgery* is completely analogous to 2-dimensional 0-surgery except that it is projected in \mathbb{R}^2 . It starts with two flattened discs which approach each other. The centers of the two discs touch and the discs merge into one. The resulting disc is a thickened segment $D^1 \times D^1$ which grows to infinity filling the complement space $\mathbb{R}^2 \setminus (S^0 \times D^2)$. The final thickened line $D^1 \times l$ corresponds to the decompactification of the thickened circle $D^1 \times S^1 = D^1 \times (l \cup \{\infty\})$. The cores of both the thickened line and the circle are shown in green in Fig. 10.1 [2–0] and Fig. 10.1 decompactified [2–0].

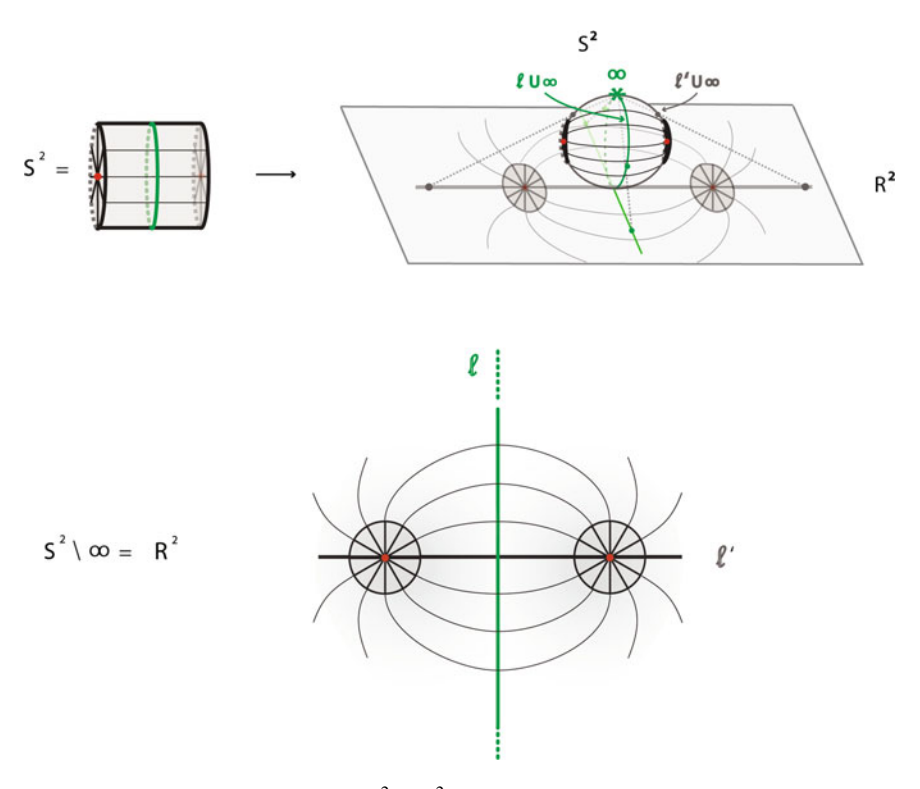


Fig. 10.2 Stereographic projection of S^2 in \mathbb{R}^2

Note that, in analogy to 2-dimensional 0-surgery, decompactified 2-dimensional 0-surgery can also be seen as a process caused by attracting forces and an attracting center. The forces are not shown here in order to keep the figures lighter.

In Sect. 10.2 we will rotate the instances of decompactified 2-dimensional 0-surgery in order to obtain our first visualization of 3-dimensional surgery in \mathbb{R}^3 .

Remark 13 The decompactified 2-dimensional 1-surgery can also be defined in analogy to the decompactified 2-dimensional 0-surgery but it is simpler to view it as its reverse process.

10.2 Visualizing 3-Dimensional Surgery in \mathbb{R}^3

As mentioned in Sect. 10.1, rotating the S^2 made of the initial and final instances of 2-dimensional surgery gives us the $S^3 = \partial D^4$ made of the initial and final instances of 3-dimensional surgery. We will now rotate the stereographic projection of S^2 in \mathbb{R}^2 , see Fig. 10.2, to obtain the stereographic projection of the initial and final

instances of 3-dimensional surgery in \mathbb{R}^3 . We will discuss the two processes of 3-dimensional surgery, namely 3-dimensional 1-surgery and 3-dimensional 0-surgery, which were introduced in Sect. 3.4. Each of these processes corresponds to a different rotation, which results in a different visualization of the initial and the final stage of 3-dimensional surgery in \mathbb{R}^3 and which, in turn, corresponds to a different decomposition of S^3 . These two decompositions are presented in Sect. 10.2.1. Then, using these visualizations of the initial and final instances, we will visualize the intermediate steps of both processes in Sect. 10.2.2.

10.2.1 Initial and Final Steps

Let us recall the initial and final instances of our two processes of 3-dimensional surgery. For 3-dimensional 1-surgery, the initial and final instances are solid tori $S^1 \times D^2$ and $D^2 \times S^1$ while for 3-dimensional 0-surgery, we have two 3-balls $S^0 \times D^3$ and a thickened sphere $D^1 \times S^2$.

Rotating our decompactified view in \mathbb{R}^2 by 180° vertically gives us the initial and final instances of 3-dimensional 1-surgery in \mathbb{R}^3 . In this case the axis of rotation is line l which is at equal distance from the two flattened discs and is shown in green in Fig. 10.3(a). We can directly see that this rotation transforms the two discs $S^0 \times D^2$ (the first instance of decompactified 2-dimensional 0-surgery) to the solid torus $S_1^1 \times D^2$ (the first instance of 3-dimensional 1-surgery), see Fig. 10.3(b). Each of the arcs connecting the two discs $S^0 \times D^2$ generates through the rotation a 2-dimensional disc, the set of all such discs being parametrized by the points of the line l in \mathbb{R}^3 . Therefore the complement of the solid torus $S_1^1 \times D^2$ is another solid torus $D^2 \times S_2^1$, see Fig. 10.3(b), where line l in \mathbb{R}^3 is circle $S_2^1 = l \cup \{\infty\}$ in S^3 .

Note that the visualization of Fig. 10.3(b) is the same as the one presented in Fig. 8.1(c), (c') of Chap. 8 where $S^3 = V_1 \cup V_2$. Here $V_1 = S_1^1 \times D^2$ and $V_2 = D^2 \times S_2^1$, the core curve c of V_1 is S_1^1 and the core curve $l \cup \{\infty\}$ of V_2 is S_2^1 .

Similarly, rotating our decompactified view in \mathbb{R}^2 by 180° horizontally gives us the initial and final instances of 3-dimensional 0-surgery in \mathbb{R}^3 . The axis of rotation is line l' which pierces the two flattened discs and is shown in grey in Fig. 10.3(a). We can directly see that this rotation transforms the two discs $S^0 \times D^2$ (the first instance of decompactified 2-dimensional 0-surgery) to two 3-balls $S_1^0 \times D^3$ (the first instance of 3-dimensional 0-surgery), see Fig. 10.3(c). The rotation of line l along l' creates a plane that cuts through \mathbb{R}^3 and separates the two resulting 3-balls $S_1^0 \times D^3$. This plane is thickened by the arcs connecting the two discs $S^0 \times D^2$ which have also rotated, see Fig. 10.3(c). This plane is the decompactified view of sphere S_2^2 in S^3 which can be viewed as a rotation of circle $l \cup \{\infty\} = S_2^1$. Therefore the complement of the two 3-balls $S_1^0 \times D^3$ is a thickened sphere $D^1 \times S_2^2$ where the plane resulting from the rotation of line l in \mathbb{R}^3 is sphere S_2^2 in S^3 .

In both cases, in Fig. 10.3(a), \hat{S}^3 is represented as the result of rotating the 2 sphere $S^2 = \mathbb{R}^2 \cup \{\infty\}$. For 3-dimensional 1-surgery, S^2 is rotated about the circle $l \cup \{\infty\}$ where l is a straight horizontal line in \mathbb{R}^2 , see also Fig. 10.2. The resulting

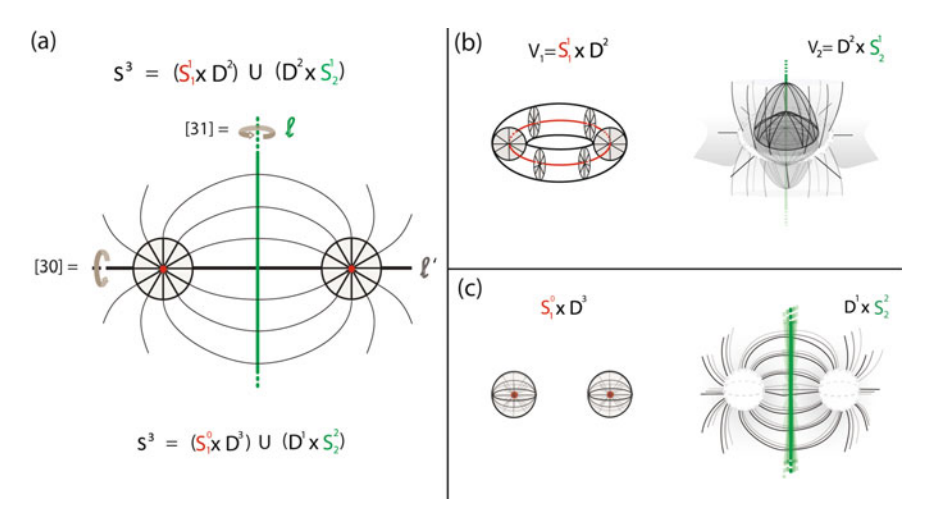


Fig. 10.3 (a) Representations of S^3 in \mathbb{R}^3 , (b) Initial and final instance of 3-dimensional 1-surgery, (c) Initial and final instance of 3-dimensional 0-surgery

decomposition is $S^3 = (S_1^1 \times D^2) \cup (D^2 \times S_2^1)$. For 3-dimensional 0-surgery, S^2 is rotated about the circle $l' \cup \{\infty\}$ where l' is a straight vertical line in \mathbb{R}^2 , see also Fig. 10.2. The resulting decomposition is $S^3 = (S_1^0 \times D^3) \cup (D^1 \times S_2^2)$.

10.2.2 Intermediate Steps

We are now ready to visualize the intermediate steps of both types of 3-dimensional surgery. By rotating the instances of decompactified 2-dimensional 0-surgery (shown in Fig. 10.1 decompactified [2–0]) around the axes l and l' (shown in Fig. 10.3(a)) we obtain the instances of 3-dimensional 1-surgery and 3-dimensional 0-surgery respectively, see Fig. 10.4.

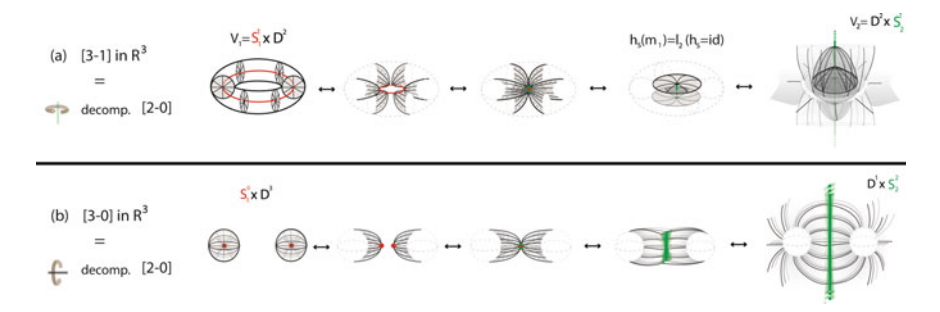


Fig. 10.4 (a) 3-dimensional 1-surgery in \mathbb{R}^3 (b) 3-dimensional 0-surgery in \mathbb{R}^3

In these two processes, as in lower dimensional surgeries, the time-evolution of surgery passes through a singular point. Namely, for 3-dimensional 1-surgery we see a solid torus $S_1^1 \times D^2$ collapsing to a singularity from which emerges the complement solid torus $D^2 \times S_2^1$. This, if visualized in \mathbb{R}^3 , fills the rest of the space, see Fig. 10.4(a). In this case we have used the standard (identity) embedding of $S_1^1 \times D^2$ denoted by h_s , which induces a 'gluing' homeomorphism along the common boundary $S^1 \times S^1$, such that the meridians of solid torus $V_1 = S_1^1 \times D^2$ are mapped to the longitudes of solid torus $V_2 = D^2 \times S_2^1$. In other words, $h_s(m_1) = l_2$.

For 3-dimensional 0-surgery, we see the two 3-balls $S_1^0 \times D^3$ collapsing to a singularity from which emerges the thickened sphere $D^1 \times S_2^2$ which, if decompactified in \mathbb{R}^3 , is a thickened plane filling the rest of the space, see Fig. 10.4(b).

10.3 The Continuity of 3-Dimensional Surgery

In this section we analyze the concept of continuity for 3-dimensional surgery.

Let us first recall from Chap. 4 that all types of 3-dimensional surgery take place inside the 4-dimensional handle $D^{n+1} \times D^{3-n}$, n < 3 and that the processes of both 3-dimensional 0- and 1-surgery can be viewed as taking the boundary of the first factor D^{n+1} , thickening it, passing through the unique intersection point $D^{n+1} \cap D^{3-n}$ and then letting the thickened boundary of the second factor D^{3-n} emerge. We will first present the core view which shows how we pass from the boundary of D^{n+1} to the boundary of D^{3-n} . We will then apply the different kinds of thickenings (or framings) to the cores in order to illustrate both processes in \mathbb{R}^4 .

More precisely, 3-dimensional 1-surgery takes place inside $D_1^2 \times D_2^2$. In this case, we go from the core $S_1^1 = \partial D_1^2$ to the core $S_2^1 = \partial D_2^2$ by passing through the unique intersection $D_1^2 \cap D_2^2$. As mentioned in Sect. 2.4.4, we consider that n-balls are centered at the origin. Hence if $D_1^2 = \{(x, y, 0, 0) : x^2 + y^2 \le 1\}$ and $D_2^2 = \{(0, 0, z, w) : z^2 + w^2 \le 1\}$ then $D_1^2 \cap D_2^2 = (0, 0, 0, 0)$. This process can be represented by looking at the (x, y) axes until core $S_1^1 = \partial D_1^2$ collapses to the singular point (0, 0, 0, 0) and then switching to the (z, w) axes as core $S_2^1 = \partial D_2^2$ uncollapses. This is shown in Fig. 10.5(a₁). We will refer to this process as the *core view of 3-dimensional 1-surgery* which will be denoted by 'core [3–1]'.

On the other hand, 3-dimensional 0-surgery takes place inside $D_1^1 \times D_2^3$. In that case, we go from the core $S_1^0 = \partial D_1^1$ to the core $S_2^2 = \partial D_2^3$ by passing trough the unique intersection $D_1^1 \cap D_2^3$. Hence, if $D_1^1 = \{(0, y, 0, 0) : y \in [-1, 1]\}$ and $D_2^3 = \{(x, 0, z, w) : x^2 + z^2 + w^2 \le 1\}$, then $D_1^1 \cap D_2^3 = (0, 0, 0, 0)$. This process can be seen by looking at the y axis until core $S_1^0 = \partial D_1^1$ collapses to the singular point (0, 0, 0, 0) and then, switching to the x, z, w axes, as core $S_2^2 = \partial D_2^3$ uncollapses. This is shown in Fig. 10.5(b₁). We will refer to this process as the *core view of 3-dimensional 0-surgery* which will be denoted by 'core [3–0]'.

We will now thicken the aforementioned cores in order to present our illustrations in \mathbb{R}^4 . Let us recall that, so far, in Sects. 10.2.1 and 10.2.2, the final instances of both 3-dimensional 0-surgery and 1-surgery were distorted due to decompactification.

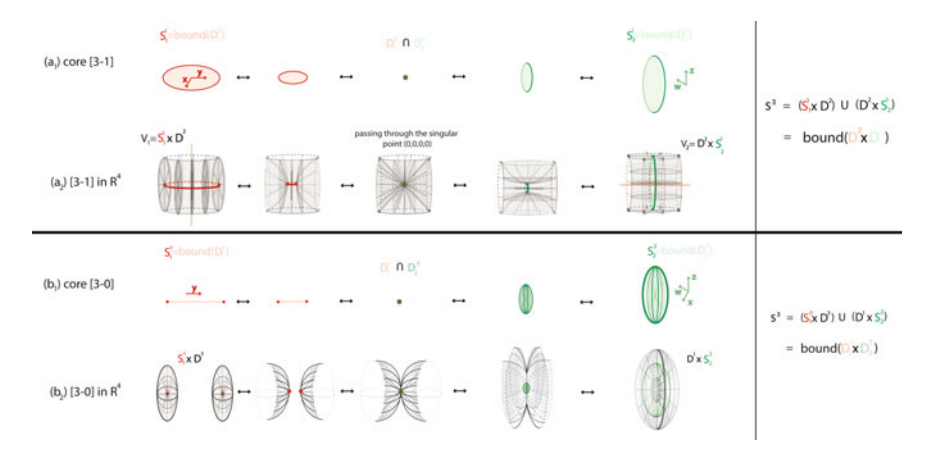


Fig. 10.5 (a₁) Core view of [3–1] surgery (a₂) [3–1] surgery in \mathbb{R}^4 (b₁) Core view of [3–0]-surgery (b₂) [3–0] surgery in \mathbb{R}^4

More precisely, in Figs. 10.3 and 10.4, both the solid torus $D^2 \times S_2^1$ and the thickened sphere $D^1 \times S_2^2$ were filling the rest of the space in \mathbb{R}^3 . Our goal here is to obtain the corresponding undistorted illustrations in \mathbb{R}^4 .

For 3-dimensional 1-surgery, we start by thickening our core view S_1^1 shown in Fig. 10.5(a₁) with a D^2 . We collapse $S_1^1 \times D^2$ to a singularity and then need to uncollapse it in a way that produces the complement solid torus $D^2 \times S_2^1$ as a thickening of its core S_2^1 . The whole process is shown in Fig. 10.5(a₂).

For 3-dimensional 0-surgery, we start by thickening our core view S_1^0 shown in Fig. 10.5(b₁) with a D^3 . We collapse $S_1^0 \times D^3$ to a singularity and then we need to uncollapse it in a way that produces the $D^1 \times S_2^2$ as a thickening of its core sphere S_2^2 . The whole process is shown in Fig. 10.5(b₂).

In both cases, we have combined the core with the \mathbb{R}^4 view and added the corresponding decomposition of S^3 in the end. We have used color coding in order to clarify how the notions presented in Sects. 10.1, 10.2 and 10.3 interplay. To complete the picture, it is worth adding that the visualizations of Fig. 10.4(a) and (b) are the decompactified versions of Fig. 10.5(a₂) and (b₂) respectively. In both cases the instances up to the singularity are identical while the uncollapsing is done in \mathbb{R}^3 and \mathbb{R}^4 respectively.

Remark 14 It is worth adding that the two last instances $D^2 \times S_2^1$ and $D^1 \times S_2^2$ of 3-dimensional 0- and 1-surgery in \mathbb{R}^4 shown in Fig. 10.5(a₂) and (b₂) can be also obtained as different rotations of the final instance $D^1 \times S^1$ of 2-dimensional 0-surgery surgery shown in Fig. 10.1 [2–0]. Indeed, starting with cylinder $D^1 \times S^1$, we first decompactify S^1 to \mathbb{R}^1 to obtain $D^1 \times \mathbb{R}^1$, see Fig. 10.6(a). Then, using the same rotational axis as the one described in Sect. 10.2.1 and shown in green in Fig. 10.6(a), we obtain the decompactified $D^2 \times \mathbb{R}^1$, where each segment D^1 has been rotated to a disc D^2 . We finally recompactify \mathbb{R}^1 to S^1 to obtain $D^2 \times S^1$. Note that the axis starts as a circle, becomes straight during decompactification and becomes a circle again when we recompactify.

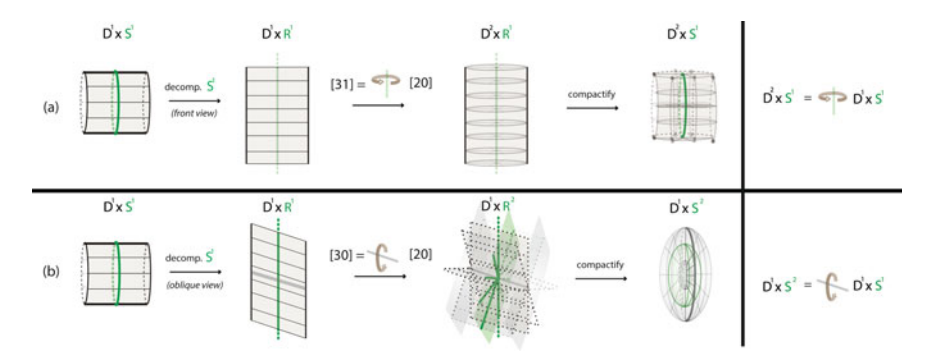


Fig. 10.6 (a) $D^2 \times S^1$ as a rotation of $D^1 \times S^1$ (b) $D^1 \times S^2$ as a rotation of $D^1 \times S^1$

Similarly, starting again with the $D^1 \times S^1$ of 2-dimensional 0-surgery, we first decompactify S^1 to \mathbb{R}^1 to obtain $D^1 \times \mathbb{R}^1$, see Fig. 10.6(b). Then, using the same rotational axis as the one described in Sect. 10.2.1 and shown in grey Fig. 10.6(b), we obtain the decompactified $D^1 \times \mathbb{R}^2$ where each line \mathbb{R}^1 has been rotated to a plane \mathbb{R}^2 . In Fig. 10.6(b), we have used an oblique view of both $D^1 \times \mathbb{R}^1$ and $D^1 \times \mathbb{R}^2$ so the effect of the rotation can be visible. We finally compactify \mathbb{R}^2 to S^2 to obtain the thickened sphere (or hollow 3-ball) $D^1 \times S^2$.

This process of decompactifying, rotating and compactifying again allowed us to visualize the final instances of 3-dimensional 1- and 0-surgery in relation with our initial visualization of $D^1 \times S^1$ of 2-dimensional 0-surgery by following a reasoning similar to the one used in Sect. 10.2 for the visualizations in \mathbb{R}^3 . The difference being that in the visualizations of Sect. 10.2, $D^1 \times S^1$ was obtained as part of the decompactification of S^2 , hence it was inevitably deformed so that its union with $S^0 \times D^2$ would form \mathbb{R}^2 . As this constrain does not exist here, when S^1 is decompactified to \mathbb{R}^1 , its framing D^1 follows without undergoing such deformation, see the passage from the first to the second instance in Fig. 10.6(a) and (b).

10.4 Modeling Black Hole Formation from Cosmic Strings

In this section we will see how the formation of black holes from cosmic strings can be modeled by 3-dimensional 1-surgery.

10.4.1 Terminology

We will first explain the terms of *Schwarzschild radius*, *event horizon* and *gravitational singularity* which will be used in the following sections.

The Schwarzschild radius is the radius of a 2-sphere such that, if all the mass of an object were to be compressed within that sphere, the escape velocity from the surface

of the sphere would equal the speed of light. If anything collapses to or below this radius, a black hole is formed. The event horizon is a boundary in spacetime beyond which events cannot affect an outside observer and is most commonly associated with black holes. For a nonrotating black hole, the Schwarzschild radius delimits a spherical event horizon.

In the center of a black hole, general relativity predicts the existence of a gravitational singularity (or space-time singularity), i.e. a region in space in which matter takes infinite density and 0 volume (basically infinitely dense and infinitely small). The singularity cannot be seen as it is covered by the event horizon.

10.4.2 Black Holes from Cosmic Strings

Cosmic strings are hypothetical 1-dimensional topological defects which may have formed in the early universe and are predicted by both quantum field theory and string theory models. Their existence was first contemplated by Tom Kibble in the 1970s. In [1], S.W. Hawking estimates that a fraction of cosmic string loops can collapse to a small size inside their Schwarzschild radius thus forming a black hole. As he mentions, under certain conditions, 'one would expect an event horizon to form, and the loop to disappear into a black hole'.

Note that other estimations of the fraction of cosmic string loops which collapse to form black holes have been made in subsequent work, see [2, 3]. While the details of the different estimations have no direct implications on this analysis, it is worth mentioning the following two statements. In [2], R.R. Caldwell and P. Casper point out that the loop 'collapses in all three directions' and in [3], J.H. MacGibbon, R.H. Brandenberger and U.F. Wichosk give the following example for a collapsing symmetric string loop: 'For example, a planar circular string loop after a quarter period will collapse to a point and hence form a black hole.'

Topologically, the aforementioned loop can be considered to be a solid torus $S^1 \times D^2$ embedded in an initial manifold M. The thickening D^2 can be considered to be very small, as the diameter of a cosmic strings is of the same order of magnitude as that of a proton, i.e. ≈ 1 fm or smaller. Further, we consider M as being the 3-space S^3 or \mathbb{R}^3 or a 3-manifold corresponding to the 3-dimensional spatial section of the 4-dimensional space-time of the universe. The loop $S^1 \times D^2$ collapses to a small size inside its Schwarzschild radius thus creating a black hole the center of which contains the singularity. In this scenario, the inital 3-space M becomes a singular manifold at that point.

Physicists are undecided whether the prediction of this singularity means that it actually exists or that current knowledge is insufficient to describe what happens at such extreme density. As we will see in the next section, we can avoid this singularity by considering that the collapsing of a cosmic string loop is followed by the uncollapsing of another cosmic string loop. In other words, we propose that the creation of a black hole is a 3-dimensional 1-surgery which changes the initial 3-dimensional space M to another 3-dimensional space $\chi(M)$ by passing through a singular point.

As detailed in Sect. 10.3, the time evolution of this process happens locally inside the handle $D^2 \times D^2$ and requires four spatial dimensions in order to be visualized but each 'slice' of the process is a 3-dimensional manifold.

Note that this process is different from the global process of embedded surgery used to model the density distribution of black hole formation in Sect. 9.3 as it describes the local process of a cosmic string collapsing to a black hole inside the event horizon.

10.4.3 Black Holes from 3-Dimensional 1-Surgery

We will now describe the process of 3-dimensional 1-surgery on M step by step. We start with an embedding of the loop $S^1 \times D^2$, which may also be knotted. Using an analogue which is two dimensions lower, M is shown as a line while the core S^1 of the embedding $S^1 \times D^2$ is shown as the core S^0 of embedding $S^0 \times D^1$. In Fig. 10.7 (initial), core S^0 is shown in red and its thickening in grey. Since the process of surgery is a local process, black hole formation can be seen independently of M. Therefore we zoom in to see this local procedure in instances (a)–(b) of Fig. 10.7 which happens inside $D^2 \times D^2$.

As mentioned in Chap. 5 and throughout this analysis, the local process of surgery is considered as a result of attracting forces. In the 3-dimensional case, we deliberately didn't show these forces in Fig. 10.5 in order to keep the illustrations lighter but as explained in Sect. 5.5, we know that the forces of our model are applied to the core 1-embedding $e = h_1 : S^1 = S^1 \times \{0\} \hookrightarrow M$ of the framed n-embedding $h: S^1 \times D^2 \hookrightarrow M$.

These forces are added in blue in Fig. 10.7(a), where we see the same process as Fig. $10.5(a_2)$ but with a knotted embedding of the core S^1 . Note that these local forces of our model correspond to the string tension, which collapses the cosmic string (see [1] for details). In instance (2) of Fig. 10.7 the cosmic string shrinks to a radius smaller than its Schwarzschild radius, thus the event horizon is formed. We are not showing the black hole inside the event horizon as we want to focus on the topological change. Further, instance Fig. 10.7(c) shows the loop shrinking to a point in the 3-dimensional space where this point is the singular point mentioned in Sect. 10.3.

According to our model, after the collapsing the process doesn't stop, but another manifold $D^2 \times S^1$, which corresponds to another cosmic string loop, grows from the singular point of instance Fig. 10.7(c), and this is the added value of our model. In Fig. 10.7(d) we show the uncollapsing of cosmic string $D^2 \times S^1$ which transforms the initial manifold M to $\chi(M) = M \setminus h(S^1 \times D^2) \cup_h (D^2 \times S^1)$, see Fig. 10.7 (final). Note that instances Fig. 10.7(a), (b), (c) and (d) are analogous to the instances of Fig. 10.5(a₂).

It is worth mentioning that Fig. 10.7 (final) is also shown two dimensions lower. Namely, as in Fig. 10.7 (initial), the core S^1 of the cosmic string loop $D^2 \times S^1$ is represented by the core S^0 of $D^1 \times S^0$. In Fig. 10.7 (final), core S^0 is shown in green and its thickening in grey. The whole process occurs inside the handle $D^1 \times D^1$

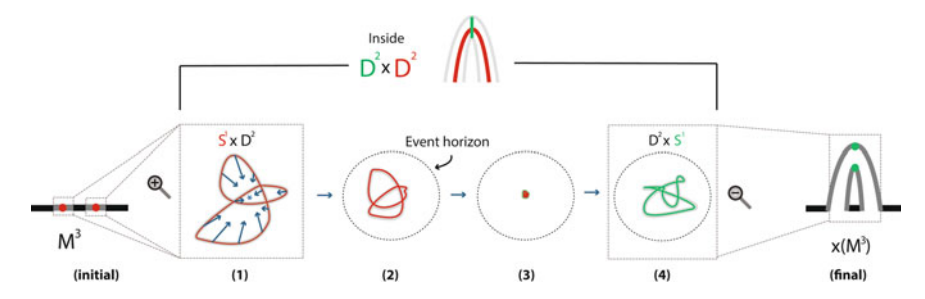


Fig. 10.7 3-dimensional 1-surgery inside the event horizon

illustrated in the upper part of Fig. 10.7 which, following this analogy, stands for $D^2 \times D^2$. The global 4-dimensional visualization of 3-dimensional 1-surgery on an initial 3-manifold such as S^3 following the line of thought of Sects. 10.2.2 and 10.3 is an intriguing subject and will be the subject of future work. However, for the purpose of this analysis we do not need to visualize the initial and final manifold but rather the idea behind the local process illustrated in instances Fig. 10.7 (a), (b), (c) and (d).

Summarizing the above, modeling the collapsing of a cosmic string loop with a 3-dimensional 1-surgery allows us to go through the singular point of the black hole without having a singular manifold in the end. Instead, we end up in the same universe with a local topology change from the 3-dimensional space M to the 3-dimensional space $\chi(M)$ and, as seen in Fig. 10.7(b), (c) and (d), this topology change happens within the event horizon.

References

- Hawking S.W.: Black holes from cosmic strings. Phys. Lett. B 231(3), 237 (1989). https://doi. org/10.1016/0370-2693(89)90206-2
- Caldwell R.R., Casper P.: Formation of black holes from collapsed cosmic string loops. Phys. Rev. D53 (1996). https://doi.org/10.1103/PhysRevD.53.3002
- MacGibbon, J.H., Brandenberger, R.H., Wichoski, U.F.: Limits on black hole formation from cosmic string loops. Phys. Rev. D 57, 2158–2165 (1998). https://doi.org/10.1103/PhysRevD. 57.2158

Chapter 11 Conclusions



In this thesis we explained many natural processes via topological surgery. Examples comprise chromosomal crossover, magnetic reconnection, mitosis, gene transfer, the creation of Falaco solitons, the formation of tornadoes and the formation of black holes. To do this we first enhanced the usual static description of topological surgery by introducing dynamics, by means of continuity and attracting forces. In order to model more phenomena, we then filled in the interior space by introducing the notion of solid surgery. Further, we introduced the notion of embedded surgery, which leaves room for the initial manifold to assume a more complicated configuration and describes how the complementary space of the initial manifold participates in the process. Thus, instead of considering surgery as a formal and static process, our new model and definitions can be used to analyze the topological changes occurring in natural phenomena.

Apart from the examples studied in this thesis, there are several other phenomena exhibiting surgery. Our topological model indicates where to look for the forces causing surgery and what deformations should be observed in the local submanifolds involved and these predictions may prove significant for the study of these phenomena. Also, it would be worth applying our modeling of the changes occurring in the complement space during embedded surgery in more natural processes as it provides a 'global' explanation of the phenomenon, which can also be of great physical value.

Equally important, all these new notions resulted in pinning down the connection of solid 2-dimensional 0-surgery with a dynamical system. This connection gives us on the one hand a mathematical model for 2-dimensional surgery and, on the other hand, a dynamical system modeling natural phenomena exhibiting 2-dimensional topological surgery through a 'hole-drilling' process. The provided dynamical system presents significant common features with solid 2-dimensional 0-surgery, in the sense that eigenvectors act as the attracting forces, trajectories lie on the boundaries of the manifolds undergoing surgery and surgery on the steady state point creates a limit cycle thus coinciding with our definition of solid surgery. A possible future research direction would be to search for other dynamical systems realizing surgery and

80 11 Conclusions

use these dynamical systems as a base for establishing a more general theoretical connection between topological surgery and bifurcation theory.

Moreover, we presented a visualization of the 4-dimensional process of 3-dimensional surgery in \mathbb{R}^3 by introducing the notion of decompactified 2-dimensional surgery. This notion could be used to visualize 3-dimensional lens spaces occurring from 3-dimensional surgery on the 3-sphere and other 4-dimensional processes.

Finally, we also modeled the formation of black holes from cosmic strings using 3-dimensional 1-surgery. As our model suggests that a black hole does not necessarily result in a spatial singularity, it would be very interesting to collaborate with physicists in order to investigate the physical implications of the proposed topological change. We are currently working in this direction.

We hope that through this study, topology and dynamics of natural phenomena, as well as topological surgery itself, will be better understood and that our connections will serve as ground for many more insightful observations and new physical implications.

Curriculum Vitae

PERSONAL INFORMATION

Name Stathis Antoniou Date of birth 25 March 1982

Address Orias 10, 11522, Athens, Greece

Phone +30 6977505932

Email stathis.antoniou@gmail.com

Public Profiles Google Scholar, ResearchGate, LinkedIn

Military duty Fulfilled

RESEARCH INTERESTS

Mathematical modeling, computational mathematics, low-dimensional topology, dynamical systems

ACADEMIC QUALIFICATIONS

2014-2018 Ph.D., Department of Mathematics, National Technical University of

Mathematical Modeling through Topological Surgery and Applica-

tions, supervisor: S. Lambropoulou

Master of Science and Technology, École Polytechnique of France 2005-2006

Specialization in Mathematical Modeling and Machine Learning

2000-2005 Diploma of Applied Mathematics and Physical Sciences, National

Technical University of Athens

Specialization in Applied and Computational Mathematics

SCHOLARSHIPS & GRANTS

2017 Ph.D. scholarship from the Papakyriakopoulos Foundation

2014-2015 Ph.D. research within grant THALES "Algebraic modeling of topo-

logical and computational structures and applications" MIS380154,

financed by Greece and the European Union

Master scholarship from the French Embassy of Athens 2005-2006

2001-2003 Diploma scholarship from the Greek National Scholarships

Foundation

RESEARCH EXPERIENCE

Publications Scientific Journals and Refereed Proceedings

> - Extending Topological Surgery to Natural Processes and Dynamical Systems, with S. Lambropoulou, PLOS ONE 12(9), DOI:

10.1371/journal.pone.0183993,2017

- Topological Surgery, Dynamics and Applications to Natural Processes, with S. Lambropoulou, Journal of Knot Theory and Its Ramifications 26(9), DOI: 10.1142/S0218216517430027, 2016

82 Curriculum Vitae

- Topological Surgery in Nature, with S. Lambropoulou, Chapter in Book, Springer Proceedings (PROMS), Vol. 219, DOI: 10.1007/978-3-319-68103-0, 2016

Technical Reports

- <u>Topological Surgery and Dynamics</u>, with S. Lambropoulou, N. Samardzija, I. Diamantis, Mathematisches Forschungsinstitut Oberwolfach Report No. 26, DOI: 10.4171/OWR/2014/26, 2014
- Fear-type emotion recognition with support vector machines ("Reconnaissance des émotions de type peur—machines à vecteurs support"), Master thesis, ENST Paris, 2006
- The chaotic attractor of a 3D Lotka-Volterra dynamical system and its relation to the topological surgery, Diploma thesis, National Technical University of Athens, 2005

Talks

- Winterbraids VII, École thématique CNRS, Université de Caen, France, 2017
- Summer School on Modern Knot Theory University of Freiburg, Germany, 2017
- Knots in Hellas 2016, International Olympic Academy, Greece, 2016
- Low Dimensional Topology and Its Relationships with Physics, 2015 AMS/EMS/SPM, Portugal, 2015
- 18th Symposium on Topological Quantum Information, Athens, Greece, 2015
- Knots and Links in Fluid Flows, Independent University, Moscow, Russia, 2015

Reviews

Invited reviewer for zbMATH

Teaching

"Programming for Mathematics and Physics", National Technical University of Athens, 2017

"Introducing Programming", National Technical University of Athens, 2002

WORK EXPERIENCE

2015-2017

Part-time Senior Consultant in R&D—Marketing and Sales, Avon Cosmetics Greece

- Behavioral analysis, incentive design and strategy
- Intern management and knowledge transfer

2012-2014

Senior Marketing Analyst, Avon Cosmetics Greece

- Data analysis, forecasting, risk evaluation and reporting
- Extensive use of Microsoft Excel, Visual Basic, and SQL databases

Curriculum Vitae 83

2010–2012 Credit Risk Analyst, Statistical Decisions

- Risk analysis for European banks using mathematical modeling, statistics and historical performance

- Extensive use of SAS and SPSS programming

2009–2010 Consultant, Planet S.A.

- Management consulting services based on data analysis and forecast

- Extensive use of Microsoft Excel, Visual Basic, and SQL databases

2006 Machine Learning Intern, Télécom ParisTech

- Detection of fear-type emotions in the human voice for future audiobased surveillance systems in cooperation with Thales Group and CNRS

- Extensive use of MATLAB, C, C++ and grid computing

PROGRAMMING

Proficient MATLAB, Mathematica, SAS, SPSS, Visual Basic, SQL

Intermediate Python, Java, R, C++, C, Lisp

LANGUAGES

Greek, French Native
English Advanced
Dutch Beginner

OTHER ACTIVITIES

From 2006 Writing (10 publications in literature magazines)

From 2015 Science outreach (5 talks at Café Scientifique and Athens Science

Festival)

2006–2008 Travel writing and volunteer work in the conservation program of

WWF in Madagascar

Index

В	\mathbf{L}
Bifurcation, 42, 47	Lotka-Volterra, 41, 53
Black hole, 3, 28, 59, 67, 74	
	M
C	Magnetic reconnection, 25, 27
Chromosomal crossover, 27, 28	Meiosis, 25
Cosmic strings, 3, 67, 74, 75	Mitosis, 28, 40
D	N
4-dimensional space, 3, 67, 75, 76	N
DNA recombination, 25, 28, 57	Nested spheres, 38, 45, 51
Dynamical system, 41, 47, 49, 52	Nested tori, 36, 37, 51
	Numerical analysis, 41, 43, 54
E	D.
Embedded topological surgery, 49, 57, 59,	R
62, 64	Recoupling, 26, 28, 30
F	S
Falaco solitons, 28, 31, 39, 47	Slow manifold, 45, 47, 53
Fractal torus, 45, 46	Solid topological surgery, 31, 33–35, 41
Fracture, 30, 40	Splicing, 25
G	Т
Gene transfer, 28, 30, 38	Three-sphere, 54, 57–59, 62, 64, 68
Gluing homeomorphism, 13, 16, 17, 27, 29,	Topological thread, 30, 39
39, 51, 72	Tornadoes, 28, 30, 33, 47, 62
07, 01, 12	1011144000, 20, 30, 33, 47, 02